ulm university universität
uulm

Institute for Inorganic Chemistry I

Synthesis and Characterization of Self-Healing Biomaterial-Based Hydrogels by Convenient Copolymerisation

Master‘s Thesis

For the Degree of

Master of Science (M.Sc.)

Submitted to the Faculty of Natural Sciences

Ulm University

By

Raphaela Leonie Thierer

796593

August 2019

Declaration

Hereby, I, Raphaela Leonie Thierer, declare that I wrote this Master's thesis myself. I have not used any sources other than those listed in the "Literature and Sources" segment and I have marked all thoughts and ideas taken directly or indirectly from these sources accordingly. Furthermore, I declare that this work has not been published nor was it part of an examination procedure.

Erklärung

Hiermit erkläre ich, Raphaela Leonie Thierer, dass ich die vorliegende Masterarbeit selbständig angefertigt habe. Ich habe keine anderen Quellen benutzt als diese, die im Abschnitt „Literature and Sources" angegeben sind. Des Weiteren habe ich alle Gedanken und Ideen aus diesen Quellen, direkt oder indirekt übernommen, als solche gekennzeichnet. Diese Arbeit wurde weder veröffentlicht, noch war sie Teil eines Prüfungsverfahrens.

Ulm, 16.08.2019

Table of Contents

Introduction

From Amino Acids to Peptide and Protein Biomaterials to Hydrogels

Peptides and Proteins

Proteins play a crucial role in every living organism. These macromolecules fulfil a wide range of functions, as they provide cells with structure, transport of various molecules, and perform highly specific reactions as enzymes. Showcasing their important role for all organisms, without proteins, DNA replication and, therefore, cell proliferation as well as cell growth could not take place. To be able to perform these versatile tasks, the correct structure of the protein is key. The basic components of naturally occurring proteins are 20 amino acids, which share a common core structure but differ in their side chains. These can be classified as hydrophilic, hydrophobic, basic, and acidic residues. The linking of these amino acids is fundamental for proteins. A condensation reaction between the amino group (N-terminus) of one amino acid and the carboxyl group (C-terminus) of another leads to the formation of a peptide bond, whereby water is released (Scheme 1).

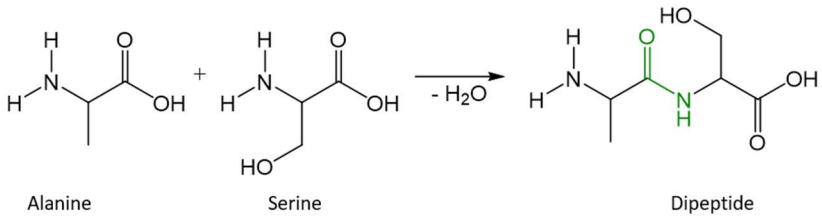

Scheme 1: Formation of a dipeptide. The carboxyl group of alanine, having a hydrophobic side chain, reacts with the amino group of serine, which has a hydrophilic side chain. A newly formed peptide bond (highlighted in green) arises while water is released.

The correct order of the amino acids dictates structure formation and, therefore, is crucial to form a functional protein. Thereby, the sequence of amino acids is described by the primary structure of a protein. The secondary structure is the spatial configuration of the peptide backbone, formed by hydrogen bonds between the carbonyl oxygen atom and the amino nitrogen atom. Main elements of the secondary structure are α-helices, β-sheets, and random coils. The tertiary structure is the overall structure of the whole polypeptide chain, which can consist of segments of different secondary structures. The conformation of the polypeptide chain is stabilized by van-der-Waals, ionic, or aromatic interactions of the amino acid residues. If a protein consists of multiple subunits, the quantity and arrangement of these is described as quaternary structure (Berg et al. 2013). Contrary to proteins, the term peptide is used if the polypeptide chain is shorter than 100 amino acids.

Folding of the polypeptide chains into the right conformation is essential for its function. The biologically active, correctly folded form is called the native conformation. The process to attain the

native conformation is driven by minimization of the peptides free energy and can be described by a folding funnel, in which the initially unfolded polypeptide chain can go different pathways to reach the native conformation (Dobson 2004). For some proteins, the energy difference between the native conformation and a misfolded, stable intermediate is very low, and as a result the process of folding is prone to errors. To avoid damage from misfolded proteins, cells have established quality control systems. Examples include heat shock proteins, which correct the misfolding, as well as rapid degradation of the misfolded chain if the native conformation cannot be reached. However, if these mechanisms fail, accumulation of misfolded proteins can occur, potentially leading to fatal diseases (Valastyan and Lindquist 2014). The widest known human disease associated with misfolded proteins is Alzheimer's disease (AD). *Post mortem* analysis of brains of patients with AD revealed plaques of aggregated fibrils, which are believed to arise from disbalance of synthesis and degradation of amyloid β (Aβ) peptide, leading to excess Aβ in neurons. The Aβ peptide self-assembles into fibrils, forming amyloid plaques (Dobson 2004; Selkoe and Hardy 2016). These are insoluble and highly resistant to degradation, consisting of peptides that self-assemble perpendicularly to the fibril axis into highly ordered, dense structures. While this strong tendency to form fibrils is linked to adverse effects when associated with disease, self-assembling and fibril forming peptides also have important physiological functions, for example during the synthesis of melanin (Fowler and Koulov et al. 2006) or in the storage of peptide hormones (Maji et al. 2009). Furthermore, this characteristic can also bear great potential for the development of new biomaterials, since amyloid fibrils provide strength and rigidity, which makes amyloid-derived biomaterials highly resistant to degradation. While biomaterials from self-assembling peptides are formed in nature, e.g. in biofilms of different bacteria, artificial biomaterials from these peptides have been proposed for utilization in cell culture or drug delivery systems (Knowles et al. 2016).

Arising from the residue structures the 20 amino acids have, there are more options to connect two amino acids than the "standard" peptide bond, involving amino acids with additional amino or carboxylic groups in their side chain which can form peptide bonds with these as well. Disulfide bridges are another possibility to connect amino acids. This is the case in insulin, whose two chains are connected via two disulfide bridges. Also, the hydroxy groups of serine or threonine can be connected with the carboxy group with another amino acid by an ester bond. Peptides containing ester bonds are called depsi peptides. In nature, the mostly cyclic depsi peptides were found in plants, marine organisms, bacteria, and fungi, where they exhibit antibiotic, antifungal, anti-inflammatory, or antitumor effects. Clinical studies showed promising results of these depsi peptides in therapeutic use (Kitagaki et al. 2015). A promising candidate for antimicrobial application is the cyclic 11-mer depsi peptide teixobactin, isolated from a bacterial strain, which showed antimicrobial properties even against antibiotic resistant bacteria while having only low toxicity on mammalian cells *in vitro* and *in*

vivo (Parmar et al. 2018). The need for new antibiotic agents is emerging greatly, since increasing and spreading antibiotic resistance poses a major threat to humanity. Teixobactin and chemically synthesized analogues therefore could be used as new antibiotic agents. As well as shown in more detail for depsi peptides, antimicrobial peptides are found in various species of life which bear a great potential since no or only low bacterial resistance was shown, but rapid degradation and clearance after application occurred, limiting bioavailability and efficacy. Synthetic peptides, based on the naturally occurring antimicrobial peptides, and chemical modification enhanced the stability and are currently reviewed in clinical trials (Kumar et al. 2018).

Apart from peptides found in nature, their derivatives as well as artificial peptides play an emerging role in various fields. One example thereof is the application of synthetic or protein-derived peptides in therapy or prevention of human diseases. Research and development of peptide-based therapeutics of various cancers is an emerging and promising field not only for treatment, but also for diagnosis and prognosis. As summarized in Xiao et al. (2015), peptides were administered in three different forms: peptide-alone therapy, peptide-based vaccines, and nanomaterials conjugated with peptides. These forms of therapy were used in anti-cancer treatments, but also to increase the survival of patients suffering from advanced cancers, where they showed higher specificity towards cancer cells and lower toxicity to healthy tissue compared to traditional chemotherapy. Application of such therapy is currently tested in clinical trials (Xiao et al. 2015).

Apart from therapy of human diseases, novel peptides with defined characteristics play an emerging role for the synthesis of biomaterials. This is realised by designing peptides that self-assemble into macromolecular structures, such as peptide nanofibers, nanotubes, or hydrogels, depending on their sequences and the solvent (Koutsopoulos 2016). These biomaterials are then used as artificial extracellular matrices to provide mechanical and structural support to cells in the fields of tissue engineering and regenerative medicine.

The emphasis in the peptide section of this work is the synthesis of depsi peptides and their self-assembly into peptide nanofibers.

Biomaterials

As previously described, biomaterials can be obtained by designing macromolecular structures made from self-assembling peptides. Since they only consist of peptides and solvents and no assembly-initiating agent is required, the yielding biomaterials are easy to obtain, well-defined, and bio-compatible, as shown from experiments in the field of regenerative medicine (Koutsopoulos 2016). In one recent example, coatings of self-assembling peptides were shown to promote neuronal cell

adhesion and outgrowth *in vitro*, as well as *in vivo* via their injection on the lesion site of a damaged nerve (Schilling and Mack et al. 2019), showcasing that biomaterials from self-assembling peptides are a viable tool for regenerative medicine. This is due to the PNFs mimicking the fibrous extracellular matrix (ECM) realised by collagen. However, the ECM also consists of other biomacromolecules, such as proteoglycan, and adhesion proteins which mediate the contact with the cell (Bosman et al. 2003). Therefore, an artificial ECM for tissue engineering or biomaterials used in regenerative medicine solely made from self-assembling peptides would not be sufficient for all potential applications, especially since problems with immunogenicity, stability, and stimuli of self-assembly were reported (Chen et al. 2019). On the other hand, proteinaceous biomaterials rapidly undergo degradation and are not able to provide sufficient mechanical stability to work as scaffold for cell culture (Wu and Ng et al. 2015; Khan et al. 2018) and can trigger immunogenic responses upon biomedical applications (Vandermeulen et al. 2004), although they are naturally occurring in each organism and are highly specific. To overcome the disadvantages of solely proteinaceous biomaterials, hybrid materials consisting of different polymers have been proposed. An extensively studied and applied technique is the covalent attachment of polyethylene glycol (PEG) chains on proteins, for example via reaction of a NHS-ester of PEG with amino groups in the protein (Kodera et al. 1998). Grafting PEG chains onto proteins decreases their immunogenicity while increasing the life time, resistance to degradation and solubility compared to the protein alone (Vandermeulen et al. 2004). However, when decorating proteins with PEG chains, the monodispersity, meaning that they possess the same molecular mass, can be lost. The degree of PEGylation of a protein can vary from batch to batch, making it difficult to exactly reproduce results from experiments with PEGylated proteins. One way to combat this is the synthesis of so-called precision polymers. By choosing a suitable PEGylation protocol, a defined number of PEG chains were shown to be grafted to different proteins. This was shown in Kuan et al. (2013), where serum albumins from human and bovine origin, as well as lysozyme, were repeatedly PEGylated with the same amount of PEG chains. In their protocol, the proteins were denatured in a first step, following PEGylation via the thiol groups of the cysteine residues in the protein backbones. Depending on the structure and the sequence of the denatured protein, all or some of the thiol groups were PEGylated, but the results could be obtained repeatedly. This protocol could principally be applied to modify a plethora of proteins that possess thiol groups (Kuan et al. 2013). The possibility to exactly modify proteins to yield in hybrid biomaterials, which originate from nature but are decorated with synthetic polymers, increases their application range in the biomaterials field. One possible method to further use these hybrid biomaterials is the formation of hydrogels (Wu et al 2014; Gačanin and Kovtun et al. 2017; Gačanin et al. 2019). This will be explained in the next section.

Hydrogels

Per definition, hydrogels are cross-linked, three-dimensional polymeric networks which are capable to adsorb large quantities of water without dissolving in it. The ability to retain water is based on the presence of hydrophilic groups in the polymer (Ahmed 2015). In a swollen hydrogel, the amount of water can be up to thousand times higher than the weight of the unswollen, dry material (Hoffman 2012). The most important features of a hydrogel are the polymers on which they are based, and the nature of the crosslinking of the polymer. Sources for hydrogels can be found in nature, but they can be synthetically made as well. Naturally occurring polymers, such as DNA, RNA, proteins, chitosan, and hyaluronic acid, amongst others, were reported to form hydrogels and are biocompatible and biodegradable by nature. DNA and RNA strands are suitable components for hydrogels due to their sugar-phosphate backbones and the possibility to specifically design them by Watson-Crick base pairing, leading in self-assembling hydrogels. Due to their mesh-like structure, they allow smaller molecules to permeate and, due to their responses to external stimuli as pH and temperature, they are capable to release small molecules on demand, making them suitable candidates for drug delivery. Furthermore, DNA and RNA can be degraded by naturally occurring enzymes, yielding in targeted disintegration of the hydrogel. As promising as this sounds, the potential of DNA and RNA based hydrogels is restricted due to their instability regarding nucleases and high cost of synthesis (Shao et al. 2017; Huang et al. 2017; Zhang et al. 2018). Similarly to DNA and RNA, naturally occurring proteins have a defined structure and function and therefore intrinsic activity. Hydrogels from a variety of proteins have been reported, spanning silk proteins (Kapoor et al. 2016), serum albumins from human (Wu et al. 2014; Gačanin et al. 2019) or bovine origin (Ma et al. 2016), and fibrin (Noori et al. 2017). Furthermore, there is the possibility to form hydrogels from polysaccharides, as for example chitosan (Furuike et al. 2017). Since all the aforementioned hydrogels are derived from naturally occurring polymers, they are tolerated by biological systems, but are prone to degradation, making them lack in long term stability. In contrast to this, hydrogels can also be prepared from synthetic polymers, such as poly(lactic acid) (Basu et al. 2016), poly(ethylene glycol) (Li and Anseth 2009), and poly(acrylic acid) (Ahmed 2015). Using hydrogels from these polymers, problems have to be faced concerning their biocompatibility, biodegradability, and polymerisation conditions which could be problematic in biological systems, while they possess stability in various environments, meaning temperature, pH, and enzymes. To combine the advantages of natural and synthetic hydrogels, hybrids were synthesized, for example in the form of a natural polymer decorated with a synthetic polymer. These hybrids are biocompatible while having enhanced stability (Ullah et al. 2015).

For the formation of a hydrogel, the crosslinking of polymers is key. Crosslinking methods can be divided in two categories: physical crosslinking, which is temporary, and permanent crosslinking via chemical reactions (Ahmed 2015; Akhtar et al. 2015). Examples for physical crosslinking are

interactions of the polymer chains via non-covalent interactions, such as hydrogen bonds, complex formation, or ionic interactions. There is a plethora of chemical crosslinking methods available, spanning polymerization, radiation, and condensation or addition reactions of different reactive groups present in the polymer backbone. In contrast to physically crosslinked hydrogels, crosslinking by chemical reactions yields in hydrogels with enhanced mechanical strength (Akhtar et al. 2015). Since the characteristics of hydrogels are highly dependent on their components, there is a wide range of areas where hydrogels can be applied. They can be found as wound dressings, drug delivery vehicles, antitumor therapy, tissue engineering scaffolds, as well as in everyday products like contact lenses and hygiene products that need to be absorbent (Wei et al. 2014; Caló and Khutoryanskiy 2015; Li et al. 2019). Furthermore, they are applied as biosensors for the detection of a variety of molecules (Jung et al. 2017).

A particularly interesting feature exhibited by some hydrogels is the ability to self-heal after damage, without addition of a healing agent or external stimulation. In physically crosslinked hydrogels, self-healing can be realised by structural re-ordering of the polymer chains due to interactions mentioned above. Via recombination of crosslinking bonds, chemically crosslinked hydrogels can exert self-healing properties. This is not possible for classical covalent bonds, but for dynamic covalent bonds, for example in boronate ester linkages. Hydrogels that are capable of self-healing have a prolonged lifetime compared to hydrogels without this feature. Furthermore, they are able to regain their functionalities after self-healing (Wei et al. 2014; Liu and Hsu 2018). Self-healing of the hydrogels is described as thixotropic behaviour, where the viscosity of the substance is dependent on applied shear forces, meaning the hydrogel is able to perform gel-to-sol transitions. This makes self-healing hydrogels particularly interesting for application via syringes, for example in targeted drug delivery (Zanna and Tomasini 2017).

Experimental Background

Synthesis of Peptides

The formation of a dipeptide (Scheme 1) via mixing two amino acids results in 4 different products, meaning statistically only 25 % of the correct dipeptide can be yielded. This decreases drastically when more amino acids are added. To overcome this problem, protective groups (PG) were developed specifically for N- and C-termini, as well as for the amino acid side chains. Application of these groups inhibit the formation of undesired products and, therefore, strongly increase the yield of the correct product. A cycle of precise cleavage of one protective group and addition of another suitable protected amino acid is applied when synthesizing peptides. Importantly, the different protective groups have to be chosen to work orthogonally, meaning one PG can be cleaved off in specific conditions, while other PGs stay bound to the peptide. Since the carboxy group is not reactive enough to form amide bonds with amino groups by itself, the C-terminus has to be activated prior coupling. This is oftentimes done by formation of active ester derivatives. The first synthetic peptide was glycylglycine (Gly-Gly), made with amino acids in solution. Since then, the field of peptide synthesis emerged greatly (Jaradat, 2017). Major progress was made by Robert Bruce Merrifield, who developed the synthesis of peptides on solid support and was therefore awarded with a Nobel Prize (Merrifield, 1963). The principle of solid phase peptide synthesis (SPPS) is illustrated in Scheme 2.

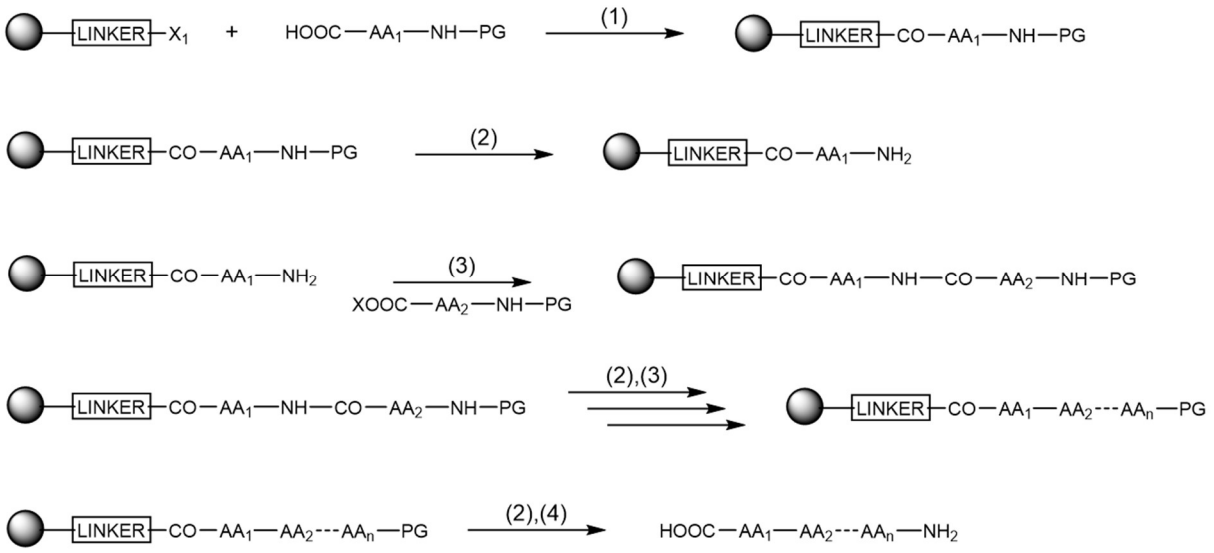

Scheme 2: Principle of the solid phase peptide synthesis after Merrifield (1963). In an initial step, the first amino acid (AA_1) is coupled to the linker on the solid support via cleavage of the functional group X_1 (1). The product of this reaction can be purchased. Binding of the C-terminus to the linker leads to the synthesis from C- to N-terminus. To make the N-terminus of the amino acid accessible, the protective group (PG) has to be cleaved off with suitable reagents (2). Coupling of a next amino acid (AA_2) occurs via its activated C-terminus (COOX), which forms a peptide bond with the unprotected N-terminus (3). The cycle of deprotection (2) and coupling (3) is repeated until the desired amino acid sequence is synthesized. After synthesis, the N-terminus is deprotected (2) and the peptide is cleaved off the solid support (4). Protective groups of amino acid side chains are also cleaved during this step. Washing steps are applied after every step to remove excess reactants and cleaved off molecules.

The basic principle of SPPS is the synthesis of a peptide on an insoluble, solid resin, via the cyclic addition of reagents and subsequent washing (Scheme 2). In a first step, the first, N-terminal protected amino acid is covalently bound to the Wang linker on the resin. After deprotection of the amino group with a suitable reagent (Scheme 3A), the next N-terminally protected amino acid can be attached. Therefore, it is dissolved, C-terminally activated via the formation of an active ester, and introduced to the peptide. The formation of a peptide bond occurs, connecting the two amino acids covalently with formally the substraction of the previously added activator in its hydroxyl form (Scheme 3B). The cycle of N-terminal deprotection and the addition of the next, activated amino acid can then be pursued until the desired peptide is synthesized. After final N-terminal deprotection, the peptide can be cleaved off the resin. With this method, high yields of peptides with specific sequences can be obtained, making it an extremely valuable method for peptide synthesis (Jaradat, 2017).

As promising and simple as this sounds, some problems in SPPS had to be faced. During the synthesis and purification of peptides rich in alanine, valine, isoleucine, asparagine, and glutamine (so called difficult peptides), aggregation occurred. This issue was first addressed using building blocks, but a much more elegant solution has been found, where no additional group has to be added. Sohma et al (2004) developed a method to synthesize O-acyl isopeptides, or depsi peptides, where serine or threonine are introduced to the sequence and the next amino acid is covalently bound to its hydroxy group, yielding in an ester bond. This led to a kinked peptide backbone, where aggregation was greatly diminished when held at acidic pH levels. Introduction of the kinked peptide to higher pH values led to an intramolecular O,N-acyl shift and subsequently to a linearized peptide (Sohma et al. 2004). A similar approach was made using the thiol group of cysteine. In a first step, the kinked S-acyl isopeptide was synthesized, followed by a S,N-acyl migration to the linear form (Yoshiya et al. 2008). Using these techniques, yields of difficult sequence containing peptides were increased via suppression of aggregation. Furthermore, the aggregation of peptides was made controllable by pH alteration.

As well as in nature, synthetic peptides can be modified after synthesis to make them accessible to further reactions. An example thereof is the introduction of an azide functional group, which can then react copper catalysed with an alkyne (Click chemistry) or with a triarylphosphine (Staudinger ligation). Another possibility is the reaction with a maleimide-N-hydroxysuccinimide ester (NHS-ester). The NHS-ester can be attached via an amide bond to the N-terminus of the peptide (Scheme 3C), or it can add to a cysteine residue via reaction of the thiol group with the free electron pair (thiol-ene reaction). These modifications, amongst others, expand the reactivity of peptides and play therefore a major role in research and development.

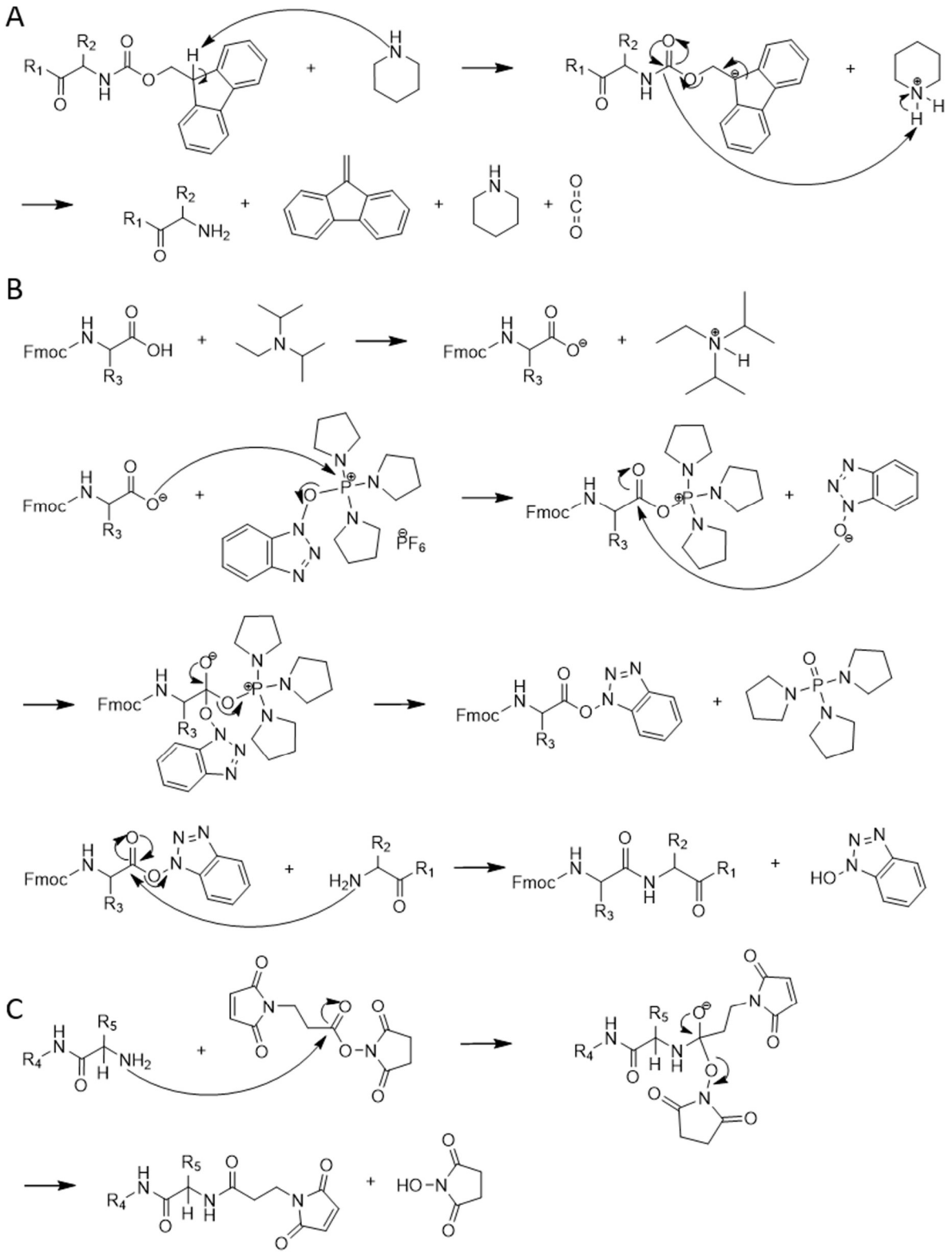

Scheme 3: Reaction mechanisms in peptide synthesis and modification used in this thesis. A) Deprotection of an N-terminally Fmoc-protected amino acid on a residue (R_1) using piperidine following an $E1_{CB}$ mechanism. B) C-terminal activation and coupling of an N-terminally Fmoc-protected amino acid. In a first step, the base DIPEA is used to activate the C-terminus. Via reaction with PyBOP, an active ester forms which is able to react with the N-terminus of the next amino acid, yielding in a dipeptide on the resin. After cycles of deprotection (A) and activation and coupling (B), the N-terminus was modified using an NHS-ester (C).

In this work, different depsi peptides were synthesized following the protocol from Gačanin et al. (2019) with a following maleimide-modification of one of the depsi peptides.

Purification and Identification Methods

Liquid Chromatography

The principle of liquid chromatography is the separation of a sample in a liquid mobile phase. The mobile phase, together with the sample, is pumped through a solid phase, with which the molecules in the sample interact due to van-der-Waals, hydrophilic/hydrophobic or ionic interactions. Depending on the constitution of the sample, its components are retained on the solid phase for a certain amount of time before their elution and detection. The retention time is characteristic for a specific component. In RP-HPLC, the stationary phase consists of a non-polar material, and a mobile phase of polar solvent. By forming a gradient using a polar hydrophilic (e.g. H_2O) and a polar organic (e.g. acetonitrile) solvent, the components of the sample can be eluted from the column depending on their hydrophobicity by interacting with the column material and the changing mobile phase. The components are then detected using absorption measurements and collected into fractions.

Matrix-assisted Laser Desorption/Ionisation (MALDI)

MALDI is a versatile tool to ionize a sample prior determination of the molecular mass of a compound, which can be applied in various fields of chemistry. Preparation of the sample consist of its cocrystallization with matrix molecules on a target plate. Using a laser, whose energy is absorbed by the matrix, parts of sample and matrix are ablated from the plate and ionized. Finally, the ions are accelerated and analyzed by a mass spectrometer. In a time-of-flight (ToF) mass spectrometer, the time of flight is measured, which correlated to the molecules mass-to-charge ratio. In a Fourier-transform ion cyclotron resonance (FT-ICR) mass spectrometer, the mass-to-charge ratio is determined by accelerating the ions in a circular orbit which separates the molecules depending on their mass and detecting, correlating again to the mass-to-charge ratio. Using MALDI and one of the mass spectrometers, the molecular masses of peptides and proteins can exactly be determined.

Characterization Methods

Transmission Electron Microscopy (TEM)

With transmission electron microscopy, higher resolution compared to light microscopy is obtained, making it a suitable method to gain insight small aggregates. In TEM imaging, an electron beam is interacting with the sample and the interaction of sample and electrons leads to acquisition of an image. Sample preparation is performed on a copper grid, where the peptides adsorb to, and counterstaining with uranyl acetate, which intercalates into fibrillary structures. Using this technique,

fibrils are characterized regarding their morphology, for example their length or interaction with other fibrils.

Conversion Assay

The conversion assay is based on the reaction of primary amines with fluorescamine, yielding in a fluorescent product while fluorescamine itself does not fluoresce (Scheme 4). Since the primary amino groups of peptides associated into fibrils cannot react with fluorescamine is reduced compared to the free depsi peptide, comparison of the fluorescence intensity of free depsi peptide and aggregated peptides can be used to determine a percentage of depsi peptide that linearized, yielding in the conversion rate.

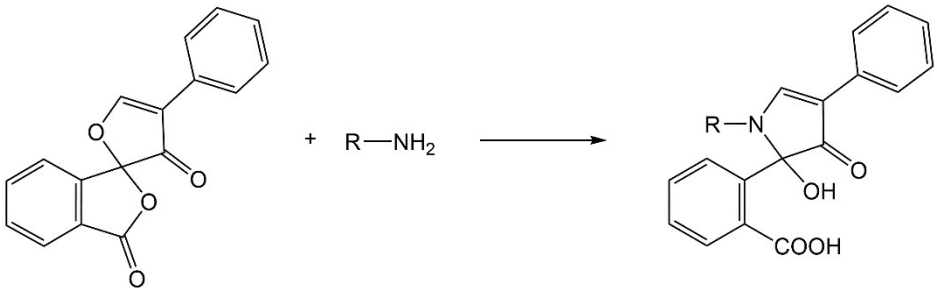

Scheme 4: Reaction of fluorescamine with a primary amine. While free fluorescamine does not show fluorescence, the product is excited at 365 nm and emits at 470 nm.

Thioflavin T Assay

Thioflavin T (ThT) is one of the most widely used fluorescent dyes for the detection of fibrils. It consists of two ring moieties which are interconnected via a C-C bond. Upon binding of ThT to fibrils in parallel fashion, the rotation of the C-C bond is limited, leading to redshifts in the excitation and emission spectra which can be related to an internal control. An increase in redshifted ThT emission therefore reports the presence of β-sheets (Biancalana et al 2010). Since only the presence or absence of β-sheets can be detected, an additional method to determine secondary structures has to be applied.

Infrared Spectroscopy

Infrared Spectroscopy is a widely used tool to determine the structure of a plethora of molecules, based on their absorption upon irradiation with light of the infrared range. Structural elucidation of proteins and peptides is performed using Fourier-transform infrared spectroscopy, where nine absorption bands are characteristic for polypeptides. From these, the amide I band (1700-1600 cm^{-1})

is the most expressive when characterizing secondary structures, since absorption in this range is correlated to C=O stretch vibrations of the amide bonds (Kong and Yu 2007).

Zeta Potential

When a charged particle is placed in a solution containing positively and negatively charged ions, counter ions form a layer around the particle (Stern layer). Around the Stern layer, a diffuse layer of ions of both charges forms, yielding in an uncharged particle. To determine the zeta potential, an electric field is applied in which ions of the diffuse layer are sheared off at the slipping plane, separating mobile and stationary ions. Thereby, the zeta potential is defined as the potential at the slipping plane, which can be determined from the electrophoretic mobility of the particle in the suspension. Although the surface charge of the particle and the zeta potential are not equal, they correlate (Bhattacharjee 2016).

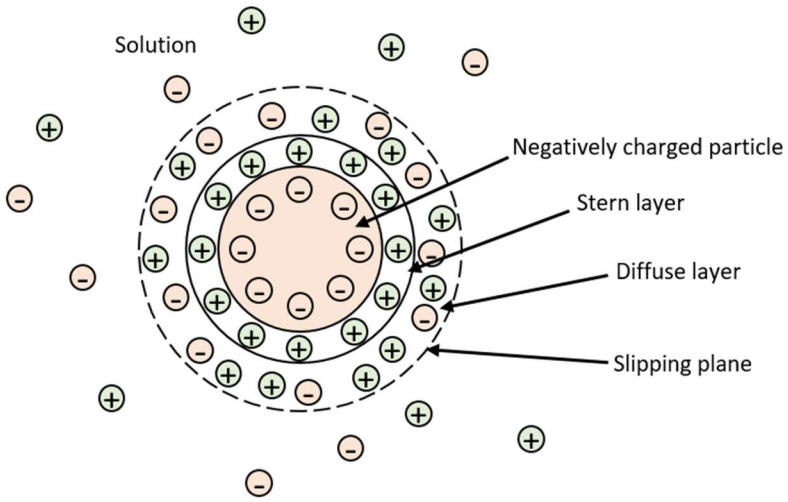

Figure 1: Schematic illustration of a negatively charged particle in a solution containing positively and negatively charged ions. Positive counter ions form the Stern layer around the particle, around which a diffuse layer containing both sorts of ions forms. The slipping plane is the border between stationary and mobile ions that can be sheared off upon application of an electric field. The zeta potential is the potential at the slipping plane. Own representation based on Bhattacharjee 2016.

Motivation

In literature, the synthesis and characterization of a peptide-protein hybrid hydrogel with highly interesting features was described (Gačanin et al. 2019). The hydrogel consisted of a polypeptide backbone, derived from the naturally occurring protein HSA, with grafted depsi peptides. The depsi peptides in their kinked form were soluble at acidic pH, while upon change to neutral pH, the peptide linearized and formation of fibrils was detected. This characteristic of the peptide was utilized to gel the hybrid material, yielding in a hydrogel that was rheologically characterized and later used in cell-based experiments. Upon instantaneous gelation, the hydrogel showed a constant mechanical strength, which was found to be independent of frequency. The hydrogel was able to compensate small strains, potentially through conformational changes of the polypeptide backbone. Upon application of higher strains, fissures in the hydrogel were described, until gel-to-sol transition occurred, whereafter the hydrogel behaved like a viscous fluid. After removal of the strain, the gel was able to immediately (< 20 sec) recover, showing superior thixotropic behavior, which could be maintained after multiple ruptures via strain. Self-healing was also shown to work on a macroscopic scale after physically cutting and rejoining pieces of the hydrogel, without the need of an external additive as stimulant. Furthermore, the herein described hydrogel was used as matrix for endothelial cells, which were able to migrate into the gel using its peptide-protein structure, yielding in a 3D cell culture. Also, the viability of neuronal cells on this hydrogel was comparable to the gold standard Matrigel. Summarized, the biomaterial-based hydrogel bears great potential as matrix in biomedical applications (Gačanin et al. 2019).

In the paper itself, the possibility of mixing free depsi peptide to the backbone during gelation is described, giving the possibility to introduce other functionalities by copolymerization. Therefore, the goal of this thesis is the alteration of the mechanical characteristics of the outstanding depsi hydrogel synthesized and analyzed by Gačanin et al. (2019) by addition of free depsi peptides. To introduce new functionalities, free depsi peptides of different characteristics were synthesized, analyzed, and, if the characteristics seemed fitting, copolymerized with the backbone. For successful copolymerization, the inducibility of fibrillation via pH increase, the fibril morphology, and a secondary structure exhibited as β-sheet were considered as crucial, since these were the characteristics of the depsi peptide used as gelator in Gačanin et al. (2019). Additionally, the zeta potential of the resulting fibrils was assessed. With these methods, suitable depsi peptide candidates were found for later application in hydrogel synthesis. Three different types of depsi peptides were quested: one with the same characteristics as the gelator to study the effect of different concentrations of the free depsi peptide on the hydrogel; one negatively charged, structurally derived from the first to evaluate the impact of a negative charge

on the hydrogel; and one showing a different fibril morphology to the first to determine the impact of the morphology on the hydrogel.

The first step consisted in provisioning the depsi peptides. Therefore, the depsi peptide that is used in its maleimide modified form as gelator of the hydrogel in Gačanin et al. (2019) is synthesized (D1, KIKI*SQINM), partly modified using maleimide (D1-Mal, Mal-KIKI*SQINM), and characterized. Next, a negatively charged equivalent of D1 is synthesized, exchanging lysine for glutamic acid, and analyzed (D4, EIEI*SQINM). Finally, depsi peptides exhibiting different fibril morphologies arising from various amino acid sequences were assessed. Possible peptides for this approach were chosen from a database of non-depsi peptides which were characterized regarding their fibril morphology and synthesized as depsi peptides via the insertion of serine and formation of an ester bond with the next amino acid. Pursuing this, three depsi peptides (D5, CKIK*SQII; D6, KIKQ*SIINMWQ; D7, KIKQI*SINMWQ) were synthesized and analyzed, and suitable candidates were chosen for copolymerization into the hydrogel.

Secondly, the peptide-protein polymer, which is the backbone of the hydrogel, is synthesized and characterized according to literature (Gačanin et al. 2019). Therefore, HSA had to be modified using cationization for additional primary amino groups, PEGylation for enhanced water retention and stability, and denaturation for accessible sulfhydryl groups. These were then used for the addition of maleimide-modified D1 peptide, which was grafted onto the backbone, yielding in a peptide-protein hybrid material as shown in Gačanin et al. (2019).

After the two components of the hydrogels were synthesized, formation of hydrogels could be started. Upon verifying the data published by Gačanin et al. (2019), copolymerisation of different equivalents of free depsi peptides was performed. Rheological characterization of the resulting hydrogels consisted of the determination of their mechanical strengths via the measurement of storage and loss moduli, as well as the examination of the frequency-dependence of these moduli. Furthermore, the mechanical strengths were measured upon application of oscillatory strain. During these measurements, the point where gel-to-sol transition occurred is assessed, revealing the maximum tolerated strain of the gels. In a final experiment, the capability to self-heal is tested via alternation of rupture of the hydrogels through application of high strains, followed by a resting period with low strain. This experiment is of particular interest, since the original published hydrogel showed superior self-healing compared to literature (Gačanin et al. 2019).

Following this outline, the aims of this thesis can be summarized as following:

1) Synthesis and characterization of new depsi peptides alongside a previously characterized one and finding suitable candidates for application in hydrogels

2) Synthesis of the peptide-protein backbone as described in literature
3) Formation and rheological characterization of the original hydrogel, as well as hydrogels copolymerized with different free depsi peptides, yielding in hydrogels with altered attributes

Potential further usage of copolymer hydrogels was not assessed during this thesis, but could be pursued in cell-based experiments. Since the original hydrogel was used as cell matrix, the herein synthesized and characterized gels could also be used in cell culture, and potentially also in biomedical applications and tissue engineering.

Results and Discussion

Synthesis and Purification of Depsi Peptides

Since the characteristics of peptides differ depending on the sequence, five depsi peptides of different sequences were synthesized and characterized for this thesis (Table 1).

The self-assembling and nanofiber-forming peptide D1 had been characterized previously and its maleimide-modified derivative (D1-Mal) had been grafted in the function as a gelator to a polypeptide backbone form a hydrogel (Gačanin et al. 2019). To make the results from this thesis comparable to literature, the hybrid peptide-protein backbone is herein also prepared with grafted D1 peptide applying maleimide chemistry. To test the impact of different concentrations of free peptide on the hydrogel properties D1 peptide was employed. However, further depsi peptides, D4, D5, D6, and D7, were synthesized to test the impact of free peptides with different charge as well as different fibril morphologies on hydrogels. On the one hand, D4 differs from D1 in an exchange of two lysine residues to glutamic acid, making D4 the negatively charged equivalent to D1 and was used to investigate the effect of negative charge on the properties of the hydrogel. On the other hand, the non-depsi serine lacking analogues of D5, D6 and D7 showed interesting fibrillary structures in TEM, spanning from short, rounded fibrils to long, heavily interconnected fibrils (Supplementary Data, Figure 14; Schilling, Mack et al. 2019) and were used to test the impact of the different fibril morphologies on the properties of the hydrogel. Therefore, the respective peptides were established as depsi peptides, synthesized and characterized. The peptide amino acid sequences and the model fibril morphologies of the serine-lacking peptide derivatives are summarized in Table 1.

Table 1: List of depsi peptides synthesized for this thesis. D1-Mal was grafted to polypeptide to afford the hybrid hydrogel backbone capable of gelation at physiological conditions. Free, non-grafted depsi peptides were additionally employed as gelators. D1 was used to test the effect on different concentrations of free peptide on the hydrogel. D4 is the negatively charged equivalent of D1 and used to study the effect of negative charge on the hydrogel. D5, D6, and D7 were chosen due to the different fibril morphologies. Asterisk indicates the location of the ester bond in the peptide main chain.

Depsi peptide	**Amino Acid Sequence**	**Characteristics**
D1	KIKI*SQINM	Literature-known gelator, used for investigation of different concentrations of free peptide (Gačanin et al. 2019)
D4	EIEI*SQINM	Negatively charged D1 derivative, lysine is exchanged for glutamic acid
D5	CKIK*SQII	Depsi derivative of CKIKQII which forms short, rounded fibrils (Supplementary Data, Figure 22; Schilling and Mack et al. 2019)
D6	KIKQ*SIINMWQ	Depsi derivative of KIKQIINMWQ which forms long, heavily crosslinked fibrils (Supplementary Data, Figure 22, unpublished data by T. Mack)
D7	KIKQI*SINMWQ	

The listed peptides were synthesized via solid phase strategy (Merrifield, 1963), either manually or in a microwave-assisted peptide synthesizer. The synthesis of D1 is shown exemplarily in Scheme 5. The other listed depsi peptides (Table 1) were afforded using the same strategy.

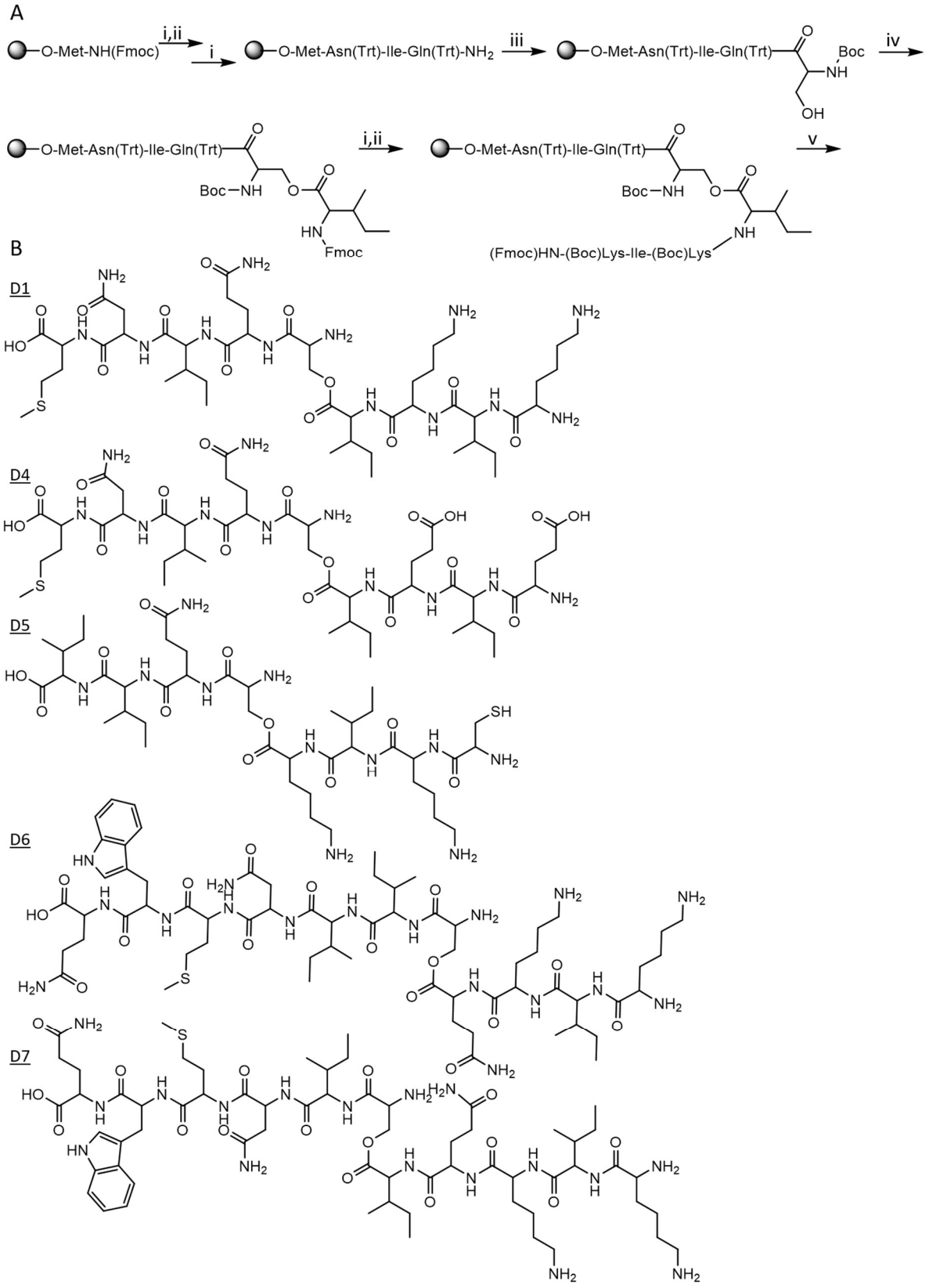

Scheme 5: Solid phase synthesis of the depsi peptide used in this thesis. A) To afford the D1 depsi peptide, following steps were performed: i) deprotection of the N-terminus using 25 vol.-% piperidine in DMF, 6 mL, 70 °C, 10 min (x2). ii) coupling of the next amino acid using Fmoc-AA-OH (5 eq.), DIPEA (11.5 eq.), PyBOP (5 eq.) in DMF, 70 °C, 60 min. iii) coupling of serine to form the ester bond using Boc-Ser-OH (5 eq.), DIPEA (11.5 eq.), PyBOP (5 eq.) in DMF, 70 °C, 60 min. iv) coupling onto the hydroxyl group of serine using Fmoc-Ile-OH (5 eq.), DIPEA (11.5 eq.), PyBOP (5 eq.) in DMF, 70 °C, 2 h (x2). v) cleavage and deprotection of the side chains using TFA (95 vol.-%), Milli-Q-H_2O (2.5 vol.-%), TIPS (2.5 vol.-%), 10 mL, RT, 2 h, 250 RPM. D4, D5, D6, and

*D7 were synthesized using the same strategy. B) Structural formulas of depsi peptides D1 (KIKI*SQINM), D4 (EIEI*SQINM), D5 (CKIK*SQII), D6 (KIKQ*SIINMWQ), and D7 (KIKQI*SINMWQ).*

After all depsi peptides were afforded as solid compounds, they were purified via HPLC and the molecular masses were verified via MALDI-FT-ICR-MS. Initially the theoretical yield was calculated using the total amount of resin, their degrees of substitution (Table 6) and the molecular mass of each peptide. This was related to the mass of crude peptide after synthesis. Yield after HPLC was calculated as ratio of input to outcome of peptide. This value, multiplied with the percentual yield of the crude peptide before HPLC, gave the total yield of each peptide. The yields differed greatly amongst the depsi peptides, depending on the amino acid sequence and spanning from 38.3 % for D5, to 4.5 % for D4.

Table 2: *Calculation of total yield per peptide. D1, D1-Mal, D4, D5, D6, and D7 were synthesized, cleaved off and purified. Total amount of resin is calculated from all batches used for the peptides, respectively. Using the total amount of resin, the substitution of the resin (Table 6) and the molecular mass of the peptide, the theoretical yield was calculated. Yields of peptides were weighed after lyophilizsation and the percentage was calculated as ratio of theoretical yield to yield before HPLC, which was calculated as ratio of input to outcome after HPLC. Total yield of peptide is the product of total yield before and after HPLC.*

	Total amount of resin	**Molecular mass of peptide**	**Theoretical yield**	**Crude peptide**	**Yield after HPLC**	**Total yield of peptide**
D1	2.6646 g	1073.63 Da	1.945 g	0.8210 g (42.2 %)	18.5 %	**7.8 %**
D1-Mal	1.3323 g	1224.65 Da	1.109 g	0.4064 g (36.6 %)	16.2 %	**5.9 %**
D4	1.7705 g	1075.52 Da	1.295 g	0.3910 g (30.2 %)	14.9 %	**4.5 %**
D5	0.1459 g	931.55 Da	0.079 g	0.0685 g (86.9 %)	44.0 %	**38.2 %**
D6	0.1739 g	1387.75 Da	0.167 g	0.0739 g (44.4 %)	34.8 %	**15.4 %**
D7	0.1749 g	1387.75 Da	0.167 g	0.0779 g (46.5 %)	11.6 %	**5.4 %**

The variation in yields of the other peptides could be lead back to the sequences. When synthesizing D4, immediate cleavage from resin after coupling and deprotecting the last glutamic acid had to be performed in order to yield correct product. MALDI-FT-ICR-MS spectra of stored D4 after purification showed a variety of masses which did not correspond to the desired EIEI*SQINM sequence, but rather IEI*SQINM (practical course, unpublished data). This led to the conclusion that the EIEI sequence is difficult to synthesize, probably due to glutamic acid. A decrease in yield compared to the positively charged D1 is therefore expected and was found to be true (7.8 % for D1 vs. 4.5 % for D4). D5 had the highest yield of all peptides (38.2 %). The CKIK*SQII sequence is the shortest and has only three hydrophilic residues, which makes it highly soluble in hydrophilic solvents, where the peptides are dissolved in prior purification. This could explain the high overall yield for D5. D6 and D7 have the same

sequence, but serine and therefore the ester bond is located on different positions. Although the yield of crude products after synthesis is similar (44.4 % for D6 vs. 46.5% for D7), yield after purification differs greatly. This may arise from the different orientation of the side chains due to the location of the ester bond and the therefore different solubilities of the two peptides.

For peptide D1, similar values were reported in literature, where the peptide was synthesized in 0.1 mmol batches via microwave-assisted SPPS. Before purification using HPLC, the yield was 34.9 %. Comparing input to outcome of HPLC, 22 % of correct product were obtained. Taken together, a total yield of 7.7 % were achieved from synthesis to purified D1 (Gačanin et al. 2019). Using manual synthesis and purification, the total yield for D1 was 7.8 % (Table 2), a slightly higher value than previously reported. This indicates that manual synthesis of depsi peptides works as well as using the established microwave-assisted protocol. Thereby, an advantage of manual synthesis is the possibility to upscale the batch sizes, as well as the synthesis of multiple batches in parallel fashion. Due to the prolonged reaction times in manual synthesis, completion of one peptide took three days, while in microwave-assisted SPPS, one peptide can be synthesized in one or two days. This disadvantage can be circumvented when synthesizing multiple batches simultaneously.

After purification via RP-HPLC, the purity of the obtained peptide was controlled via LC-MS. The LC-MS spectrum of purified D1 is shown in Figure 2.

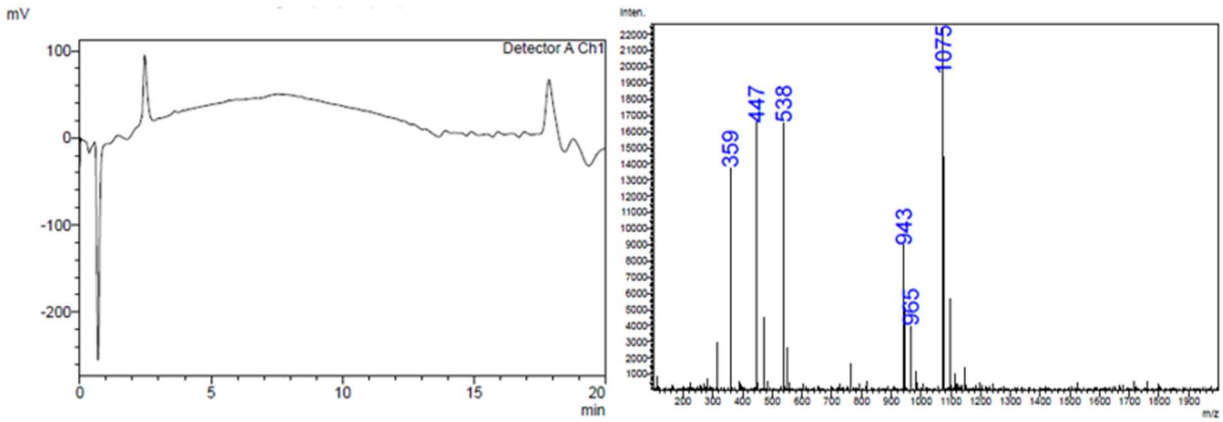

*Figure 2: LC-MS spectrum of D1 (KIKI*SQINM). The main peak at t = 2.5 min (left panel) was analyzed for its contained masses. The mass for D1 was calculated as 1073.6 Da. Products found (right panel) were m/z = 1075 $[M+H]^+$, 965 $[943+Na]^+$, 943 [unknown], 538 $[M+2H]^+$, 447 [unknown], and 359 $[M+3H]^+$. The peak at 0.8 min arose from injection of the sample.*

In the LC spectrum of D1 (Figure 2, left panel), multiple peaks were detected, the first of which at 0.8 min arose from injection of the sample into the column. The components in the main peak at 2.5 min were analyzed via MS (Figure 2, right panel). A plethora of masses were found in this peak, where some of them corresponded to the desired peptide (m/z = 1075, 538, 395). For some of the found products, no adequate molecular constitution could be found to explain the molecular mass (m/z = 965, 943,

447). In the initial purification of D1 via RP-HPLC (Supplementary Data, Figure 23), the product peak slightly overlapped with other peaks, containing unwanted by-products, which could lead to some unwanted by-products in the collected fraction. The peak at 1.6 min, as well as the peaks from 13.5 min on, were not analyzed. The first could potentially arise from the injection as well, while the final peaks could result from the gradient returning to the initial conditions.

The same analysis was performed for the maleimide-modified D1-Mal. The LC-MS spectrum of purified D1-Mal is shown in Figure 3.

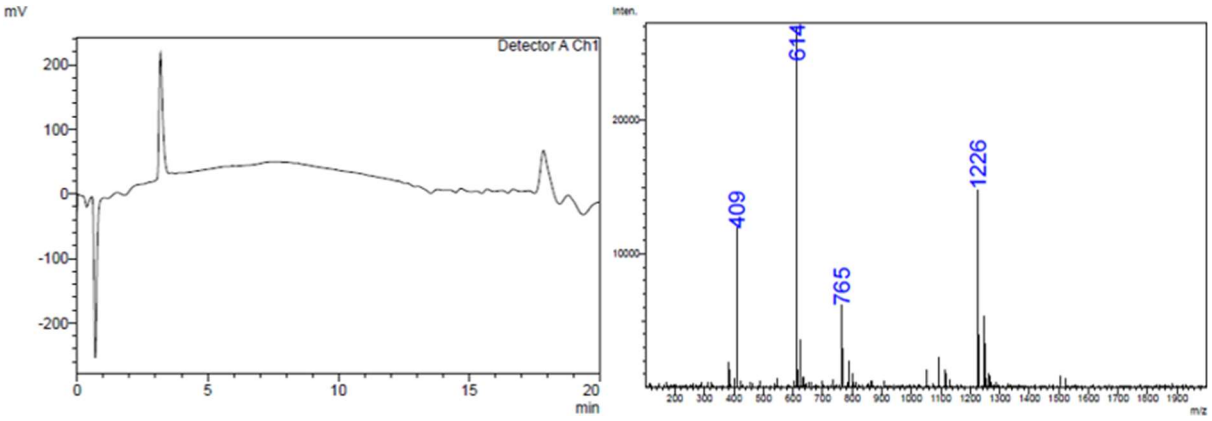

*Figure 3: LC-MS spectrum of D1-Mal (Mal-KIKI*SQINM). The main peak at t = 3.5 min (left panel) was analyzed for its contained masses. The mass for D1-Mal was calculated as 1224.6 Da. Products found (right panel) were m/z = 1226 $[M+H]^+$, 765 [unknown], 538 $[M+2H]^+$, and 409 $[M+3H]^+$. The peak at 0.8 min arose from injection of the sample.*

As well as detected for D1 previously, multiple peaks in the LC spectrum of D1-Mal (Figure 3, left panel) were found, the first one at 0.8 min emerging from injection of the sample into the column. Analysis of the components of the main peak at 3.5 min via MS (Figure 3, right panel) revealed products with masses corresponding to the desired D1-Mal depsi peptide (m/z = 1226, 538, 409). One mass could not be aligned to an adequate peptide structure (m/z = 765). Purification of the crude product occurred via RP-HPLC (Supplementary Data, Figure 24), where the product peak slightly overlapped with other peaks, potentially yielding in impurities which were detected via LC-MS. Further peaks, for example at 1.6 min and from 13.5 min on, were not analyzed. The latter could arise from the change of gradient to the initial conditions, the first could emerge from injection, as previously seen in D1 LC spectrum.

Next, the purified depsi peptide D4 was analyzed via LC-MS. The spectrum of this experiment is shown in Figure 4.

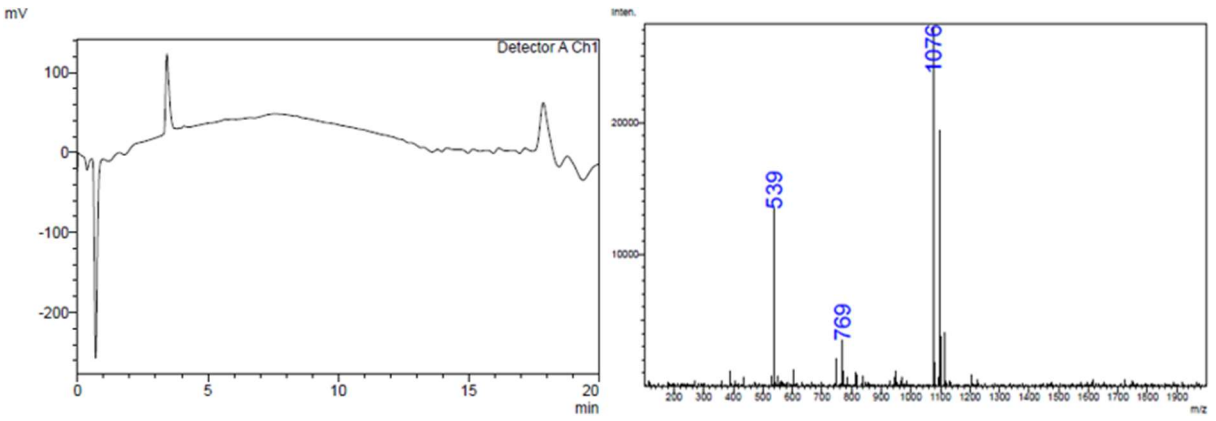

*Figure 4: LC-MS spectrum of D4 (EIEI*SQINM). The main peak at t = 3.4 min (left panel) was analyzed for its contained masses. The mass for D4 was calculated as 1075.5 Da. Products found (right panel) were m/z = 1076 $[M+H]^+$, 765 [unknown], and 539 $[M+2H]^+$. The peak at 0.8 min arose from injection of the sample.*

In the LC analysis of D4, multiple peaks were found (Figure 4, left panel). The first peak, at 0.8 min, likely emerged from injection, as well as the peak at 1.6 min, which was also found in the LC spectra of D1 (Figure 2) and D1-Mal Figure 3). The main peak at 3.4 min was analyzed and masses corresponding to D4 were found (m/z = 1076, 539), but also one mass could not be aligned with D4 (m/z = 765) (Figure 4, right panel). As previously described, the product peak during the initial purification of D4 (Supplementary Data, Figure 25) overlapped with other peaks, which could be a potential source for masses in the MS chromatogram. After 13.5 min, further peaks emerged in the LC spectrum. These were not analyzed, since they potentially arise from the change in gradient, also seen in the previous analyses.

The LC-MS analysis of previously purified D5 is shown Figure 5.

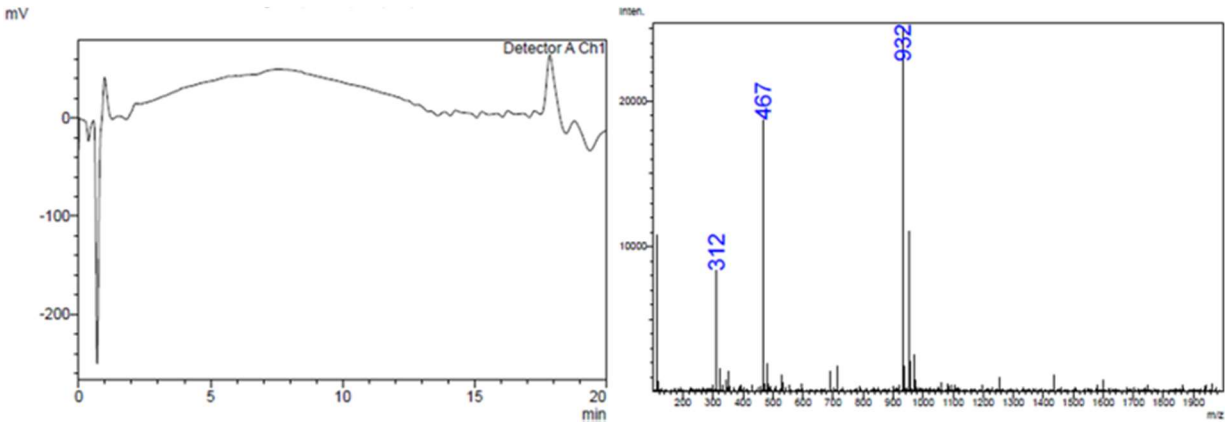

*Figure 5: LC-MS spectrum of D5 (CKIK*SQII). The main peak at t = 1.2 min (left panel) was analyzed for its contained masses. The mass for D5 was calculated as 931.5 Da. Products found (right panel) were m/z = 932 $[M+H]^+$, 467 $[M+2H]^+$, and 312 $[M+3H]^+$. The peak at 0.8 min arose from injection of the sample.*

In the LC spectrum of D5 (Figure 5, left panel) showed one injection peak at 0.8 min, followed by the product peak at 1.2 min that was subsequently analyzed regarding the contained masses (Figure 5, right panel). All found masses could be aligned with D5 depsi peptide (m/z = 932, 467, 312). In the initial purification of crude D5 via RP-HPLC (Supplementary Data, Figure 26), the product peak was clearly separated from other occurring peaks, containing by-products of synthesis. Therefore, manual collection of the product fraction was readily feasible and yielded in a high percentage of purified D5 (Table 2). As well as in the other LC spectra, a peak at 1.6 min occurred, potentially arising from injection. Since D5 is the shortest of all peptides, its retention time is shorter than these of the other depsi peptides previously analyzed via LC-MS. Besides, the peaks after 13.5 min were not analyzed for the same reasons described previously.

The next depsi peptide to analyze was D6. In Figure 6, the LC-MS spectrum of purified D6 is shown.

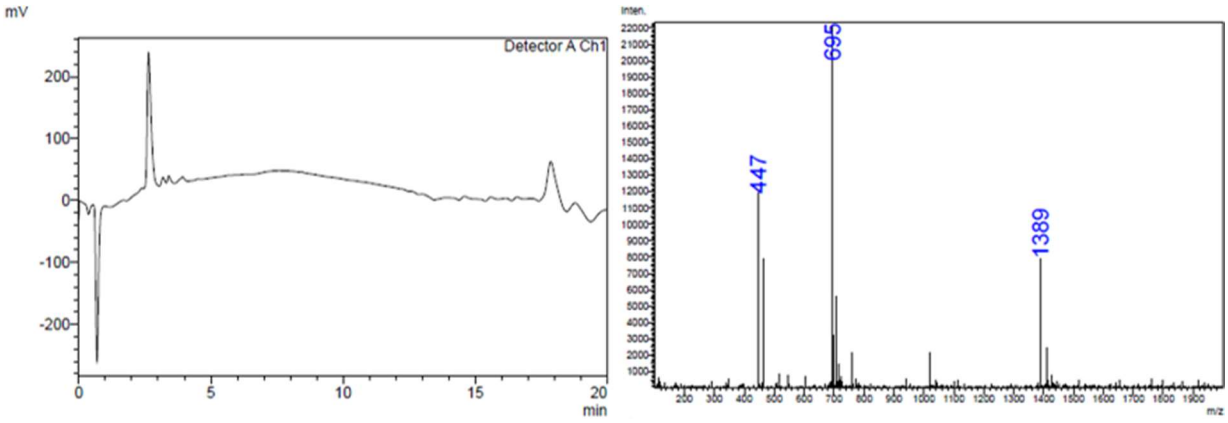

*Figure 6: LC-MS spectrum of D6 (KIKQ*SIINMWQ). The main peak at t = 2.9 min (left panel) was analyzed for its contained masses. The mass for D6 was calculated as 1387.7 Da. Products found (right panel) were m/z = 1389 $[M+H]^+$, 695 $[M+2H]^+$, and 447 [unknown]. The peak at 0.8 min arose from injection of the sample.*

As previously discussed, the peak at 0.8 min in the LC spectrum of D6 (Figure 6, left panel) arose from injection of the probe into the column. The main peak, at 2.9 min, was further analyzed regarding the masses it contained (Figure 6, right panel). Two of the main masses found could be aligned to D6 (m/z = 1389, 695), for the other peak, no adequate molecular structure could be found (m/z = 447). After the main peak in LC, three smaller peaks were detected whose products were not analyzed. In the chromatogram of purification of crude D6 via RP-HPLC (Supplementary Data, Figure 27), the product peak overlapped with other peaks, containing by-products of the synthesis, making the manual collection of the purified product more challenging. This could explain the unallocated mass in the main peak, as well as the occurrence of the smaller peaks thereafter. Further peaks occurred after 13.5 min of LC, which are likely due to the gradient change to its initial conditions.

Finally, the purity of the last depsi peptide was analyzed. The LC-MS spectrum of D7 is displayed in Figure 7.

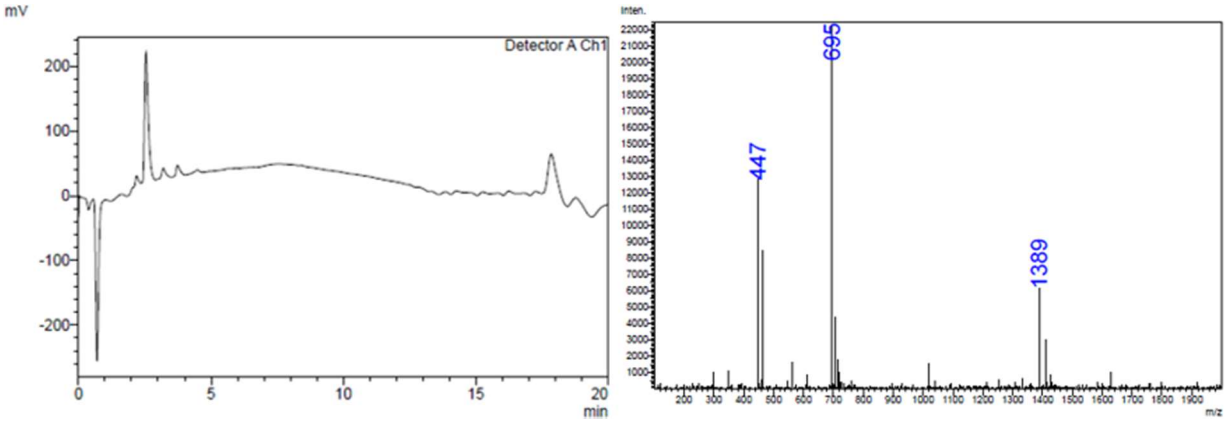

*Figure 7: LC-MS spectrum of D7 (KIKQI*SINMWQ). The main peak at t = 2.7 min (left panel) was analyzed for its contained masses. The mass for D7 was calculated as 1387.7 Da. Products found (right panel) were m/z = 1389 $[M+H]^+$, 695 [M+2H], and 447 [unknown]. The peak at 0.8 min arose from injection of the sample.*

In the LC spectrum of D7, the injection peak at 0.8 min is seen (Figure 7, left panel), as previously described. The main peak, at 2.7 min, was further analyzed and the contained masses were allocated to possible products (Figure 7, right panel). Two of the masses, the same as seen in the MS spectrum of D6 (Figure 6, right panel) could be aligned to D7 (m/z = 1389, 695), and one mass could not be allocated equally (m/z = 447). Since D6 and D7 only differ in the placement of serine into the original sequence, detection of the same masses seemed adequate, especially since the retention time of the product peaks were not equal. Purification of crude D7 was the most difficult of all peptides, since the product peak of RP-HPLC was very small and greatly merged into peaks containing unwanted by-products of the synthesis (Supplementary Data, Figure 28). This could explain the small peaks in the LC spectrum, before and after the main peak, as well as the unaligned mass found in the MS spectrum. As described before, the peaks after 13.5 min arose from the change in gradient.

For the initial purification of D6 and D7, optimization of the gradient of RP-HPLC could have beneficial effects on purity, as well as on the yield of synthesis. An optimization could be realized through flattening of the gradient at the detected H_2O-ACN-ratio of the two peptides. This theory could not be elaborated further due to the lack of time, but could be kept in mind for following purifications.

After all LC-MS spectra were recorded, a contamination of the acetonitrile reservoir with an unknown substance was reported. This, next to the difficulties during purification of the crude products, could explain the small peaks in the LC spectra and potentially also the unallocated masses in the MS spectra. Since the pollutant is of unknown nature, it could also interact with the purified depsi peptides and yield in the formation of by-products whose masses remained unclear and that were not detectable

during the initial purification. Therefore, the reason for the unaligned masses could not be determined exactly and the contamination with by-products during purification of the crude product could not be excluded completely. The LC-MS spectra of all depsi peptides were assessed once more using fresh acetonitrile, after the samples were stored over the weekend at 4 °C. In these spectra, other peaks and products were found, that could mostly not be allocated to possible molecular structures (data not shown). Thus, storage of dissolved depsi peptide in acidic conditions for prolonged time should be avoided. *De novo* analysis of freshly dissolved depsi peptides via LC-MS could not be pursued due to lack of time and material shortage.

However, for all peptides, the purity was evaluated as adequate and were used in further experiments, where fibrillation upon pH change, secondary structure elements, and zeta potential of the fibrils were assessed. Finally, the depsi peptides could then be used as components in hydrogel synthesis.

Characterization of Peptide Nanofibrils

Inducibility of Fibrillation and Resulting Fibril Morphology

After synthesis and purification, the obtained peptides were tested for their potential use as gelators in hydrogel preparation. Therefore, the pH-inducible nature of the self-assembling peptides resulting from an intramolecular O,N-acyl shift at physiological conditions was elucidated via TEM and quantification of fibrillation via conversion assay at acidic and neutral conditions was conducted as summarized in Figure 8A and B, while a schematic visualization of reaction mechanism of the O,N-acyl shift is shown in panel C.

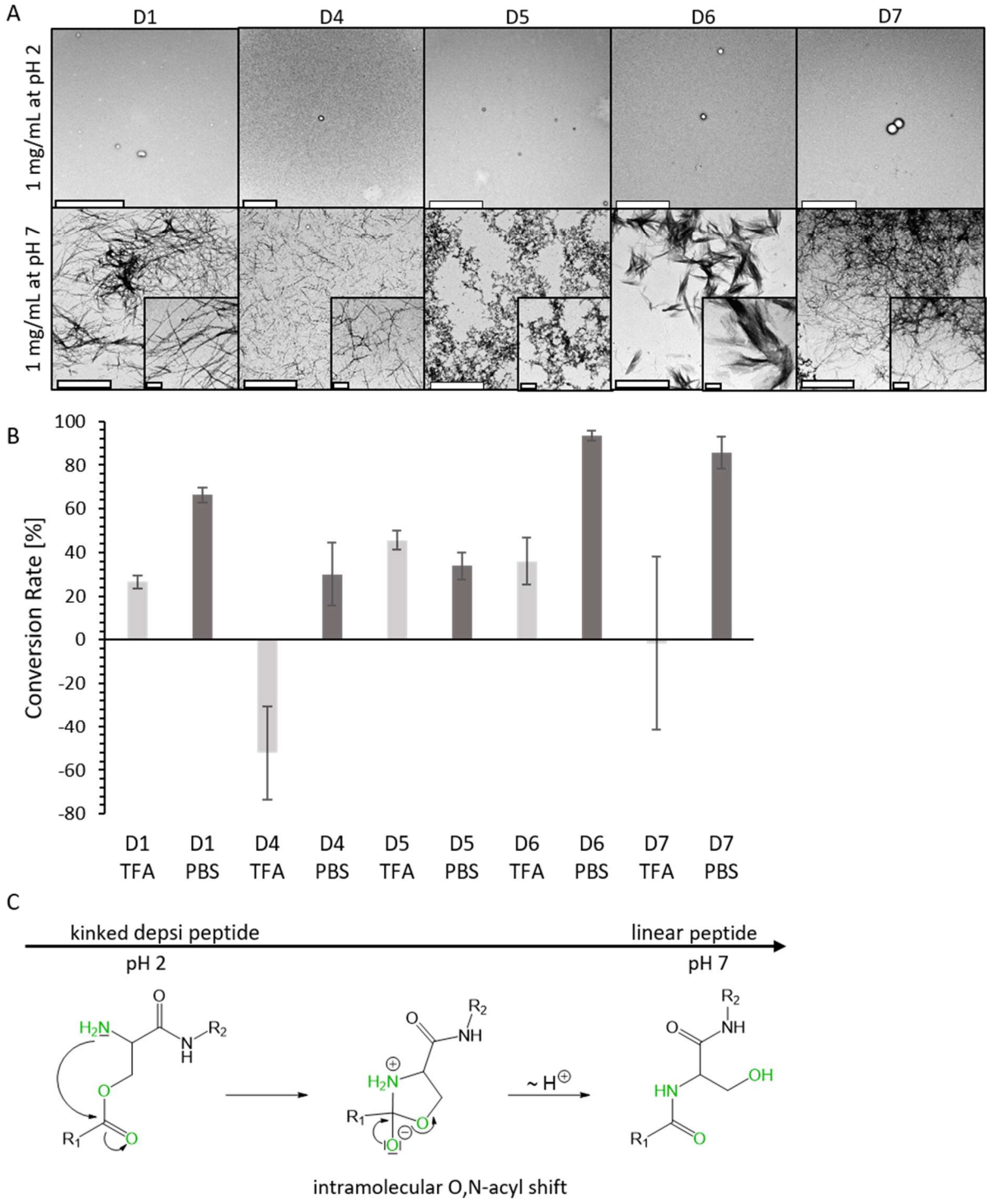

*Figure 8: Evaluation of the pH-induced fibrillation – fibril morphologies and conversion rates. A) Transmission electron microscopy images of 1 mg/mL solutions of D1, D4, D5, D6, and D7. Representative images of samples incubated for 24 h in 0.1 % aqueous TFA (pH 2) are shown in the upper panel. Upon incubation in PBS (pH 7.4) for 24 h, fibrillation occurred, the different fibril morphologies are shown with representative images in the lower panel. Scale bars are 2 µm and 200 nm in the insets. B) Quantification of fibrillation via conversion assay of D1 (KIKI*SQINM), D4 (EIEI*SQINM), D5 (CKIK*SQII), D6 (KIKQ*SIINMWQ), and D7 (KIKQI*SINMWQ). Peptides were incubated in 0.1 % aqueous TFA or PBS (1 mg/mL) overnight, one half was filtered and the fluorescence readout using fluorescamine of the filtered half was compared to the unfiltered. Readout was performed with multiple reads per well. Values are mean ± s.d., n = 2-3. C) Mechanism of the intramolecular O,N-acyl shift, forming a linear peptide from the kinked depsi peptide. Upon increase of pH, the free electron pair of the serine amino group attacks the carbonyl C. Via an intermediate five-membered ring and a proton shift, the ester is cleaved and the amide bond is created, leading to a linear peptide backbone.*

TEM pictures in Figure 8A show the fibrillation of all peptides upon increased pH. However, when incubated for 24 h in 0.1 % aqueous TFA (pH 2), none of the peptides aggregated into fibrillary structures. This indicates that all synthesized depsi peptides exhibit the pH-controlled structure formation upon inducing the intramolecular shift, linearizing the kinked peptide (Figure 8C). Depending on their amino acid sequence, the peptides assembled to different fibril morphologies upon incubation at physiological pH (PBS, pH 7.4). D1 fibrils were several micrometers long, 10.79 ± 1.86 nm thick and formed crosslinked networks. In comparison to literature, which is in good comparison with literature (11.30 ± 1.26 nm, Gačanin et al. 2019). The negatively charged equivalent of D1, D4, also formed fibrils of lengths in the micrometer range but with a lower diameter of 8.80 ± 1.83 nm. In contrast to the interwoven fibril networks formed from D1, D4 rather formed single fibrils. While the non-depsi model peptide was observed to form short rounded fibrils (Supplementary Data, Figure 22), D5 was found to aggregate rather than form defined fibrils. This might be caused by the addition of serine and the following change of orientation of the residues. D6 and D7 are derived from the same model peptide, KIKQIINMWQ, which formed heavily crosslinked fibrils in the nanometer range (Supplementary Data, Figure 22). The first depsi derivative, D6, was discovered to form short stacks of fibrils which were 133.34 ± 44.63 nm in diameter. The length of these stacks was in the micrometer range. In contrast, D7 formed fibrils of 9.35 ± 1.20 nm in diameter, and of micrometers in length, which are strongly interconnected. D7 therefore resembled more the structure of the original peptide.

Further characterization of the pH-inducible O,N-acyl shift and quantification of the subsequent fibril formation was performed via conversion assay (Figure 8B). This assay is based on the measurement of the ratio of soluble depsi peptide to insoluble, aggregated peptide and was performed at both, acidic and neutral pH. D1, the peptide which will be functionalized with a maleimide group and used as gelator in the final hydrogel formation, as well as in its non-modified form to test concentration effects of free D1 on hydrogel properties, showed a low aggregation rate of 26.5 ± 3.0 % (n = 2) at acidic pH which is similar to literature (24.5 ± 4.7 %, n = 3, Gačanin et al. 2019). At neutral pH, where fibril formation was clearly visible via TEM, the conversion rate was 66.4 ± 3.0 % (n = 3), which is a lower rate than described in literature (88.5 ± 2.2 %, n = 3, Gačanin et al. 2019). Importantly, the pH-inducible change in the backbone of D1 could be validated, making its maleimide derivative D1-Mal a suitable gelator for hydrogel formation, and a good candidate to analyze different concentrations of free D1 on the hydrogels. For D4, the negatively charged equivalent of D1, a conversion rate of -52.0 ± 21.3 % at acidic pH, and 29.9 ± 14.5 % at neutral pH (n = 2, respectively) were measured. Upon incubation in 0.1 % aqueous TFA, all measurements of the conversion rate of D4 were negative, which meaned higher fluorescence in the filtrate than in the original untreated solution. This effect could be explained by the presence of a quencher of fluorescence at pH 2. Although the conversion rate at neutral pH was low, fibrils were seen via TEM. The prolongation of incubation time could have beneficial effect on the

formation of PNFs using the D4 sequence, possibly also leading to higher conversion rates. Since an increase in conversion and the formation of fibrils could be detected only upon pH change, D4 seems to be a possible candidate for application in hydrogel formation, but one must keep in mind that its weak conversion at physiological pH might impede stable hydrogel crosslinking. For D5 the conversion rate at acidic pH of 45.5 ± 4.3 (n = 2) was found to be higher than at neutral pH with 33.8 ± 6.0 (n = 3). For this sequence, TEM revealed structures of aggregation rather than fibril formation, and no fibrils were found in acidic conditions. The original peptide, CKIKQII, showed conversion rates of 55 % at neutral pH which is on the lower end of all peptides characterized (Schilling, Mack et al. 2019). This rate could not be reached by D5, probably due to the insertion of a serine for the formation of the depsi peptide. For D6, conversion rates were found to be 36.0 ± 10.7 % (n = 3) at acidic pH, where no fibrillary structures were seen in TEM, and as high as 93.2 ± 2.3 % (n = 3) at neutral pH, where the formation of fibrillary stacks was seen via TEM, confirming the inducibility of fibrillation at increased pH and making D6 a suitable and highly interesting candidate for hydrogel testing, as high conversion rates indicate efficient PNF formation and, thereby, hydrogel crosslinking. Negative values for D7 in acidic pH were found in 2 of 3 measurements, leading to a conversion rate of -1.6 ± 39.7 % (n = 3), whereby the only positive value was as high as 54.1 %. At neutral pH, a conversion rate of 85.6 ± 7.2 % (n = 3) was found, which means an increase upon pH change, also visible in TEM images. Therefore, the pH-inducible O,N-acyl shift could be confirmed for D7, making it a suitable candidate for hydrogel testing.

The incubation time used throughout this thesis was based on results from literature. In Gačanin et al. (2019), the conversion from kinked to linear peptide was pursued in an HPLC based assay, where incubation of D1 peptide at neutral pH was quenched at different time points. Upon linearization, elution time shifted, and an incubation time of 12 h, the longest time period tested, showed the biggest area under the curve of the shifted peaks, representing the total amount of linearized peptides. Since this was not tested for peptides characterized in this thesis, the incubation times were chosen to be 24 h, assuming that linearization would be completed by this time. If the transition from kinked to linear peptide could not be completed by some of the newly characterized peptides, prolongation of incubation times could lead to higher conversion rates, as well as the formation of more PNFs. Longer incubation times in combination with the HPLC based quantification of linearization at different time points could not be elaborated within the scope of this thesis due to the time restriction but would definitely be interesting for future investigations.

Execution and evaluation of the conversion assay turned out to be difficult. The overall results were generally in line with results from TEM, but oftentimes negative conversion rates were obtained, implying higher fluorescence in the filtrate than in the unfiltered solution. In most cases, a negative result was an outlier, but in others, the value remained negative during multiple testings (D4 TFA, D7

TFA). Negative values were exclusively found in samples incubated with TFA, although no inhibiting action of TFA on fluorescamine has been reported. Fluorescence quenching could be a possible explanation for the negative values, but the quencher itself could not be elucidated thus far. Furthermore, results from conversion assay could be falsified if the resuspension of the lyophilized peptide in DMSO was incomplete. This led to the conclusion that conversion assay works in general, but is prone to errors when performing it under acidic conditions. The given results of samples incubated in acidic solvent have to be used with caution and another way of testing of inducible fibrillation, as done in TEM images here, would be advisable.

Since the inducibility of fibrillation was demonstrated and a range of PNF morphologies could be detected for all synthesized peptides, further experiments were performed to analyze their secondary structure elements and charge.

Analysis of the Secondary Structures

The secondary structure of all peptides was analyzed via Thioflavin T assay and FT-IR measurement. ThT assay is based on its binding to β-sheets, limiting the rotation of the C-C-bond between the two ring moieties and leading to a redshifted emission compared to unbound ThT (Biancalana et al. 2010). Secondary structure of peptides can be spectroscopically measured via FT-IR. Here, characteristic absorption bands can be correlated to secondary structure elements. For the analysis of the peptides, absorptions in the amide I region (1600-1700 1/cm) are used. These are characteristic for the stretching vibration of the C=O bond, which is involved in hydrogen bonding and therefore allows conclusion to secondary structure elements (Byler and Susi 1986; Kong and Yu 2007). Results of ThT assay and FT-IR measurements are given in Figure 9.

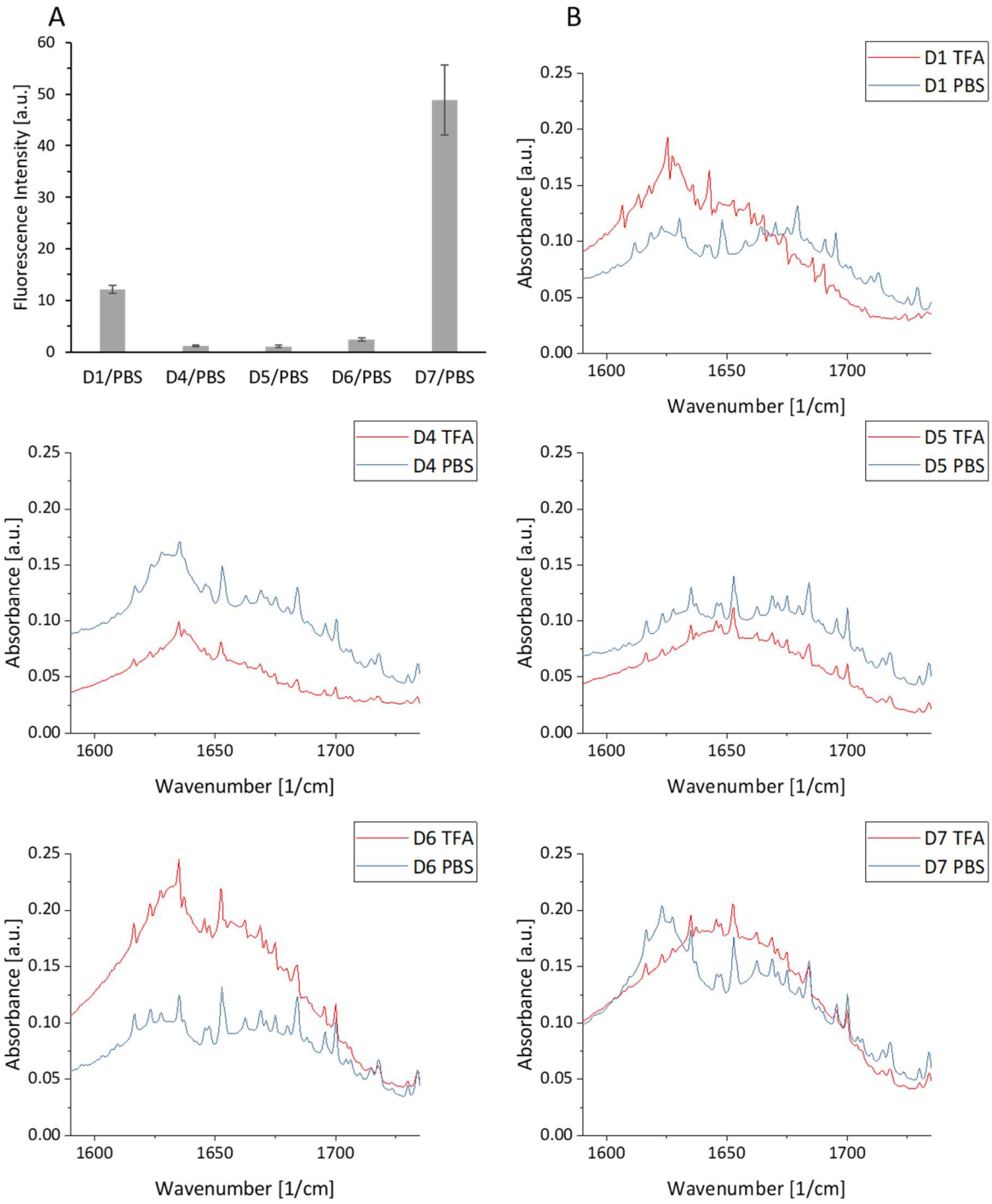

*Figure 9: Secondary structure analysis of the peptides. A) Thioflavin T assay of 1 mg/mL solutions of D1 (KIKI*SQINM), D4 (EIEI*SQINM), D5 (CKIK*SQII), D6 (KIKQ*SIINMWQ), and D7 (KIKQI*SINMWQ). Samples were incubated in PBS overnight to allow fibrillation and mixed with 50 µM ThT solution prior to fluorescence readout with multiple reads per well. Values of each measurement were normalized by dividing through the value for PBS, which was used as control. Data is shown as mean ± s.d. with n = 3. B) FT-IR spectra of 1 mg/mL solutions of D1, D4, D5, D6, and D7. Samples were incubated in 0.1 % aqueous TFA or PBS overnight, respectively, and lyophilized. Absorbance in the amide I region (wavenumbers 1600 – 1700 1/cm) of peptides incubated at pH 2 is shown in red, while pH 7 is shown in blue.*

The results of three independently measured ThT assays are pictured in Figure 9A. Results are displayed as quotient of the fluorescence intensity of each peptide and PBS, used as a control,

respectively. For D1, the emission of ThT was enhanced by 12.2 ± 0.7 in comparison to ThT in PBS, leading to the conclusion that D1 forms β-sheets when incubated in PBS. Binding to D4, the negatively charged equivalent of D1, led to a 1.2 ± 0.2 fold enhancement in ThT fluorescence. A similar factor was seen in D5, where an enhancement of 1.0 ± 0.2 was measured. Since binding of ThT to amyloid fibrils enhances its fluorescence by 2 orders of magnitude (Amdursky et al. 2012), it can be concluded that fibrils from these peptides do not form β-sheets but rather α-helices or random coils. It is also possible that these peptides are not ThT active (Cloe et al. 2011). D6 is exactly on the border with an enhancement of ThT fluorescence of 2.4 ± 0.3 times, making β-sheets a possible secondary structure. D7 showed the biggest factor in enhancement with 48.9 ± 6.8, which leads to the assumption of a β-sheet rich fibril formation.

The secondary structures of all peptides were further characterized via FT-IR. Using this technique, possible transitions in secondary structures from kinked and non-assembled to linear and assembled form of the peptides can be elaborated. For that, the spectra of lyophilized peptide, incubated in 0.1 % TFA or PBS, were overlaid and the shifts in maxima in the amide I region (1600 – 1700 1/cm) were analyzed (Cabiaux et al. 1989; Goormaghtigh et al. 1990; Adochitei and Drochioiu 2011). For D1, a transition of maxima from 1625 1/cm at acidic pH, corresponding to β-sheets, to 1676 1/cm for the linearized peptide was found, resembling β-sheets or β-turns. This is in line with the results from the ThT assay, where D1 incubated in PBS led to a strong increase in fluorescence, most likely due to binding to β-sheets. Similar results were published for this peptide. In Gačanin et al. 2019, this depsi peptide had its maximum absorbance at 1638-1639 1/cm, resembling unordered structures. Upon fibrillation, the maximum was shifted to 1680 1/cm, which corresponds to β-sheets. Although their results could not be exactly reproduced, similar structural findings were made for D1. From the FT-IR analysis and the high increase in ThT fluorescence, it can be concluded that D1 forms secondary structures high in β-sheet content at neutral pH, as it is also visible via TEM (Figure 8A). For D4, the maxima of absorbance are at 1635 1/cm upon incubation at both pH values, indicating the presence of β-sheets. This result is not in line with the ThT assay, where D4 did not interact with ThT, leading to the assumption of unordered structures. An explanation for these contradictory results could be the missing ThT activity of D4. A deletion mutation of the well-known amyloid β precursor peptide, which forms fibrils but does not increase ThT fluorescence has already been reported (Cloe et al. 2011). Also, it could be possible that a contamination quenches the ThT fluorescence by absorbing light at the excitation wavelength or the emitted light from ThT fluorescence (Hudson et al. 2009). To further examine the secondary structure, Congo red assay or measurement of circular dichroism spectra could have been performed as an alternative. This was not done, since ThT is the more specific dye for amyloid structures (Khurana et al. 2001). For D5, FT-IR revealed maxima of absorbance at 1653 1/cm at both, acidic and neutral pH, which corresponds to the formation of α-helices. This is in line with the

ThT assay. Its precursor CKIKQII, characterized by Schilling and Mack et al. (2019), showed a maximum absorbance at 1630 1/cm after incubation at neutral pH, which corresponds to β-sheets. This indicates that the introduction of serine for depsi peptide formation had severe effects on the secondary structure. For D6, the maximum peak at 1635 1/cm at pH 2, resembling β-sheets, shifts to 1684 1/cm at pH 7, corresponding also to β-sheets. Interaction with ThT was not increased, possibly to missing interaction with the fibrils, or the presence of a quencher. D7, which differs from D6 only in the placement of serine, shows a maximum at 1652 1/cm at pH 2, which corresponds to α-helices. Upon change to pH 7, the maximum is shifted to 1623 1/cm, resembling β-sheets. This is in line with the results from ThT assay, where D7 generated the highest increase in fluorescence, and the TEM images, where highly crosslinked fibrils were found (Figure 8A). This led to the conclusion that the secondary structure of D7 is β-sheets.

Taken together ThT assay and FT-IR measurements showed that D1, D4, D6, and D7 formed β-sheets, while D5 formed α-helices at neutral pH.

Characterization of Charge

Characterization of the PNFs surface charge via determination of the zeta potential was performed as electrophoretic mobility of peptides after fibrillation. Results from these measurements are shown in Figure 10.

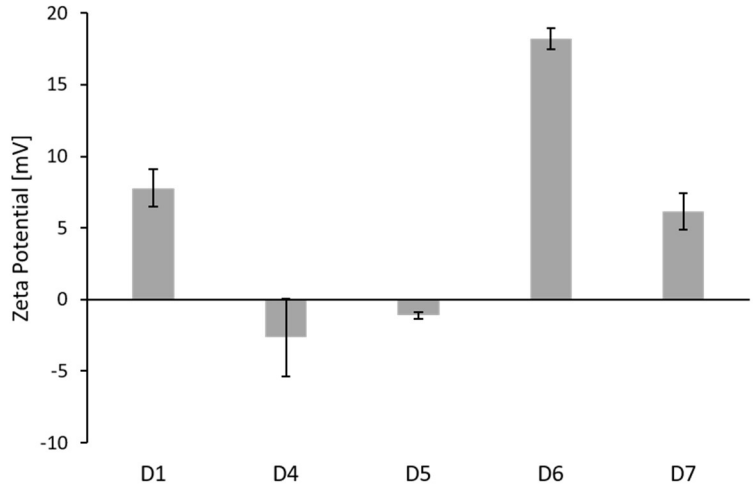

*Figure 10: Characterization of the surface charge of pre-incubated solutions of D1 (KIKI*SQINM), D4 (EIEI*SQINM), D5 (CKIK*SQII), D6 (KIKQ*SIINMWQ), and D7 (KIKQI*SINMWQ) at pH 7.4 (1 mg/mL, PBS, 24 h). The peptides were diluted in 1 mM KCl solution (0.05 mg/mL) and zeta potential was measured by electrophoretic mobility assay. Data is presented as mean ± s.d. with n = 3-6.*

For D1, a zeta potential of 7.8 ± 1.3 mV (n=6) was measured. The positive value was expected, since positively charged and neutral amino acid residues are present in the peptide, which led to an overall positive zeta potential. A negative zeta potential of -2.7 ± 2.7 mV (n=4) was found for D4, where two lysine residues are exchanged for glutamic acid in order to yield a negatively charged equivalent of D1, which was confirmed by the overall negative zeta potential. D5, which does not contain any negatively charged amino acids, was found to have a negative zeta potential of -1.1 ± 0.3 mV (n=6), although no negatively charged amino acids were used in this peptide. A possible explanation could be that the two positively charged lysine residues, as well as the N-terminus, could be spatially oriented into the aggregation this peptide formed (Sudhakar et al. 2017), which could conceal these positive charges or inhibit their protonation (Okuda et al. 2006). In contrary to this, the C-terminus could be accessible and deprotonated, yielding in an overall negative zeta potential for D5. D6 showed the highest zeta potential with 18.2 ± 0.7 mV (n=3). Although containing the same amino acids with neutral and positively charged residues as D6, D7 has a lower zeta potential of 6.2 ± 1.3 mV (n=4). This difference may arise from the placement of serine and therefore the ester bond in the depsi precursor. Upon O,N-acyl shift and fibrillation into different morphologies (Figure 8A and C), the orientation of the amino acid residues of both peptides changed, which could mask charged residues inside of the PNF or inhibit their protonation (Okuda et al. 2006), leading to different positive zeta potentials for peptides comprising the same amino acids.

Overall, the expected positive zeta potentials for D1, D6, and D7 were confirmed, as well as the negative zeta potential of D4. Surprisingly, D5 exhibited a negative zeta potential, which could be explained by the aggregation this peptide showed.

Summary: Peptide Nanofibrils

Peptide D1 was found to have similar characteristics as described in literature (Gačanin et al. 2019). The pH inducible shift from kinked to linear form and following fibrillation could be demonstrated via TEM, which also showed similar fibrillary morphologies compared to literature. The conversion rates were found to be lower than reported but still adequate. Furthermore, fibrils consisted of β-sheets, as seen in ThT assay and also in FT-IR measurements at pH 7. Zeta potential was shown to be positive. Thus, D1 and its maleimide-derivative D1-Mal can be used for hydrogel synthesis, where D1-Mal works as gelating agent grafted onto the polypeptide backbone, and D1 is used to test effects of additional free peptide of the same sequence on the rheological properties of the gels.

D4 is inspired by D1, where two lysine residues are exchanged for two glutamic acid residues. Despite that, it showed different characteristics and was more challenging to synthesize and analyse. The peptide had the lowest overall yield. In TEM images, the inducibility of fibrillation could be

demonstrated, but in comparison to D1 thinner and weaker interconnected fibrils were found. Conversion rates could not be completely elaborated since the values for D4 incubated at pH 2 always turned out negative. FT-IR revealed β-sheets as secondary structure, but the peptide did not interact with the well-established fluorescent marker thioflavin T. Zeta potential was found to be negative as expected but varied greatly. Overall, it can be said that substitution of two positively charged to two negatively charged amino acids changed the properties of the peptide in an higher extent than expected and made the characterization more difficult. Nevertheless, D4 showed the desired properties, as pH induced fibrils consisting of β-sheets and the negative charge, making it a suitable candidate to test the effects of free negatively charged peptide, with similar characteristics as the gelator, on the hydrogel.

D5, the depsi variation of CKIKQII, was chosen as candidate due to the interesting structure of its precursor (Supplementary Data, Figure 22; Schilling and Mack et al. 2019). Depsi peptide D5 showed the highest overall yield. However, the found characteristics did not live up to the expectations. TEM images showed no defined fibrillary structures but rather aggregations. Although the inducible conversion upon pH increase was seen there, conversion rates at lower pH were raised compared to higher pH. ThT assay and FT-IR revealed α-helices as secondary structure, corresponding to the aggregations visible in TEM. Zeta potential was found to be slightly negative, potentially arising from the aggregations it formed. Peptide CKIKQII consists of β-sheets and had higher conversion rates, zeta potential was not determined in the publication. From these results, it can be concluded that the establishment of a depsi peptide with the desired characteristics is harder than expected. Insertion of a single serine changed the features drastically. This has to be kept in mind for the future when trying to establish new depsi peptides. Characterization of the serine containing non-depsi form would be a better starting point than comparing to a peptide lacking in serine. Nonetheless, with D5, the impact of an α-helical peptide with negative zeta potential on hydrogel properties can be tested. However, D5 was not used for hydrogel testing in this work.

Depsi peptides D6 and D7 were selected due to the fibrillary structure of their precursor KIKQIINMWQ (Supplementary Data, Figure 22). Serine, required for the formation of a depsi peptide, was inserted in different places to test the effect thereof. D6 showed stacks of fibrils in TEM, which was not expected from the structure of the original peptide. Fibrillation upon pH increase was highly inducible as seen in conversion rates. D6 did not interact with ThT but FT-IR revealed a secondary structure of β-sheets. Zeta potential was found to be the highest of all peptides. In contrary, D7 showed fibril morphologies closer to the original peptide. Conversion rates were difficult to determine exactly, but the pH inducible fibrillation could be verified nevertheless. The secondary structure was found to be β-sheets, seen by the strong interaction of D7 with ThT and FT-IR measurements. Zeta potential was found to be positive, but to a lower extent than D6. These findings lead to the conclusion that the insertion of serine for

depsi formation does not only alter the characteristics in great manner, but also the place where it is inserted is crucial. The comparison of D6 and D7 to their serine containing non-depsi analogues would allow to conclude where the changes of properties arise. For hydrogel testing, both D6 and D7 are interesting candidates due to the different fibril morphologies and zeta potentials.

Synthesis and Characterization of the Protein Backbone

The hydrogel which inspired the experiments in this thesis was formed from peptides grafted onto a protein backbone. A naturally occurring protein was chosen as backbone, since its biocompatibility in *in vivo* applications is granted. Thus, HSA is used as raw material and gradually modified to introduce desired characteristics. An overview of the reactions performed from HSA to the final peptide-protein hybrid material is shown in Figure 11.

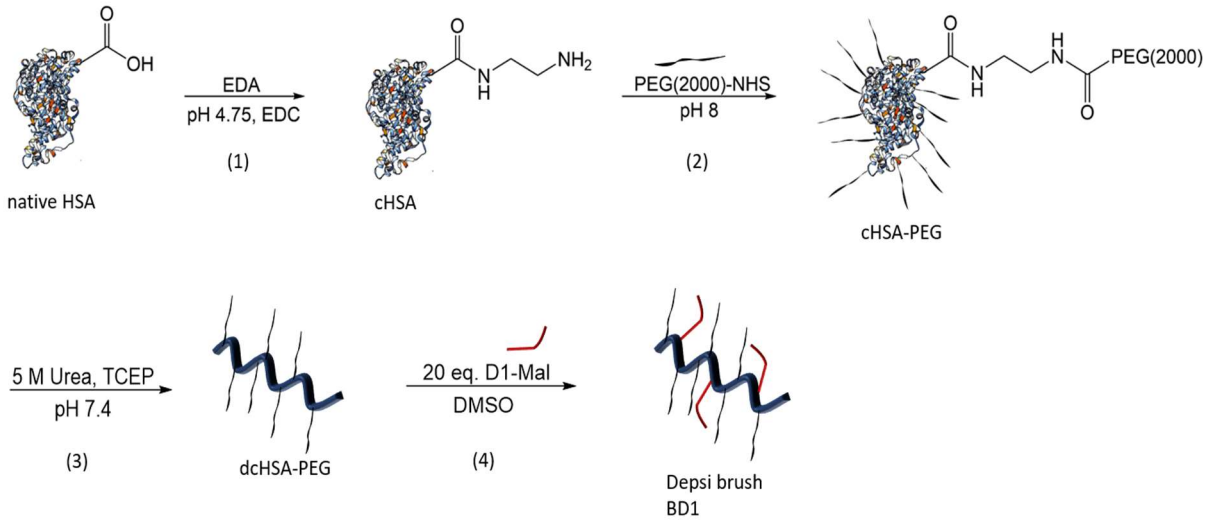

Figure 11: Schematic overview of reactions converting HSA to the depsi-brush BD1. In an initial step, natural HSA is cationized using EDA and EDC (1). These additionally added amino groups are used for the subsequent PEGylation (2). In a next step, the protein backbone is denatured using urea and TCEP (3). Finally, the denatured modified protein is mixed with the maleimide-modified depsi peptide D1-Mal (4l, yielding in the depsi-brush BD1.

The first step in backbone preparation is the cationization of HSA, providing more amino groups for the following reaction (Figure 11, step 1). MALDI-ToF measurement revealed a mass to charge ratio of m/z = 72539 and a yield of 0.5153 g (7.1 µmol, 95 %) was obtained. The molecular weight difference of HSA and cHSA implies the addition of 142 EDA chains (Figure 12). In literature, different amounts of introduced EDA chains were reported spanning 117 (Wu et al. 2014), 152 (Gačanin et al. 2019), and 156 (Gačanin and Kovtun et al. 2017). It was concluded that obtained 142 EDA molecules were adequate. These additional amino groups are further used for the reaction with MeO-PEG(2000)-NHS-ester (Figure 11, step 2). PEGylation is performed to increase the water capacity and decrease the immunogenicity of the gel (Wu et al. 2014). Yields of the reactions, performed in 3 different batches, are shown in Table 3.

Table 3: Yields of the PEGylation of cHSA, shown in reaction step 2 in Figure 11. After PEGylation, ultrafiltration and lyophilization, cHSA-PEG was obtained as a white solid. m/z was measured via high molecular mass MALDI-ToF. Amount of PEG chains was calculated via molecular mass difference of cHSA and cHSA-PEG.

	Batch 1	**Batch 2**	**Batch 3**
Amount of cHSA	0.1005 g (1.38 µmol)	0.1001 g (1.38 µmol)	0.3147 g (4.34 µmol)
m/z	114857	106240	109096
Yield of cHSA-PEG	0.1349 g (1.17 µmol, 85 %)	0.1367 g (1.29 µmol, 93 %)	0.4155 g (3.81 µmol, 87 %)
Amount of PEG chains	21	16	18

PEGylation of cHSA resulted in the addition of 21, 16, and 18 PEG chains, respectively (Table 3, Figure 12). These results are close to literature, where 22 PEG chains were added to cHSA (Gačanin et al. 2019), thus the number of PEG chains were found to be sufficient and no second round of PEGylation of one batch had to be done. Preparation of the protein backbone was pursued by denaturation of cHSA-PEG (Figure 11, step 3). The yields of this reaction, performed in 4 different batches, are listed in Table 4. Batches 1 and 2 from dcHSA-PEG are derived from cHSA-PEG batch 1, dcHSA-PEG batches 3 and 4 arised from cHSA-PEG batch 2.

Table 4: Yields of the denaturation of cHSA-PEG, shown in reaction step 3 in Figure 11. After denaturation, ultrafiltration and lyophilization, dcHSA-PEG was obtained as a white solid.

	Batch 1	**Batch 2**	**Batch 3**	**Batch 4**
Amount of cHSA-PEG	25.3 mg (218 nmol)	25.2 mg (218 nmol)	35.5 mg (334 nmol)	35.4 mg (334 nmol)
Yield of dcHSA-PEG	24.6 mg (97 %)	24.3 mg (96 %)	32.7 mg (92 %)	32.3 mg (91 %)

Yields of 91-97 % of dcHSA-PEG were obtained (Table 4). This is lower than in literature, where the reaction was performed quantitatively (Gačanin et al. 2019), but still good with values over 90 %. Probably, product was lost during the purification using ultrafiltration. Subsequently, the batches of dcHSA-PEG were used to generate the peptide-protein hybrid BD1 (Figure 11, step 4). Results from these reactions, carried out in 5 different batches, are presented in Table 5. BD1 batch 1 resulted from dcHSA-PEG batch 1, BD1 batches 2 and 3 arose from dcHSA-PEG batch 3, BD1 batches 4 and 5 were derived from dcHSA-PEG batch 4. Due to problems with the MALDI-ToF apparatus, the mass to charge ratios and therefore the number of grafted D1-Mal chains onto the backbone could not be performed.

Nevertheless, BD1 batches 1 and 2 were used for hydrogel synthesis. Their mass to charge ratio was presumed as m/z = 145000 Da with 20 D1-Mal chains grafted onto the polymer backbone, as it was determined in literature (Gačanin et al. 2019).

Table 5: Yields of the formation of the peptide-protein hybrid, BD1, shown in reaction step 4 in Figure 11. After reaction with D1-Mal, ultrafiltration and lyophilization, BD1 was obtained as a white solid. Determining of the mass to charge ratio and the following calculation of the number of grafted D1-Mal chains could not be performed due to difficulties with the apparatuses (n.d. indicates not determined).

	Batch 1	**Batch 2**	**Batch 3**	**Batch 4**	**Batch 5**
Amount of dcHSA-PEG	21.0 mg (0.18 µmol)	16.3 mg (0.15 µmol)	16.7 mg (0.16 µmol)	16.2 mg (0.15 µmol)	16.2 mg (0.15 µmol)
m/z	n.d.	n.d.	n.d.	n.d.	n.d.
Yield of BD1	20.7 mg	17.3 mg	16.0 mg	16.1 mg	16.1 mg
Amount of D1-Mal	n.d.	n.d.	n.d.	n.d.	n.d.

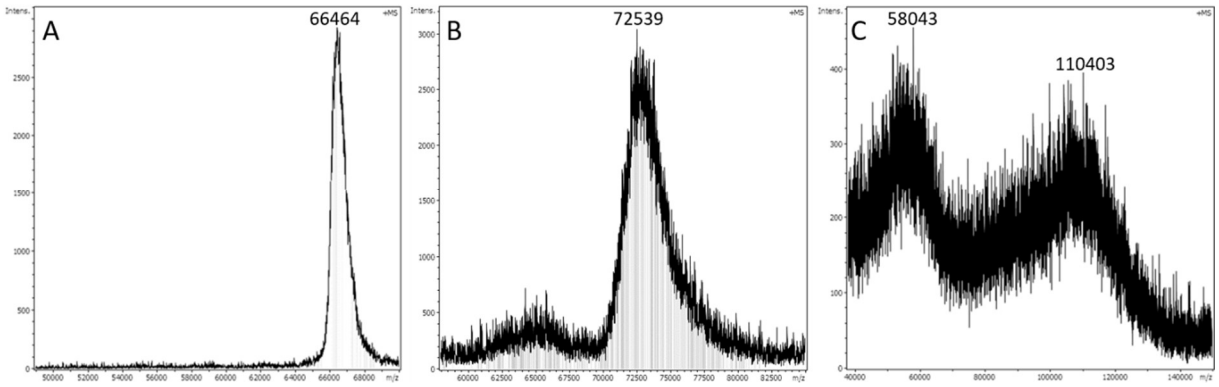

Figure 12: MALDI-ToF mass spectra. A) Native HSA with m/z = 66464 is gradually modified to serve as a backbone for hydrogel synthesis. As a first step, HSA is cationized (Figure 11, step 1) yielding in B) cHSA with m/z = 72539. Furthermore, PEG chains were grafted onto the backbone (Figure 11, step 2), affording C) cHSA-PEG, here an exemplary batch with m/z = 110403. The peak with m/z = 58043 approximately represents the twofold charged molecule (z=2).

Characterization of the Protein-Peptide Hydrogels

Prior characterizing the hydrogels with additional free depsi peptide, H1 hydrogels were prepared according to literature to reproduce the expected properties (Gačanin et al. 2019). Results from these measurements are shown in Figure 13.

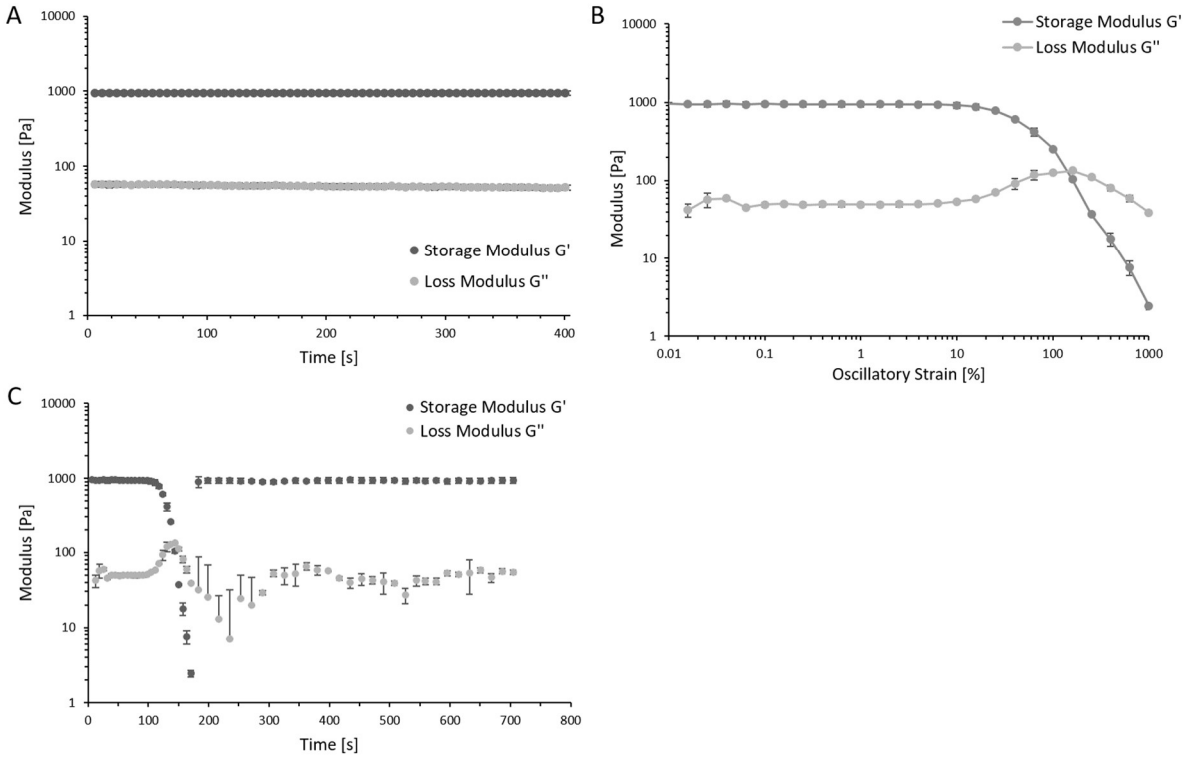

Figure 13: Rheological characterization of H1. A) Oscillatory time sweep with fixed strain (1 %) and fixed frequency (1 Hz). A time period of 400 s where storage modulus (G') and loss modulus (G'') were constant is displayed. B) Oscillatory strain sweep (0.01-1000 %) with fixed frequency (1 Hz). C) Thixotropy measurement, consisting of an oscillatory strain sweep (0.01-1000 %) with fixed frequency (1 Hz), followed by a 500 s time sweep with fixed strain (0.1 %) and fixed frequency (1 Hz) to show the self-healing properties of the hydrogel. All measurements were performed at 25 °C. Data is presented as mean ± s.d. with n=2.

First, the mechanical properties of H1 were assessed via oscillatory time sweep measurements (Figure 13A). Gelation happened instantaneously, and storage modulus of G'=950 Pa and loss modulus of G''=55 Pa were constant over the 400 s time period. Furthermore, G' and G'' remained constant until an oscillatory strain of 15 % was applied (Figure 13B), where the strains could be compensated by the hydrogel. Oscillatory strains of over 15 % led to the steady decrease of G', while G'' increased slowly until a crossover point at 140 % oscillatory strain, where gel-to-sol transition occurred and the material showed the characteristics of a fluid. The reported capability of self-healing was tested via the application of increasing oscillatory strain followed by a time period with low fixed strain. After disruption of the gel by high strain, H1 was able to recover seconds after the strain was removed (Figure 13C). The efficiency of immediate recovery was quantified by comparison of G' values before and after disruption, and found to be 95 %. In Gačanin et al. (2019), the original H1 was reported with

G'=700 Pa and G''=40 Pa, which is a similar range to the hereby reported hydrogels. Analogously, the mechanical properties remained constant until an oscillatory strain of 15 % was applied, but gel-to-sol transition occurred as early as at 41 % strain. The exact reason for this difference could not be elaborated, but it could possibly arise from a difference in number of grafted D1-Mal chains to the backbone, since the exact number of these remained unclear. The number of PEG chains (21 here and 22 in Gačanin et al. 2019) is nearly the same, hence do not provide a sufficient reason for the big difference in disruption resistance. However, the superior self-healing properties of the published hydrogel could be reproduced, since it had been shown to instantaneously return to the initial G' value after removal of the strain in a nearly quantitative fashion.

Since the herein prepared H1 hydrogel could reproduce the published data, addition of different equivalents of free depsi peptides prior gelation was performed and the alterations of the rheological properties was analyzed. Since the addition of 20 eq. free depsi peptide showed no change in rheological properties (unpublished data from J. Gačanin), 50 eq. or 100 eq. of free depsi peptide were copolymerized with the brush. The rheological characteristics of the first candidate, H1 with 50 eq. of D1 depsi peptide, are displayed in Figure 14.

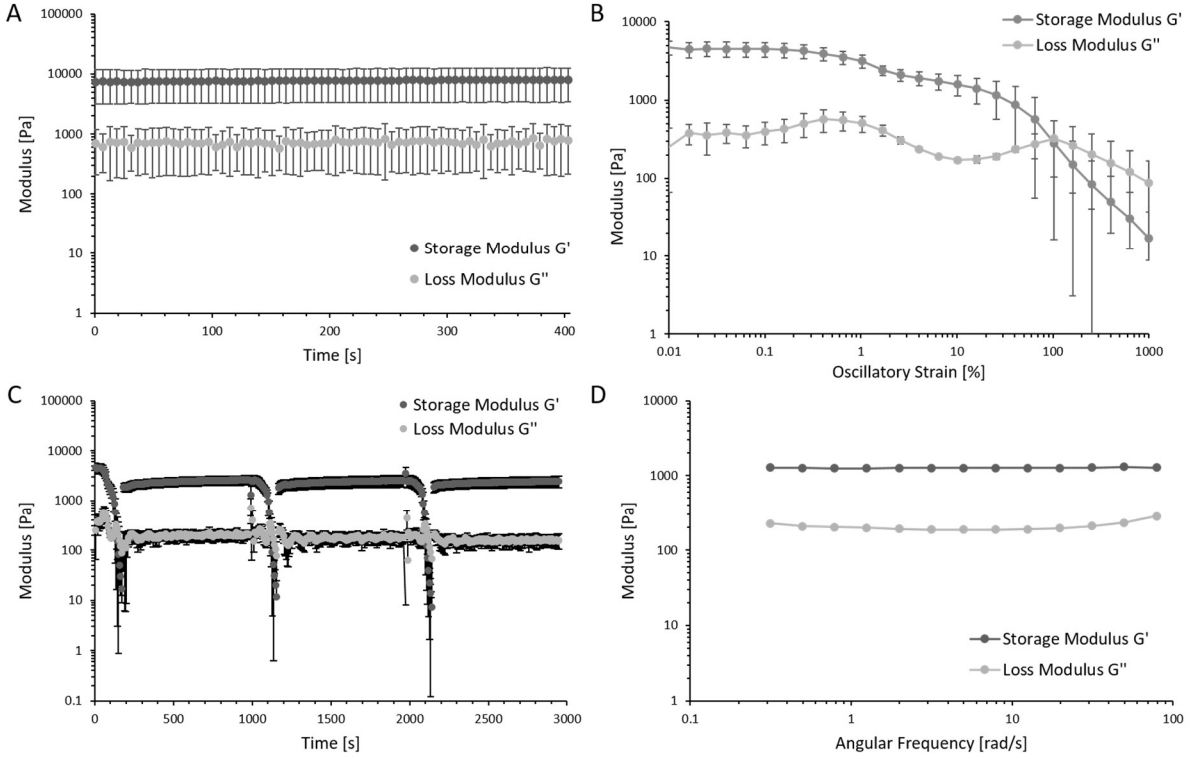

*Figure 14: Rheological characterization of H1 with additional 50 eq. of free D1 depsi peptide (KIKI*SQINM). A) Oscillatory time sweep with fixed strain (0.1 %) and fixed frequency (1 Hz). A time period of 400 s where storage modulus (G') and loss modulus (G'') were constant is displayed. Data is presented as mean ± s.d. with n=3. B) Oscillatory strain sweep (0.01-1000 %) with fixed frequency (1 Hz). Data is presented as mean ± s.d. with n=3. C) Thixotropy measurement, consisting of oscillatory strain sweeps (0.01-1000 %) with fixed frequency (1 Hz), followed by 800 s time sweeps with fixed strain (0.1 %) and fixed frequency (1 Hz) to show the self-healing properties of the hydrogel. Data is presented as mean ± s.d. with n=3. D) Frequency sweep (0.05-100 Hz) with fixed strain (0.1 %) (n=1). All measurements were performed at 25 °C.*

Time sweep measurements revealed that complete gelation of H1+50 eq. D1, detectable in constant G' and G'' values, took a longer time period than gelation of H1 (Supplementary Data, Figure 30). Mechanical properties of G'=7700 Pa and G''=720 Pa were measured (Figure 14A) and stayed constant until an oscillatory strain of 1 % was applied (Figure 14B). Here, a peak followed by a decrease in G'' and slight decrease in G' is visible, as well as at 15 % strain. When strains over 100 % were applied, gel-to-sol transition occurred and the gel collapsed. After disruption of H1+50 eq. D1 via high strains, it was able to recover in seconds but G' didn't return to the initial G' value during the recovery time (Figure 14C). Quantification of self-healing revealed an efficiency of 41 %. Frequency sweep showed constant values for G' and G'' until 50 rad/s, further increase in frequency led to an increase in G'' but no intersection could be seen, showing the independence of mechanical properties over all tested frequencies.

In comparison to H1, addition of free D1 depsi peptide for H1+50 eq. D1 made the hydrogel 7-fold stiffer. Since the mechanical properties of H1 are unaffected of measurement with 0.1 % or 1 % strain (G'=1000 Pa for 0.1 % strain; Supplementary Data, Figure 29 vs. G'=950 Pa for 1 % strain, Figure 13A), the difference in applied strain is no valid explanation for this occurrence. This increased hardening most probably arose from the additional D1 peptide which interacts with the D1-Mal grafted onto the polypeptide backbone. Since D1 fibrils formed a crosslinked network in TEM images (Figure 8A), presumably a fibrillary network is formed that interacted with the BD1 brush due to hydrogen bonding.

In literature, time and frequency sweeps were performed at 1 % oscillatory strain (Gačanin et al. 2019) whereas they had to be performed at 0.1 % strain here. Performing time sweeps of H1+50 eq. D1 with 1 % strain yielded in G'=3050 Pa and G''=450 Pa (Supplementary Data, Figure 31A). In frequency sweeps with 1 % strain, G'' was found to be higher than G', leading to the conclusion that it is not a gel, but a viscous fluid (Supplementary Data, Figure 31B). Furthermore, in oscillatory strain sweeps, a peak at 1 % strain could be seen. Since rheological characteristics should be determined when storage and loss modulus are in linear regions with respect to the applied sweep (Zuidema et al. 2014), hydrogels with free peptides were examined with an oscillatory strain of 0.1 % in time and frequency sweeps. The oscillatory strain sweep of H1 (Figure 13B) showed no peak at 1 % strain, therefore the parameter did not have to be changed. Since the peak arose with addition of free D1 peptide, it could be possible that at this percentage of strain, a fibrillary network disrupts within the gel. Presumably, applied strains under 1 % show the interaction of the hydrogel with the fibrillary network, which could be displaceable and movable until a strain of over 1 % is applied, where the fibrillary network disrupts and the properties of the hydrogel alone are displayed. This thesis is also supported by the course of G' and G'' of H1+50 eq. D1 after strains of approx. 3 % are applied. From there on, the curves for H1 and H1 + 50 eq. D1 proceed similarly. In both hydrogels, strains of under 15 % are compensated by the

material, while strains over 15 % led to a decrease in G' and increase in G'', until a gel-to-sol transition occurs at strains of over 100 % where the gels collapsed. This underlines the proposed hypothesis.

Efficiency of self-healing of H1+50 eq. D1 was impaired when compared to H1 (41 % vs. 95 %). In the time sweep after disruption of H1, an instantaneous recovery of G' to a constant level is seen, while G' of H1+50 eq. D1 stayed lower than the initial value and was not able to return during the 800 s recovery period. This led to the conclusion that the rearrangement of the presumably disrupted fibrillary network needs more time than rearrangement of the polypeptide backbone of the gel. This is also underlined by the gelation time of H1+50 eq. D1, which is prolonged in comparison to H1.

Since the impact of 50 eq. of free D1 depsi peptide showed interesting results, the impact of 100 eq. of free D1 on the rheological properties of H1 was elaborated as a next step. Rheological data from H1+100 eq. free D1 depsi peptide is shown in Figure 15.

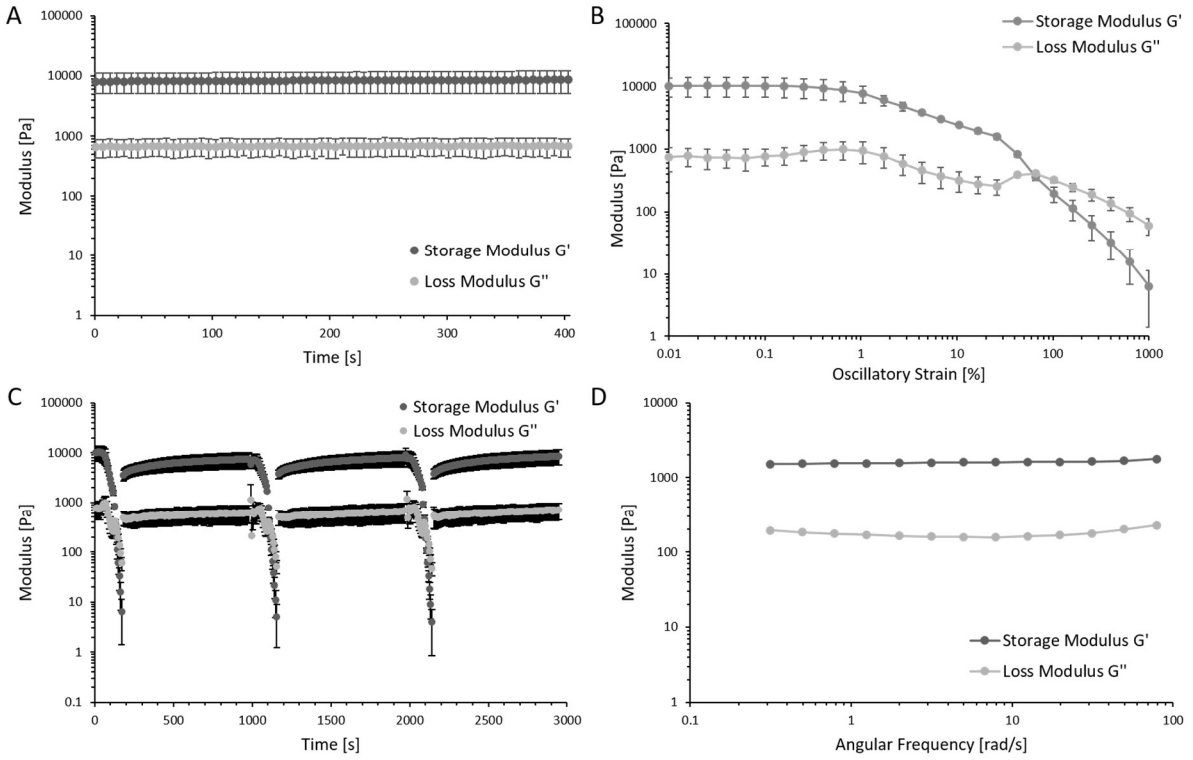

*Figure 15: Rheological characterization of H1 with additional 100 eq. of free D1 depsi peptide (KIKI*SQINM). A) Oscillatory time sweep with fixed strain (0.1 %) and fixed frequency (1 Hz). A time period of 400 s where storage modulus (G') and loss modulus (G'') were constant is displayed. Data is presented as mean ± s.d. with n=3. B) Oscillatory strain sweep (0.01-1000 %) with fixed frequency (1 Hz). Data is presented as mean ± s.d. with n=2. C) Thixotropy measurement, consisting of oscillatory strain sweeps (0.01-1000 %) with fixed frequency (1 Hz), followed by 800 s time sweeps with fixed strain (0.1 %) and fixed frequency (1 Hz) to show the self-healing properties of the hydrogel. Data is presented as mean ± s.d. with n=2. D) Frequency sweep (0.05-100 Hz) with fixed strain (0.1 %) (n=1). All measurements were performed at 25 °C.*

The mechanical properties of H1+100 eq. D1 were assessed via oscillatory time sweep, in which storage modulus of G'=8400 Pa and loss modulus of G''=680 Pa were found after gelation time (Figure 15A).

When stressed via application of oscillatory strain, G' and G'' were constant until 1 % strain (Figure 15B). Forces of over 1 % strain led to a peak followed by a decrease in G'' and a decrease in G', as well as when strains over 15 % were applied. Gel-to-sol transition and therefore collapse of H1+100 eq. D1 happened at an oscillatory strain of 60 %. After this collapse, the hydrogel was able to recover immediately after removal of the strain but G' didn't return to the original value during the 800 s recovery period (Figure 15C). Efficiency of self-healing was quantified as 35 %. The mechanical properties of H1+100 eq. D1 showed no dependency on the tested frequency range, as G' and G'' remained constant until 50 rad/s. Increase in frequency led to the increase of G'', but no intersection and therefore gel-to-sol transition could be seen (Figure 15D).

The addition of another 50 eq. of free D1 depsi peptide led to an 1.1-fold increase in G' when compared to H1+50 eq. D1 (Figure 14A). This shows a non-linear relation between addition of D1 and the storage modulus G'. H1+100 eq. D1 could bear less oscillatory strain than H1+50 eq. D1 and had lower self-healing properties. This underlies the hypothesis that the network of D1 fibrils is disrupted more easily than the structure of the polypeptide backbone, and the rearrangement of this network after shear stress needs more recovery time than H1. Since the amount of free D1 peptide is very high compared to the backbone, the characteristics of H1 could be superimposed by the fibrillary network of D1, visible in the earlier rupture by oscillatory strain.

Since the further increase in D1 content seemed unpractical, further hydrogels were made by adding the negatively charged equivalent to D1, D4, to the brush. Rheological characterization of H1+50 eq. D4 is shown in Figure 16.

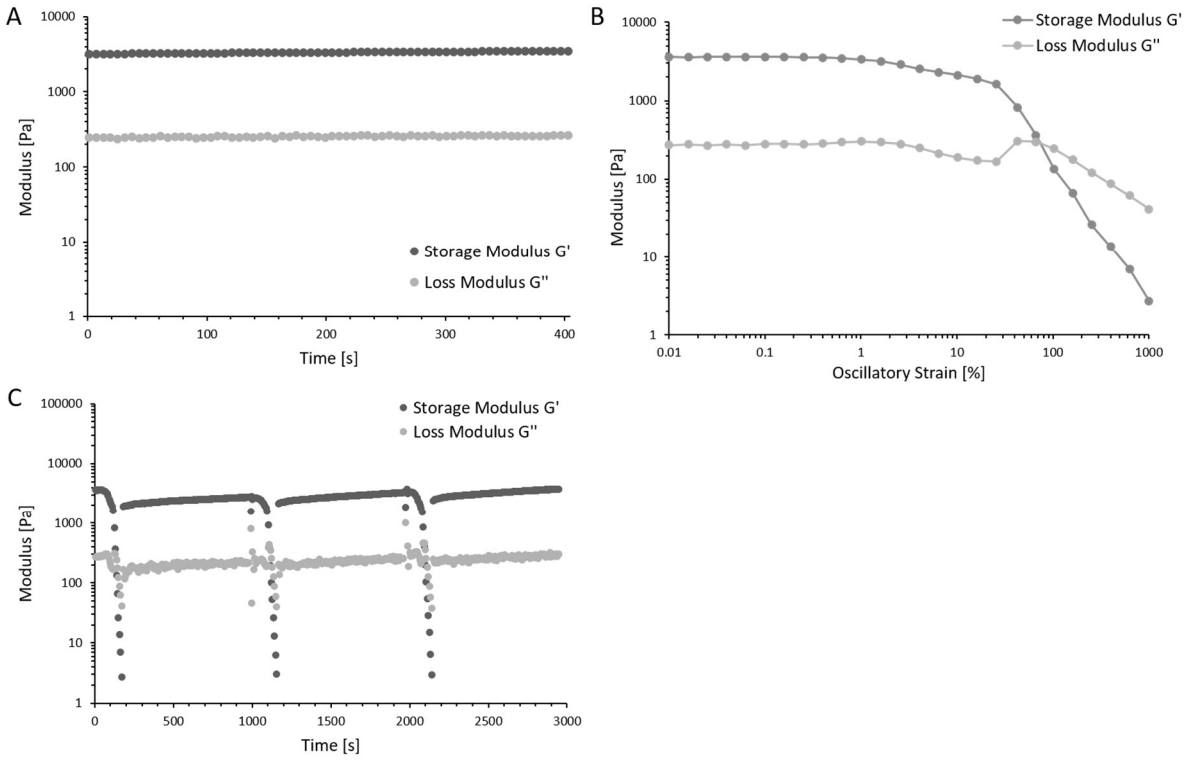

*Figure 16: Rheological characterization of H1 with additional 50 eq. of free D4 depsi peptide (EIEI*SQINM). A) Oscillatory time sweep with fixed strain (0.1 %) and fixed frequency (1 Hz). A time period of 400 s where storage modulus (G') and loss modulus (G'') were constant is displayed. B) Oscillatory strain sweep (0.01-1000 %) with fixed frequency (1 Hz). C) Thixotropy measurement, consisting of oscillatory strain sweeps (0.01-1000 %) with fixed frequency (1 Hz), followed by 800 s time sweeps with fixed strain (0.1 %) and fixed frequency (1 Hz) to show the self-healing properties of the hydrogel. All measurements were performed at 25 °C with n=1.*

After appropriate gelation time, oscillatory time sweeps revealed mechanical properties of G'=3300 Pa and G''=260 Pa (Figure 15A). Upon application of shear forces through oscillatory strain, G' and G'' remained constant until 1 % strain, where G'' peaked and decreased afterwards, and G' decreased. A strain of 15 % could be compensated by the hydrogel, further increase to 70 % led to disruption and gel-to-sol transition (Figure 15B). After disrupting via high strains, the hydrogel immediately recovered after the strain was removed, and therefore self-heal, during the recovery time period, but stayed under its initial G' value (Figure 15C). The efficiency of immediate self-healing was quantified to 54 %.

Although D4 depsi peptide was expected to interact via hydrogen bonding and electrostatic interaction due to its negative charge and the positive charge of the grafted D1-Mal peptide and therefore lead to a harder hydrogel, addition of 50 eq. of free D4 did not lead to a formation of a stiffer gel compared to 50 eq. D1 (G`=3300 Pa vs. G'=8300 Pa). This may arise from the weaker fibrillary network from D4 seen in TEM images (Figure 8A) and may also explain the smaller peak at 1 % oscillatory strain. H1+50 eq. D4 could bear lower oscillatory stress as the original H1 hydrogel. A possible explanation for this could be the interaction of the disrupted negatively charged fibrillary network on the grafted D1-Mal, with

which D4 interacts via electrostatic and potentially weakens the interaction between D1-Mal chains that hold the polypeptide backbone together. A higher rate at recovery than H1+50 eq. D1 (54 % vs. 41%) was found, which could arise from the weaker crosslinking of the D4 fibrillary network, which then needed less time to rearrange. Since D1 and D4 showed different fibrillary networks and converted to fibrils in different rates (Figure 8A+B), and their impact on hydrogel properties are different, it can be concluded that although consisting of the same core sequence, they cannot be treated as equivalents of each other.

The impact of 100 eq. of free D4 depsi peptide was tested, but due to the lack of time, only one oscillatory time sweep could be performed. This is shown in Figure 17.

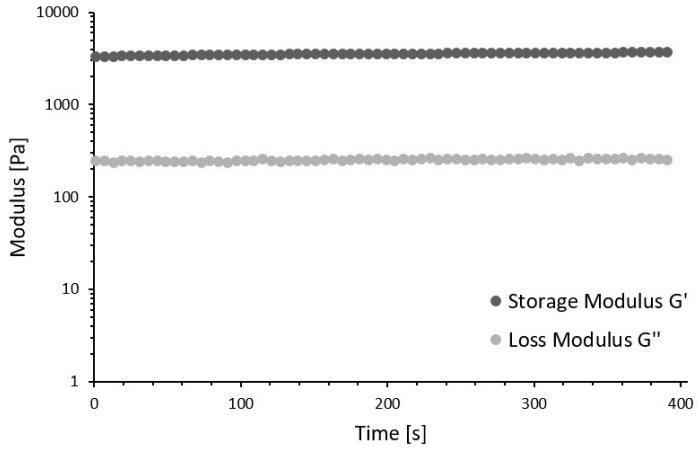

*Figure 17: Oscillatory time sweep of H1+100 eq. free D4 depsi peptide (EIEI*SQINM) with fixed strain (0.1 %) and fixed frequency (1 Hz). A time period of 400 s where storage modulus (G') and loss modulus (G'') were constant is displayed. Measurement was performed at 25 °C with n=1.*

The oscillatory time sweep of H1+100 eq. D4 revealed G'=3600 Pa and G''=250 Pa after appropriate gelation time (Figure 17). Interestingly, the addition of another 50 eq. of free D4 depsi peptide led to a 1.1-fold increase in G' when compared to H1+50 eq. D4 (G'=3300 Pa, Figure 16A). This was also the factor of enhancement in storage modulus from H1+50 eq. D1 to H1+100 eq. D1. This confirmed the non-linear correlation of storage modulus and addition of free depsi peptide equivalents. Although the expected effect of opposite charges, the formation of a stiffer, denser hydrogel compared to addition of a positively charged depsi peptide, could not be verified, and it was shown that D1 and D4 cannot be treated as equivalents, the factor of enhancement of G' when adding the same number of equivalents, stayed the same. This could possibly arise from the same core structure D1 and D4 possess.

Since D6 showed highly interesting fibrillary structure, had good conversion rates and percentual yield, it was chosen to form a hydrogel. The rheological properties of H1+50 eq. D6 are shown in Figure 18.

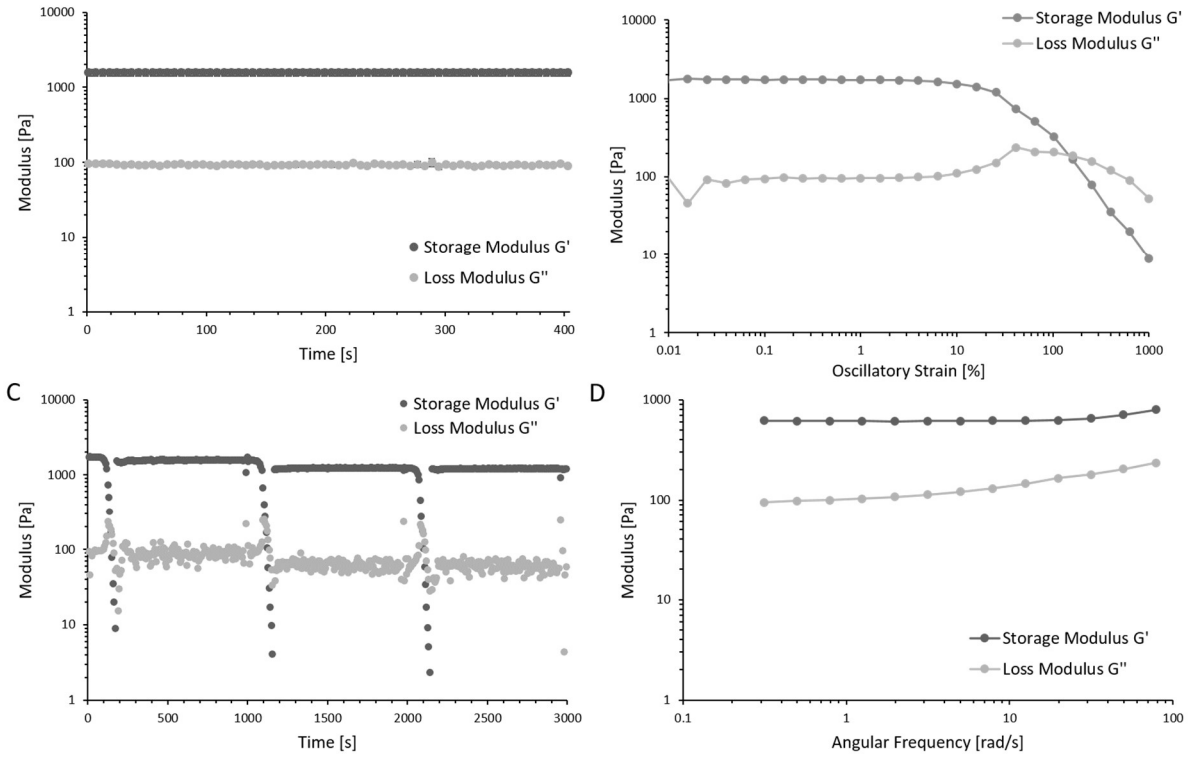

*Figure 18: Rheological characterization of H1 with additional 50 eq. of free D6 depsi peptide (KIKQ*SIINMWQ). A) Oscillatory time sweep with fixed strain (0.1 %) and fixed frequency (1 Hz). A time period of 400 s where storage modulus (G') and loss modulus (G'') were constant is displayed. Data is presented as mean ± s.d. with n=2. B) Oscillatory strain sweep (0.01-1000 %) with fixed frequency (1 Hz) (n=1). C) Thixotropy measurement, consisting of oscillatory strain sweeps (0.01-1000 %) with fixed frequency (1 Hz), followed by 800 s time sweeps with fixed strain (0.1 %) and fixed frequency (1 Hz) to show the self-healing properties of the hydrogel (n=1). D) Frequency sweep (0.05-100 Hz) with fixed strain (0.1 %) (n=1). All measurements were performed at 25 °C.*

The mechanical properties were assessed via oscillatory time sweep, which revealed G`=1600 Pa and G''=100 Pa (Figure 18A). G' and G'' stayed constant with increasing oscillatory strain until 15 % strain were applied, where G'' increased and G' decreased until the crossover at 140 % strain, where gel-to-sol transition happened and the gel disrupted (Figure 18B). After disruption of the gel, the self-healing capacity was tested and found to be immediate after removal of the strain. G' after the first disruption returned very close to the initial G' value (Figure 18C). Quantification of the self-healing efficiency was found to be 88 %. An increase in frequency showed no dependency of G' and G'' thereof. At frequencies above 15 rad/s, G'' increased steadily, but no intersection happened (Figure 18D).

Addition of free D6 depsi peptide, which formed fibrillary stacks in TEM images (Figure 8A), led to a 1.6-fold increase in mechanical strength. Preparation of this hydrogel was easier and it didn't need as much time to fully gel as the other hydrogels with additional free depsi peptide. The oscillatory strain showed no peak at 1 % strain, where the other hydrogels had peaked, which was hypothesized to arise from the fibrillary network D1 and D4 form. Since D6 formed fibrillary stacks, a disruption of a fibrillary network at 1 % strain could not be detected, underlining the proposed hypothesis. Furthermore, time

sweep measurements with 1 % fixed strain showed G'=1700 Pa, which is in the same range when measured with 0.1 % strain (Supplementary Data, Figure 32). The self-healing properties of H1+50 eq. D6 were closer to the original H1 than other hydrogels with additional free peptide. This potentially also arose from the fibrillary stack structure, which showed no disruption but rather got displaced or rearranged faster since no fibrillary networks had to be formed. This could also be the reason why H1+50 eq. D6 formed a softer hydrogel compared to these with fibrillary networks, but stiffer as H1.

Unfortunately, the impact of 100 eq. D6 on the rheological characteristics could not be elaborated, due to the lack of peptide and time. Also, hydrogels with additional D7 depsi peptide could not be characterized due to the same reasons.

Comparison of the Rheological Characteristics

Prior adding free depsi peptides to the polypeptide backbone, the properties of the hydrogel reported in literature (Gačanin et al. 2019) could be reproduced. The here synthesized H1 hydrogel gelled instantaneously, was resistant against high oscillatory strains and able to immediately recover after strains were removed, thus having the ability to self-heal. Furthermore, its mechanical properties were constant in the tested frequency range.

Addition of free depsi peptides led to the formation of a stiffer hydrogel for all peptides. The mean values for the storage modulus G' of all hydrogels, assessed at a constant oscillatory strain of 0.1 %, are shown in Figure 19.

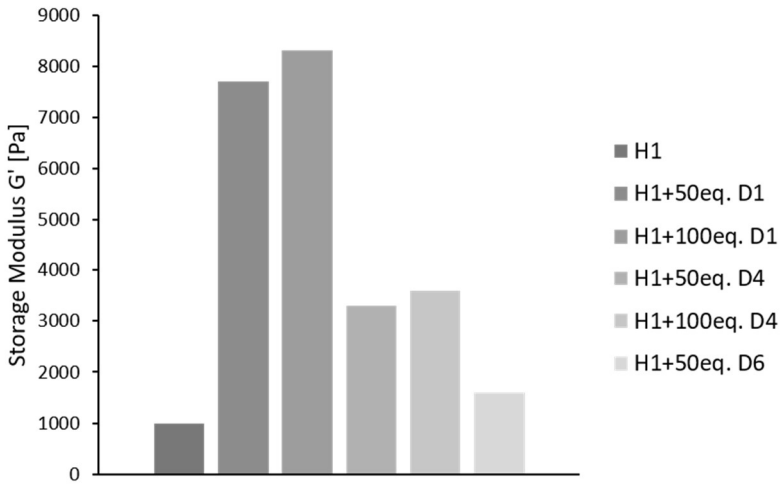

Figure 19: Comparison of mean storage moduli (G') from oscillatory time sweeps with fixed oscillatory strain (0.1 %) and fixed frequency (1 Hz) of all synthesized hydrogels in this thesis.

Addition of D1 led to the highest increase in G' of all peptides. D4, which was treated as the negatively charged equivalent, showed a lower increase in G' at both tested equivalents. Interestingly, further

addition of 50 eq. D1 or D4 led to an approximately 1.1-fold increase in G' when compared to only 50 eq. of free D1 or D4, meaning that the stiffnesses could be enhanced by the same factor upon adding the same equivalents of different peptides. This is most probably due to the sequence similarity of D1 and D4, since they possessed the same amino acids except the exchange of lysine in D1 to glutamic acid in D4. However, 50 eq. of both peptides did not increase G' of H1 by the same factor, which led to the conclusion that D1 and D4 could not be treated as equivalents. A hypothesis for this behavior is the formation of a fibrillary network of D1 and D4, as seen in the TEM images of both (Figure 8A), which interacted with the brush and led to an increase in G', which may be specific to the form of network both peptides possessed. By addition of 100 eq. free D1 or D4, the interaction of fibrils formed from free depsi peptide and the backbone could be limited or saturated and the interaction occurred mainly amongst the fibrils, leading to the same factor in increase. It was expected that the addition of D4 would lead to a stiffer and denser hydrogel, since the interaction of the grafted D1-Mal and D4 could be realized via hydrogen bonds and electrostatics. This could not be confirmed, most probably because D4 fibrils were too weak. The lowest increase in G' was found to happen after D6 was added to the gel. Since D6 fibrils showed a very different morphology than D1 or D4, the interaction with the backbone could differ from the one hypothesized before, namely the insertion of fibrillary stacks between the grafted D1-Mal chains on the backbone. Summarized, addition of any free depsi peptide increased G', leading to a stiffer gel than the published H1. For this behavior, two plausible explanations could be given, depending on how the free depsi peptides interacted with the polypeptide backbone. The first possibility would be the formation of a fibrillary network that is located on top of the brush, interacting with the grafted D1-Mal peptides, occurring when depsi peptides forming fibrillary networks are added. Another theory is the intercalation of free depsi peptide between grafted D1-Mal strands, when peptides were added that formed fibrillary stacks. These findings indicate that the interaction of the protein-peptide hybrid with additional free depsi peptide is dependent on the structure the fibrils exhibited. Also, it could be concluded that the addition of peptides that form fibrillary networks increased G' stronger than addition of peptides that form fibrillary stacks. However, these theories require further experiments to be verified or corrected accordingly. A possible method to determine the form of interaction of free depsi peptide and polypeptide backbone would be the characterization via cryo-SEM (Aston et al. 2016), which could not be pursued due time restriction.

In contrary as reported in Gačanin et al. (2019), the here synthesized H1 hydrogel was able to tolerate higher oscillatory strains. The exact reason for this remained unclear, but the hydrogels with added peptides also tolerated higher oscillatory strains than the original hydrogel, respectively depending on the added depsi peptide and also its amount. For all reported hydrogels, G' decreased gradually while G'' increased with increasing oscillatory strain. This led to the conclusion that the hydrogels didn't collapse suddenly, but compensated increasing strains probably through changing the spatial

arrangement of the polypeptide backbone assembled with the fibrillary structures, similarly to the previously reported H1 hydrogel (Gačanin et al. 2019). The percentages of oscillatory strains that were tolerated by the tested hydrogels, before gel-to-sol transition occurred, are displayed in Figure 20.

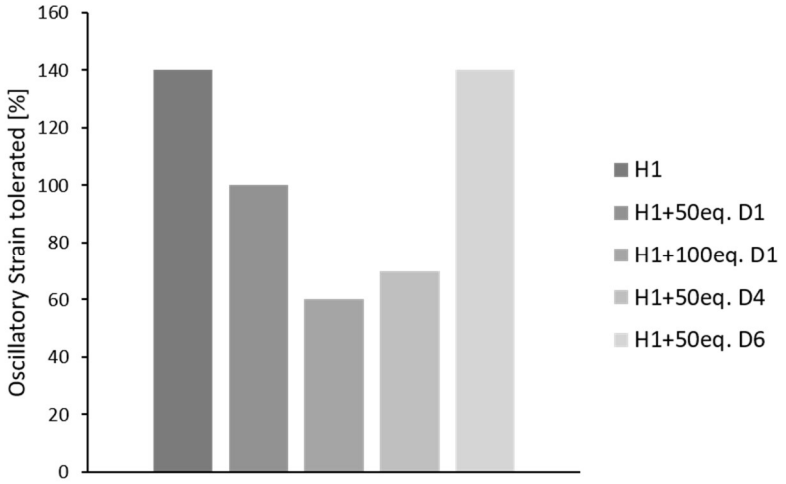

Figure 20: Comparison of the percentage of oscillatory strain that was tolerated by the hydrogels. Values of oscillatory strains were assessed before gel-to-sol transition occurred during oscillatory strain sweeps (0.01-1000 %) in all tested hydrogels.

The addition of 50 eq. free D1 depsi peptide led to a decrease of tolerated oscillatory strain of 40 %. Interestingly, addition of 100 eq. D1 reduced the maximum endured strain again by 40%. In contrast to the storage modulus G', the tolerance of oscillatory strain was found to depend linearly on the amount of added D1. This may arise from the formation of a fibrillary network interacting with the grafted D1-Mal peptides, which could restrict the ability of the polypeptide backbone to spatially rearrange upon application of strain, leading to a lower tolerance and an earlier gel-to-sol transition. Addition of 50 eq. of the negatively charged D4 peptide bisected the tolerated oscillatory strain (70 % vs. 140 %). This could be due to the electrostatic interaction between D4 and the grafted D1-Mal peptides, which could potentially weaken the ability to rearrange the polypeptide chains or diminish the interaction between D1-Mal strands which connected the polypeptide chains to form the hydrogel. In contrary to that, addition of 50 eq. D6 had no effect on the tolerated oscillatory strain. This may be due to the different morphology of fibrils from D6 and the therefore different interaction with the polypeptide backbone. While the fibrillary networks extensively interact with the brush, making it stiffer and less flexible, the fibrillary stacks formed by D6 seemed to be easily displaceable against the polypeptide backbone, leading to a slightly harder but equally as flexible hydrogel. Moreover, these experiments showed a very interesting behaviour of the hydrogels at an oscillatory strain of 1 %. While G' and G'' of H1 behaved constant, some of the hydrogels with added depsi peptides showed a peak in G'' and a steady decrease of G' and G'' at this strain. This peak was most dominant when D1 was

added, which also formed a crosslinked fibrillary network in TEM. For H1+50 eq. D4, the peak was only very small, correlating to the weaker fibrillary network it showed in TEM images. No peak was visible when D6 was added, which was shown to not form fibrillary networks but stacks. This led to the hypothesis that this peak arose from the fibrils. At strains of up to 1 %, properties of the hydrogel associated with the fibrillary networks were depicted, while the hydrogels with added peptides behaved like the H1 hydrogel at oscillatory strains of over 1 %. To correctly represent the behaviour of the hydrogels, frequency sweeps were performed at 0.1 % oscillatory strain. However, the exact structural alteration of the hydrogels upon increasing strain still needs to be elucidated.

The most remarkable feature of the previously reported H1 hydrogel was its capability to self-heal, meaning G' returning to its initial value, immediately after its disruption via high oscillatory strains. Via comparison of G' before and seconds after the first rupture, self-healing efficiency was assessed and is displayed in Figure 21.

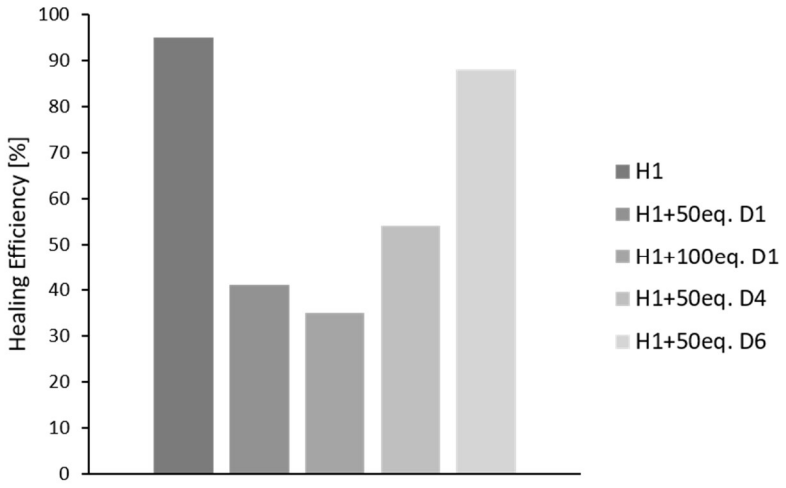

Figure 21: Comparison of the self-healing efficiencies from thixotropy measurements. Values were generated by comparing G' values before and after the first disruption of the hydrogels by application of high oscillatory strains (0.01-1000 %) with a following healing period with low oscillatory strain applied (0.1 %).

Similarly to the published H1, the herein synthesized H1 showed a nearly quantitative (95 %) ability to self-heal immediately after disruption. Upon addition of 50 eq. D1, the self-healing efficiency decreased to 41 %. This may arise from the prolonged time H1+50 eq. D1 needed to fully gel compared to H1. During the 800 sec. healing time, it could be seen that G' rose gradually until it was disrupted again by oscillatory strain, but did not reach the initial G' value. The same findings were made for H1+100 eq. D1, where the self-healing ability was further decreased to 35 %. A possible explanation is the even longer time the excess D1 needed to reassemble compared to H1+50 eq. D1, which could also be seen in the gelation time. When 50 eq. of D4 were added, the immediate self-healing decreased

to 54%. This could be due to the weaker fibrillary network D4 formed, which potentially also needed less time to build than the network of D1 fibrils, leading to a better self-healing of H1+50 eq. D4 compared to H1+50 eq. D1. A self-healing efficiency as high as 88 % was found for H1+50 eq. D6, which is a similar range than for H1. Analogically to the findings before, this could be due to the fibrillary stacks, which possibly are displaceable within the polypeptide backbone, and whose fibrillation could be less time-consuming compared to the assembly into fibrillary networks. This could also be seen in the gelation time of H1+50 eq. D6, which was not as time consuming than the gelation of H1 with additional fibrils that assembled into networks.

Due to time and material restriction, frequency sweeps could only be performed for three hydrogels and were performed with 0.1 % oscillatory strain, instead of 1 % as described in Gačanin et al. (2019). For G' and G'' of H1+50 eq. D1, H1+100 eq. D1, and H1+50 eq. D6, no frequency dependence was found in the tested range. In first frequency sweep, performed for H1+50 eq. D1 at 1 % oscillatory strain, G'' was found to be higher than G', which would correspond to a material that behaved like a viscous fluid instead of a gel (Supplementary Data, Figure 31B). Taken together with the findings of the oscillatory sweeps, showing a peak at 1 % strain for hydrogels with added fibrillary networks, it was concluded that these conditions didn't represent the characteristics of the hydrogels correctly and therefore the parameter had to be adjusted for time and frequency sweeps, since G' and G'' should behave constantly in the range of the fixed parameter (Zuidema et al. 2014).

From the conducted experiments, it could be concluded that the impact of fibrillary structures on the peptide-protein hybrid material is heavily dependent on the characteristics of the fibrils, and to a lower extent on the charge. Addition of the depsi peptide which had the same sequence as the gelator (D1) or had two amino acids exchanged for a negative charge (D4) led to a stiffer hydrogel, which could not tolerate as much oscillatory strain and whose self-healing was impaired with increasing number of equivalents. These depsi peptides formed fibrillary networks. Addition of a depsi peptide which formed a different fibril morphology, described as fibrillary stacks, led to the formation of stiffer hydrogels which could tolerate the same percentage of oscillatory strain and whose self-healing was only slightly less effective.

Summary and Outlook

In literature, a peptide-protein hybrid material was described, which showed some highly interesting characteristics (Gačanin et al. 2019). Due to the depsi structure the crosslinking peptide had, its fibrillation and therefore gelation was inducible upon pH increase. Characterization of the hydrogel using rheology revealed that it gelled instantaneously, was able to bear oscillatory strain and, most importantly, showed efficient self-healing on microscopic and macroscopic levels. Copolymerisation of the hybrid with additional free depsi peptide was described to introduce other functionalities. Derived from this, the aim of this thesis consisted in the alteration of the mechanical characteristics described by Gačanin et al. (2019) by addition of free depsi peptides during polymerisation. For this, the depsi peptides should exhibit the following characteristics, derived from the peptide that was used as gelator: inducibility of fibrillation via pH increase, fibril morphology, and a β-sheet secondary structure. Using different characterization methods, three types of depsi peptides were quested: one that has the same characteristics as the gelator to test the impact of the same free depsi peptide on the gel; one negatively charged that is structurally equivalent to the first one to evaluate the effect of opposite charges on the hydrogel; and one with a different fibril morphology to study its impact on the hydrogel.

To pursue this, the first step consisted of the synthesis of depsi peptides utilizing manual as well as microwave-assisted SPPS. Using manual synthesis, yields of D1 (KIKI*SWINM) were comparable to published data for the same peptide (Gačanin et al. 2019), demonstrating that manual synthesis as viable alternative, especially when synthesizing multiple batches at once when large quantities of depsi peptides are needed. As a negative peptide, the lysine residues of D1 were exchanged for glutamic acid residues, yielding in D4 (EIEI*SQINM). Furthermore, three new depsi peptides were synthesized based on the fibril morphology of their peptide precursors, which exhibited short, rounded fibrils and a heavily crosslinked network. From this, D5 (CKIK*SQII), D6 (KIKQ*SIINMWQ), and D7 (KIKQI*SINMWQ) were synthesized. Upon characterization, it was found that D1 behaved similarly to D1 described in literature (Gačanin et al. 2019). D4, the negative equivalent of D1, formed less connected fibrillary networks compared to D1. These depsi peptides were chosen as suitable candidate for the application in the hydrogel, as they fulfil the requirements of depsi peptides that are structurally similar to the gelating peptide (D1) and structurally similar but negatively charged (D4). Characterization of D5, D6, and D7 revealed that D5 formed aggregations instead of fibrils, consisting of α-helices, excluding it from hydrogel testing. D6 exhibited a highly interesting fibril morphology consisting of fibrillary stacks, and was therefore chosen as an excellent candidate which fulfilled the requirement for a depsi peptide showing a different fibril morphology compared to D1. D7, which differed from D6 in the placement of serine, showed a highly interesting fibrillar network which was denser than that formed from D1, making it an interesting candidate, but the yield was too low to actually perform copolymerisation experiments. From these two candidates compared to the

precursor, as well as D5 compared to its precursor, it could be concluded that the placement of serine and therefore the placement of the ester bond is crucial and can change the characteristics of the resulting fibrils drastically compared to fibrils formed from the original peptide. Likely, this arose from the alteration of the orientation of the amino acid side chains, yielding in a different morphology. In conclusion, three depsi peptides could be synthesized that fulfilled the listed requirements and could be used in copolymerisation experiments: D1, D4, and D6.

The next step consisted in the synthesis and characterisation of the backbone, a peptide-protein hybrid. For that, HSA was cationized using EDA, making more primary amino groups available for following reactions. Afterwards, PEGylation was performed to enhance water retention and stability of the hydrogel. Finally, the sulfhydryl groups were made accessible via denaturation, which were later used to graft maleimide-modified D1 depsi peptides onto the backbone, yielding in the hybrid material described in literature (Gačanin et al. 2019). Characterization via MALDI revealed that the number of grafted EDA chains, as well as PEG chains, was close to the values from literature. Therefore, it could be concluded that the backbone could be used for hydrogel synthesis.

The final and main part of this thesis was the preparation of hydrogels from the provided components. First, a hydrogel without any free depsi peptide was made to verify and reproduce the published data (Gačanin et al. 2019). The herein prepared H1 hydrogel was slightly stiffer and was able to tolerate higher percentages of strain. Additionally, self-healing efficiency was similar to H1 from literature, leading to the conclusion that it could be reproduced successfully, although the reason for the enhanced stiffness and strain tolerance remained unclear. H1+50 eq. D1 built a stiffer hydrogel whose mechanical properties were independent of the applied frequency, which tolerated less oscillatory strain. Furthermore, the immediate self-healing efficiency was impaired. The results from H1+100 eq. D1 were in line with these findings. This hydrogel was even stiffer, its mechanical properties were still independent of frequency, and it tolerated even less oscillatory strain. Additionally, self-healing efficiency was further impaired. Summarized, the copolymerisation of H1 with free D1 led to stiffer hydrogels, lower tolerance and lower self-healing efficiency with increasing D1 content, but not in a proportional relation, except for strain tolerance, where a linear relationship was found. H1+50 eq. D4 was stiffer, tolerated less oscillatory strain, and also had an impaired self-healing efficiency compared to H1. H1+100 eq. D4 was even stiffer, but also not in a proportional manner. Since both depsi peptides, D1 and D4, were shown to form fibrillary networks, it could be concluded that these findings could be explained by the fibrillary network, which interacted with the backbone either by intercalating into the grafted D1-Mal strands, or the formation of a network that laid over the backbone, yielding in stiffer hydrogels. Tolerance of oscillatory strain decreased, likely due to the earlier rupture of the fibrillary structures rising from D1 and D4, which is indicated by the additional peak in the oscillatory strain cures compared to H1. Similarly, the self-healing is impaired because the reconstruction of the

fibrillary network needed more time compared to the backbone. H1+50 eq. D6 was also stiffer than H1, its stiffness was frequency independent, it tolerated the same percentage of oscillatory strain, and self-healing efficiency was only slightly weaker. These findings arose from the fibril morphology of D6 forming fibrillary stacks, which could intercalate into the grafted D1-Mal chains. Since no fibrillary network is formed, the rearrangement of fibrils and backbone could be performed quicker, as well as the possibility to move the fibrillary stacks against the brush. However, the exact interaction between backbone and fibrils needs to be further elucidated.

In summary, it can be concluded that alterations of rheological characteristics could be realised by convenient copolymerisation of the peptide-protein hybrid and additional free depsi peptides. Since the time was restricted, no more experiments for n=3 or with other numbers of equivalents or depsi peptides could be performed. This would be a prerequisite to precisely determine the properties of the hydrogels. The herein introduced hydrogels could be, as previously reported for the H1 hydrogel (Gačanin et al. 2019), used as cell matrices for different cell types. Using copolymerisation with free depsi peptides, the mechanical properties of the hydrogels could be fine-tuned to provide an optimal scaffold for various cell types, and possibly also be applied in biomedical applications, since the components of the hydrogel are biomaterial-derived. Furthermore, since H1 was shown to be injectable (Gačanin et al. 2019) the hydrogels could be used as a tool for targeted drug delivery. This could be realized via the modification of the free depsi peptides and the controlled release of their cargo via degradation of the components. Further possibilities for follow up experiments seemed endless in this topic, since there are various depsi peptide sequences that could be tested as well. From these possibilities, the impact of a negatively charged depsi peptide that forms fibrillary stacks would be particularly interesting, since copolymerisation with fibrillary stacks showed better self-healing properties. Also, hydrogels with mixed depsi peptides could be a possibility. Pursuing this, a neutral hydrogel could be synthesized by mixing D1 and D4 into the gel. Furthermore, D1 and D6 could be copolymerized into the hydrogel for better self-healing than D1 alone, possibly also with modified depsi peptides for added functionalities by utilizing the side chains or termini for additional reactions prior copolymerisation. Apart from possible modifications by changing the free depsi peptide, the backbone could be altered as well, for example by grafting more or less D1-Mal. Interesting results could possibly be obtained upon maleimide modification of D6 and utilizing D6-Mal as a gelator for hydrogel formation. Also, different quantities of the backbone could be used for a higher or lower weight percentage in the hydrogel. By alterations of all components of the hydrogel, it would be possible to obtain hydrogels with a range of mechanical properties and characteristics, which could then be used in biomedical or regenerative medicine.

Material and Methods

Synthesis and Characterization of Peptides

Manual Synthesis of Peptides via SPPS

All peptides used for this project were synthesized via automated and mostly manual solid phase strategy according to Merrifield (1963). The peptides were synthesized from C- to N-terminus on solid support. Therefore, the needed amount of Wang resin (Table 6), covalently loaded with the initial Fmoc-protected amino acid, was swollen in dimethyl formamide (DMF) for at least 3 h at RT.

Table 6: Calculated masses of resins used for the synthesis of peptides, depending on the degree of substitution and the batch quantity. Resins were swollen in DMF for a minimum of 3 h.

Resin type	Substitution [mmol/g]	Batch quantity [mmol]	Mass [g]
Fmoc-Met-Wang	0.68	0.2	0.295
		0.1	0.147
Fmoc-Ile-Wang	0.69	0.1	0.145
Fmoc-Gln(Trt)-Wang	0.58	0.1	0.172

After washing with DMF, the first amino acid bound to the resin was deprotected. For deprotection, 25 vol.-% piperidine in DMF was added to the resin and incubated for 10 min at 70 °C (Heraeus B12, Thermo Electron Corporation), twice, followed by a washing step. To couple the next amino acid, five equivalents of the protected amino acid (Table 8) were dissolved in DMF. In order to activate the C-terminus, benzotriazol-1-yl-oxytripyrrolidinophosphonium hexafluoro-phosphate (PyBOP) and N,N-diisopropylethylamine (DIPEA) were added to the amino acid solution. Coupling was performed for 1 h at 70 °C while rotating the vials (rotary mixer 34526, snijders). After coupling, the resin was washed with DMF.

The volumina of reactants, depending on the batch size, are given in Table 7.

Table 7: Summary of volumina of reactants used for the synthesis of peptides for this thesis.

Synthesis step	Batch size [mmol]	Volume and amount of reactant
Wash	0.2	7.5 mL DMF, four times
	0.1	3 mL DMF, four times
Deprotection	0.2	6 mL 25 vol.-% piperidine in DMF, twice
	0.1	3 mL 25 vol.-% piperidine in DMF, twice
Activation	0.2	1 mL PyBOP (1 mmol, 5 eq) 400 µL DIPEA (2.30 mmol, 11.5 eq)
	0.1	1 mL PyBOP (0.5 mmol, 5 eq) 200 µL DIPEA (1.15 mmol, 11.5 eq)
Coupling	0.2	1 mmol amino acid in 2.5 mL DMF (5 eq)
	0.1	0.5 mmol amino acid in 2.5 mL DMF (5 eq)

In order to synthesize depsi peptides, the strategy had to be changed in order to couple the next amino acid to the hydroxy group of the serine side chain. The following amino acid was dissolved, activated and reacted with the peptide for 2 h at 70 °C. This procedure was repeated without prior deprotection. Subsequently, the following sequence was synthesized using the described standard protocol.

Peptides were stored in DMF at 4 °C with Fmoc-protected N-terminus.

Table 8: Calculated masses of amino acids used for the synthesis of peptides. The fivefold amount, in comparison to the respective amount of resin, was completely diluted in 2.5 mL of DMF and activated using PyBOP and DIPEA.

Amino acid	Used derivative	Molecular mass [g/mol]	Fivefold equivalent of batch quantity [mmol]	Mass [g]
Asn, N	Fmoc-Asn(Trt)-OH	596.67	1	0.597
			0.5	0.298
Gln, Q	Fmoc-Gln(Trt)-OH	610.70	1	0.611
			0.5	0.305
Ile, I	Fmoc-Ile-OH	353.41	1	0.354
			0.5	0.178
Lys, K	Fmoc-Lys(Boc)-OH	468.54	1	0.469
			0.5	0.234
Glu, E	Fmoc-Glu(OtBu)-OH	425.47	1	0.425
			0.5	0.213
Ser, S	Boc-Ser-OH	205.21	1	0.205
			0.5	0.103
Cys, C	Fmoc-Cys(Trt)-OH	585.72	0.5	0.293
Met, M	Fmoc-Met-OH	371.45	0.5	0.186
Trp, W	Fmoc-Trp(Boc)-OH	526.58	0.5	0.263

Maleimide-Functionalization of the N-Terminus

Prior functionalization of the N-terminus of peptides, the resin-bound peptides were split into 0.05 mmol batches. The reactions were performed in a microwave-assisted peptide synthesizer (Biotage Initiator+). The volumina of reactants used for this reaction are listed in Table 9. Deprotection of the N-terminus was performed using 25 vol.-% piperidine in DMF twice, respectively, incubating for 3 min and 10 min, followed by a washing step, using DMF and shaking four times. The maleimide-NHS-ester (3-(maleimido)propionic acid N-hydroxysuccinimide ester) was used in 2.5 fold surplus and added to the deprotected peptide. The functionalization was performed microwave-assisted for 2 h at 40 °C and 500 rpm. After functionalization, the vial was washed with DMF. The resin-bound functionalized peptide was stored in DMF at 4 °C.

Table 9: Summary of volumina of reactants used for the functionalisation of peptides with maleimide.

Synthesis step	**Volume and amount of reactants**
Wash	3 mL DMF, four times
Deprotection	3 mL 25 vol.-% piperidine in DMF, twice
Functionalization	33.28 mg (0.125 mmol) in 1.8 mL DMF

Cleavage and Precipitation of Peptides

To obtain the solid peptide, it had to be cleaved off the resin, precipitated, resuspended and lyophilized. Volumina of the reactants depended on the batch size, and are given in Table 10. For cleavage, a cocktail of 95 vol.-% trifluoroacetic acid (TFA), 2.5 vol.-% H_2O and 2.5 vol.-% triisopropylsilane (TIPS) was prepared and added to the resin. Cleavage occurred for 2 h at RT and mild shaking at 250 RPM (HLC MKR13). To precipitate the cleaved off peptide, the solution was introduced into ice cold diethyl ether. Upon centrifugation for 5 min at 4 °C and 3500 RPM (Beckman Coulter Allegra X15R, Brea, CA, USA), a pellet of crude peptide was obtained. To wash the peptide pellet, the ether was decanted and the tube was refilled with cold diethyl ether. After resuspension of the pellet, the solution was centrifuged again. The precipitation step was performed twice. After final decanting, the pellet was dried for 2 h in the fume hood. The dried pellet was resuspended in 0.1 vol.-% TFA in H_2O, and lyophilized for 2 d (Alpha 2-4 LD, Christ). After lyophilization, the peptide was obtained as a white solid.

Table 10: Volumina of reactants for cleavage, precipitation and resuspension of peptides, depending on the amonunt of substance of the batch.

Reactant	Volume for 0.1 mmol batch	Volume for 0.05 mmol batch
TFA	9.5 mL	4.75 mL
H_2O	250 µL	125 µL
TIPS	250 µL	125 µL
Total cleavage cocktail	10 mL	5 mL
Diethyl ether	40 mL	20 mL
0.1 vol.-% TFA in H_2O	20 mL	10 mL

Purification via High Performance Liquid Chromatography (HPLC)

To purify the synthesized peptides, reversed phase chromatography was performed. Therefore, a non-polar stationary phase (LiChroCART 250-10 RP-18, Merck) and a mobile phase consisting of a gradient (Table 11) of acetonitrile (ACN) and H_2O, each mixed with 0.1 vol.-% TFA, were used.

Table 11: Gradient used to purify the peptides via HPLC. Acetonitrile and H_2O, each mixed with 0.1 vol.-% TFA, were used as mobile phase.

Time [min]	ACN + 0.1 vol.-% TFA [%]	H_2O + 0.1 vol.-% TFA [%]
2	5	95
10	10	90
20	40	60
37	100	0
42	5	95
44	5	95

The crude peptide was dissolved in acidic water (0.1 vol.-% TFA, 1.2 mg/mL), filtered (Corning Costar Spin-X centrifuge tube filters with nylon membrane, 0.45 µm pore size) and 2 mL were injected into the HPLC unit per run. Peptides were detected via absorption measurement at 214 nm, where peptide bonds absorb, and at 280 nm, where absorbance of aromatic amino acids can be detected. Peptides were collected manually.

To remove the ACN from the fractions, they were centrifuged under vacuum for 1.5 h using speedvac (Univapo 150H, UniEquip). They were lyophilized for 2 d. Thus, the peptides were obtained as white solids. Purity was assessed via LC-MS.

Mass Analysis via Matrix-assisted Laser Desorption Ionisation (MALDI-ToF-MS or MALDI-FT-ICR-MS)

Identification of synthesized products was done via MALDI-MS. Peptides were measured via MALDI-FT-ICR, the identification of proteins was done via MALDI-ToF-MS.

To identify crude products, a sample of solvent free resin-bound peptide was mixed with 40 µL of TFA and incubated for 20 min at 250 RPM. An aliquot of 20 µL was diluted in 40 µL of an ACN/H_2O-mixture (1:1) and submitted to measurement. Purified peptides were measured either using an aliquot of 20 µL of the HPLC fraction or dissolving the lyophilized product in 20 µL of ACN/H_2O-mixture (1:1). Until further preparation, samples were stored at 4 °C. For the measurement, the peptide was crystallized in a matrix consisting of a saturated solution of α-cyano-4-hydroxycinnamic acid in H2O/ACN (1:1) with 0.1 vol.-% TFA. From the peptide samples, 1 µL was mixed with 1 µL of matrix solution, and 1 µL of the resulting solution was placed on the target plate. The remaining sample was further diluted with 1 µL of matrix solution, and 1 µL of this mixture was spotted on the target as well. Preparation and measurement were performed by Dr. Markus Lamla on a Bruker solariX Hybrid 7T FT-ICR mass spectrometer (Bruker Corporation).

For the measurement of proteins, an 1 µL aliquot was taken while ultrafiltration and diluted in 9 µL of Milli-Q-H_2O or 0.1 % aqueous TFA in case of BD1 samples. Protein samples were crystallized using a saturated solution of sinapinic acid in H_2O/ACN (1:1) as matrix. Therefore, 1 µL of sample was mixed with 1 µL of the matrix, and 1 µL of the resulting solution was spotted on the target plate. The remaining sample was diluted once more with 1 µL of matrix, and 1 µL was spotted on the plate as well. Preparation and measurement were performed by Marco Hebel on a Bruker Reflex III MALDI-ToF mass spectrometer (Bruker Corporation).

Preparation of Peptide Stock Solutions

Stock solutions of all peptides were prepared in DMSO in a 10 mg/mL concentration. Until further utilization, they were stored at 4 °C.

Transmission Electron Microscopy (TEM)

To prepare samples for TEM, 10 µL of the 10 mg/mL peptide stock solution were introduced into 90 µL sterile filtered (0.22 µm pore size) 0.1 % aqueous TFA or phosphate buffered saline (PBS), yielding a 1 mg/mL peptide solution. Upon incubation on a shaker (600 rpm) at 37 °C for 24 h, the solutions were centrifuged shortly (< 2000 rpm, 5 sec) and vortexed. 3 µL of each peptide solution were placed on a

copper grid and incubated at RT for 5 min. After removing the solution using filter paper, 7 µL of aqueous 2 % uranyl acetate solution were pipetted on the grids to counterstain fibrillary structures. Subsequent to an incubation of 5 min at RT, the grids were washed three times with Milli-Q-H_2O, excess liquid was removed using filter paper and the grids were air dried for 30 min at RT. Imaging was performed with a JEOL 1400 transmission electron microscope in vacuum and an acceleration voltage of 120 kV was used.

Conversion Assay

Peptide solutions were prepared adding 20 µL of each 10 mg/mL stock solution to 180 µL sterile filtered (0.22 µm pore size) 0.1 % aqueous TFA or PBS, yielding a 1 mg/mL solution. After incubation at 37 °C and 600 rpm overnight, short centrifugation (< 2000 rpm, 5 sec) and mixing thoroughly, 100 µL of each sample were ultra-filtered using Vivaspin 500 tubes (3000 Da MWCO) at 13.2 krpm and 4 °C for 99 min. Upon centrifugation, the filtrate and the remaining 100 µL of original sample were lyophilized overnight. The obtained solids were dissolved in 25 µL DMSO. 10 µL of these solutions were placed in a 384 well plate (Greiner 384 Flat Bottom Transparent Polystyrol small volume) in duplicates. As a control, 10 µL of DMSO were used instead of peptide solution, twice. To perform fluorescence measurement, a 3 mg/mL fluorescamine solution was prepared in DMSO, whereof 3 µL were mixed into the samples. During incubation for 20 min at RT in the dark, fluorescamine interacts with free amino groups of the peptides. Fluorescence reading was performed at λ_{ex} = 365 nm and λ_{em} = 470 nm with multiple reads per well (3x3; infinite M1000 reader, TECAN). The conversion rate (CR) of each peptide in both solvents (0.1 % aqueous TFA and PBS) was calculated according to equation 1, whereby the value for DMSO is set to 1.

$$CR = 100 - \frac{100 * fluoresc.\ intensity\ (filtrate)}{fluoresc.\ intensity\ (original)}\ [\%] \qquad 1$$

The measurement was performed three times with independently prepared samples.

Thioflavin T (ThT) Assay

As described before, 100 µL of a 1 mg/mL peptide solution was obtained from diluting a 10 mg/mL stock solution and in sterile filtered (0.22 µm pore size) PBS. These solutions were incubated over night at 37 °C and 600 rpm. After short centrifugation (< 2000 rpm, 5 sec) and mixing thoroughly, 4 µL of each solution were introduced into 20 µL ThT in PBS (50 µM) in a 384 well plate (Greiner 384 Flat Bottom Black Polystyrol). As control, 4 µL PBS were used instead of peptide solution. All peptides and

the control were prepared in quadruplets. After an incubation time of 10 min at RT in the dark, fluorescence reading was performed. The measurement was executed upon excitation at λ_{ex} = 440 nm and emission was captured at λ_{em} = 488 nm (infinite M100 reader, TECAN). Each well was read multiple times (3x3). Three measurements with independently prepared samples were performed.

Fourier-Transform Infrared Spectroscopy (FT-IR)

Peptides were prepared using 10 µL of DMSO stock and 90 µL sterile filtered (0.22 µm pore size) 0.1 % aqueous TFA or PBS, leading to a 1 mg/mL solution. Upon incubation at 37 °C and 600 rpm overnight, samples were shortly centrifuged (< 2000 rpm, 5 sec), vortexed, and lyophilized for 1 d. Transmittance of solid compounds was measured on a spectrometer (Bruker Tensor 27, Bruker Corpopration). For analysis, absorbance of the peptides in the amide I region (1600-1700 1/cm) were used.

Zeta Potential

Two 1 mg/mL peptide solutions were prepared using 10 µL of stock solution and 90 µL sterile filtered (0.22 µm pore size) PBS per peptide. Upon incubation on a shaker (600 rpm, 37 °C) overnight, short centrifugation (< 2000 rpm, 5 sec) and vortexing, the solutions were split into 50 µL aliquots and 1 mM KCl solution was added to give 1 mL of sample (0.05 mg/mL). Measurement of zeta potential was performed in 1 mL folded capillary cells on a zetasizer (Zetasizer Nano ZS, Malvern Instruments) and analyzed using zetasizer software (Malvern Panalytical). Values were generated using at least three independently measured samples.

Preparation of the Protein Backbone

Cationization of Human Serum Albumin (cHSA)

The synthesis of cHSA was performed as previously described in the literature (Gačanin, Kovtun et al. 2017). In brief, native HSA (500 mg, 7.5 µmol) was dissolved in 50 mL ethylenediamine (EDA) solution (2.5 M, pH 4.75). Upon the addition of 1-ethyl-3-(3-dimethylaminopropyl)carbodiimide hydro-chloride (EDC; 2.56 g, 13.3 mmol), the solution was stirred for 3 h at RT. To stop the reaction, acetate buffer (3.4 mL, 4 M, pH 4.75) was added and stirred for another 5 min. The solution was concentrated via ultrafiltration (Vivaspin 20 tubes, 30 kDa MWCO), washed 2 times using acetate buffer (100 mM, pH 4.75) and 6 times using Milli-Q-H_2O. Thereafter, cHSA was lyophilized (Christ Alpha 2-4 LD) for 2 days and obtained as a white solid.

PEGylation of cHSA (cHSA-PEG)

The procedure was performed as described in literature (Gačanin, Kovtun et al. 2017). The exact volumina and masses for all three individually prepared batches are listed in Table 12. In an initial step, phosphate buffer (50 mM, pH 8) was degassed, where cHSA was subsequently dissolved. After that, MeO-PEG(2000)-NHS ester was dissolved in DMSO and added to the cHSA solution. The reaction was stirred for 135 min at RT. The product was concentrated using ultrafiltration (Vivaspin 20 tubes, 30kDa MWCO) and washed 8 times using Milli-Q-H_2O. Finally, cHSA-PEG was lyophilized (Christ Alpha 2-4 LD) for 2 days and obtained as a white solid.

Table 12: Masses of cHSA and MeO-PEG(2000)-NHS ester and volumina of phosphate buffer (50 mM, pH 8) and DMSO used for the PEGylation of cHSA.

	Batch 1 (100 mg)	**Batch 2 (100 mg)**	**Batch 3 (315 mg)**
Volume of phosphate buffer	50 mL	50 mL	175 mL
Amount of cHSA	0.1005 g (1.38 µmol)	0.1001 g (1.38 µmol)	0.3147 g (4.34 µmol)
Amount of MeO-PEG(2000)-NHS ester	0.1022 g (37 eq)	0.1025 g (37 eq)	0.3515 g (40 eq)
Volume of DMSO	400 µL	400 µL	1 mL

Denaturation of cHSA-PEG (dcHSA-PEG)

Denatured cHSA-PEG was prepared according to the literature (Gačanin et al. 2019). Masses of solids and solvents used for all individually prepared batches are listed in Table 13. After degassing of urea sodium buffer (5 M urea, 50 mM sodium phosphate, pH 7.4) using Schlenk technique, cHSA-PEG was added under argon atmosphere. The solution was stirred under argon for 15 min to denature the cHSA-PEG. Subsequently, tris(2-carboxyethyl)phosphine hydrochloride (TCEP, 95 eq), was dissolved in the same urea sodium buffer (10 µL) and introduced into the protein solution to reduce all disulfide bridges and transfer them into reactive sulfhydryl groups. The reaction was stirred overnight under argon for complete protein denaturation. The product was concentrated using ultrafiltration (Vivaspin 20 tubes, 30 kDa MWCO) and washed 5 times with Milli-Q-H_2O. Upon lyophilization (Christ Alpha 2-4 LD) for 2 days, dcHSA-PEG was obtained as a white solid.

Table 13: Masses of cHSA-PEG and TCEP and volume of urea sodium phosphate buffer (5 M urea, 50 mM sodium phosphate, pH 7.45) used to synthesize dcHSA-PEG.

	Batch 1	Batch 2	Batch 3	Batch 4
Volume of buffer	12.5 mL	12.5 mL	15 mL	15 mL
Amount of cHSA-PEG	25.3 mg (218 nmol)	25.2 mg (218 nmol)	35.5 mg (334 nmol)	35.4 mg (334 nmol)
Amount of TCEP	5.962 mg (20.8 µmol)	5.967 mg (20.8 µmol)	9.102 mg (31.7 µmol)	9.031 mg (31.5 µmol)

Preparation of the Depsi-Brush (BD1)

The backbone for hydrogel formation was prepared following a protocol described in literature (Gačanin et al. 2019). The exact masses and volumes of all needed materials for this synthesis are listed in Table 14. In a first step, dcHSA-PEG was dissolved in DMSO. Next, D1-Mal, a maleimide modified depsi peptide, was predissolved in DMSO and added to the dcHSA-PEG solution. After mixing the solutions thoroughly, the reaction was stirred for 24 h at RT and 1150 rpm. The product was washed 5 times via ultrafiltration (Vivaspin 6 tubes, 30 kDa MWCO) using 0.1 % aqueous TFA. The depsi-brush was obtained as a white solid upon lyophilization (Christ Alpha 2-4 LD) for 2 days.

Table 14: Masses of dcHSA-PEG and D1-Mal peptide and volumina of DMSO to solve both solids in order to form the depsi-brushes (BD1)

	Batch 1	Batch 2	Batch 3	Batch 4	Batch 5
Amount of dcHSA-PEG	21.0 mg (0.18 µmol)	16.3 mg (0.15 µmol)	16.7 mg (0.16 µmol)	16.2 mg (0.15 µmol)	16.2 mg (0.15 µmol)
Volume of DMSO for dcHSA-PEG	200 µL	170 µL	170 µL	170 µL	170 µL
Amount of D1-Mal	4.444 mg (3.63 µmol)	3.7362 mg (3.05 µmol)	3.8712 mg (3.16 µmol)	3.760 mg (3.07 µmol)	3.764 mg (3.07 µmol)
Volume of DMSO for D1-Mal	60 µL	50 µL	50 µL	50 µL	50 µL

Synthesis of Hydrogels

Hydrogels without additional free peptide were prepared according to literature. In brief, 1.2 mg of the depsi-brush (BD1) were swollen in 30 µL of 100 mM phosphate buffer (pH 7.4), yielding in a 4 wt.-% hydrogel (Gačanin et al. 2019). To test effects of additional free peptide, BD1 was added to 50 eq. or 100 eq. of peptide in solid form (Table 15). After mixing the two solid compounds, 30 µL of 100 mM phosphate buffer (pH 7.4) were added to initialize hydrogel formation.

Table 15: Masses of peptides to form hydrogels with 50 eq. or 100 eq. of free peptide. Hydrogels were formed using 1.2 mg of BD1 and 30 µL 100 mM phosphate buffer, yielding in a 4 wt.-% hydrogel.

	D1	**D4**	**D5**	**D6**	**D7**
Mass for 50 eq.	0.44 mg	0.44 mg	0.39 mg	0.57 mg	0.57 mg
Mass for 100 eq.	0.89 mg	0.89 mg	0.77 mg	1.15 mg	1.15 mg

Rheological Characterization of the Hydrogels

For the rheological characterization, a DHR3 rheometer (TA Instruments) was used. The test geometry consisted of 8 mm parallel plates with solvent trap to prevent the hydrogels from drying, and gap sizes from 420 µm to 500 µm for 30 µL of hydrogel were used. Hydrogels were prepared as previously described and placed on the test geometry. Following an initial time sweep measurement, either strain sweeps with following time sweeps or a frequency sweep was performed. Following experiments were conducted at 25 °C:

1. Time sweep: To determine the mechanical properties of the hydrogels, time sweeps were performed at fixed strain (1 % or 0.1 %) and fixed frequency (1 Hz). This experiment was performed until the storage modulus (G') and the loss modulus (G'') were constant.

2. Strain sweep: Oscillatory strain sweeps (0.01-1000 %) were performed at a fixed frequency (1 Hz) to determine the percentage of strain the hydrogels tolerated until gel-to-sol transition occurred.

3. Thixotropy measurements: Cycles of oscillatory strain sweeps (0.01-1000 %) with fixed frequency (1 Hz) followed by a 800 s oscillatory time sweep with fixed strain (0.1 %) and fixed frequency (1 Hz), conducted three to four times in a row. With this experiment, the self-healing of the hydrogels after disruption via shear stress is analysed. Comparison of the self-healing capacities was performed by comparing the storage modulus of the hydrogels before and after (13 s) the initial disruption.

4. Frequency sweep: Frequency sweeps (0.05-100 Hz) were conducted at a fixed oscillatory strain (1 % or 0.1 %) to determine the frequency dependence of the mechanical properties of the hydrogels.

Annex

Supplementary Data

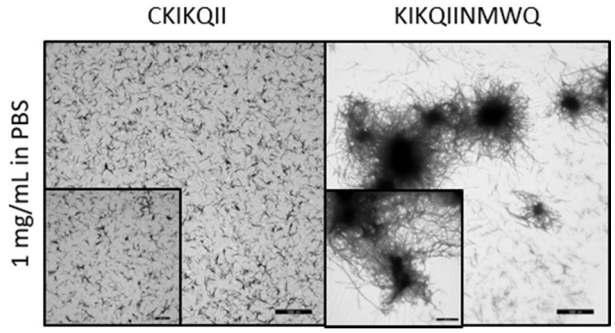

Figure 22: Transmission electron microscopy images of 1 mg/mL solutions of CKIKQII (D5 precursor) and KIKQIINMWQ (D6 and D7 precursor). Samples were incubated in PBS (pH 7) for 24 h to allow fibrillation. Scale bars are 1 µm and 500 nm in the insets. Laboratory work and imaging were performed by Thomas Mack.

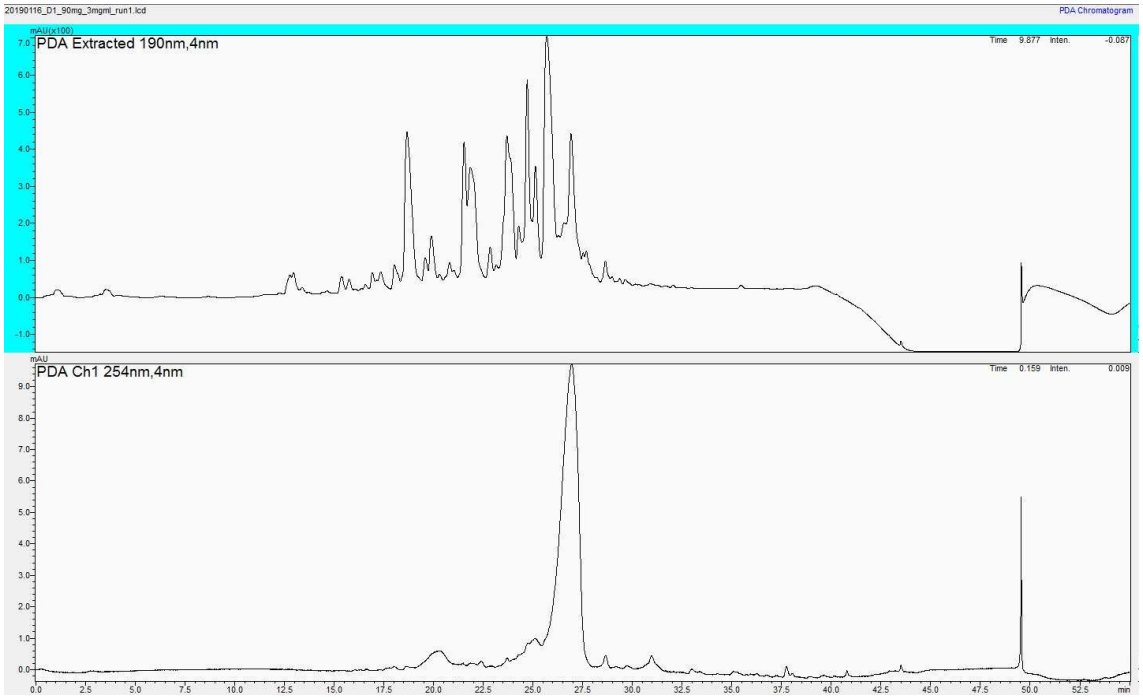

*Figure 23: HPLC chromatogram of D1 (KIKI*SQINM). The upper panel shows absorbance at 190 nm (peptide bonds). The lower panel shows absorption at 254 nm, which should be 280 nm but was set wrongly. The peak at a retention time of 25.6 min (upper panel) contained the desired peptide.*

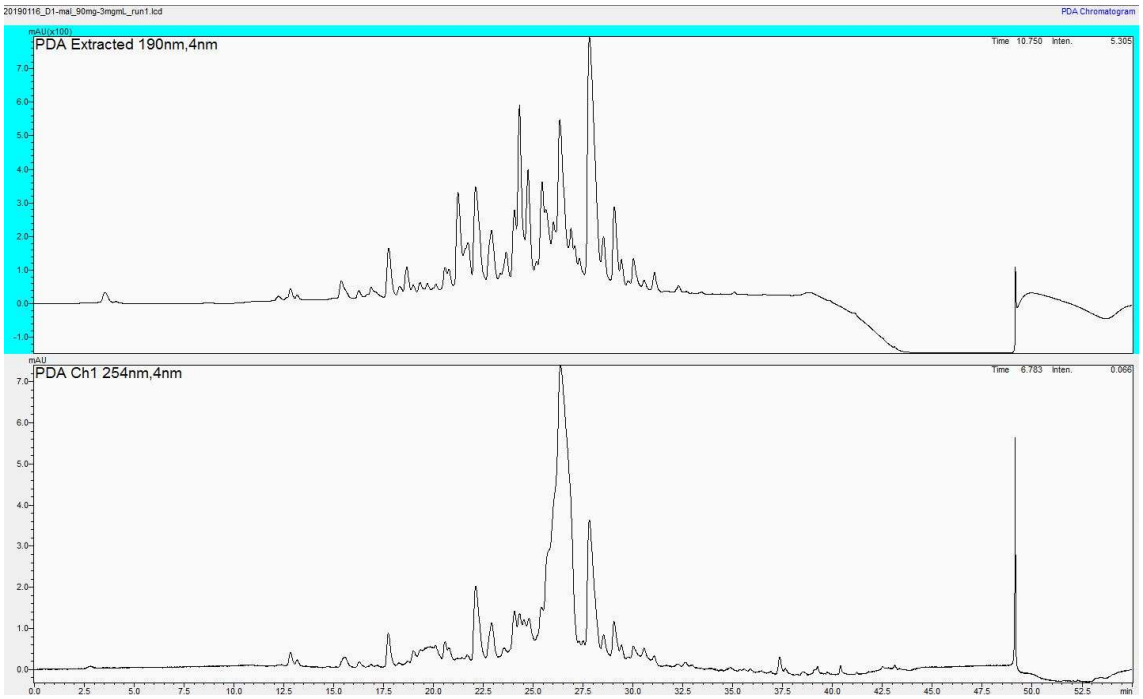

*Figure 24: HPLC chromatogram of D1-Mal (Mal-KIKI*SQINM). The upper panel shows absorbance at 190 nm (peptide bonds). The lower panel shows absorption at 254 nm, which should be 280 nm but was set wrongly. The peak at a retention time of 27.2 min (upper panel) contained the desired peptide.*

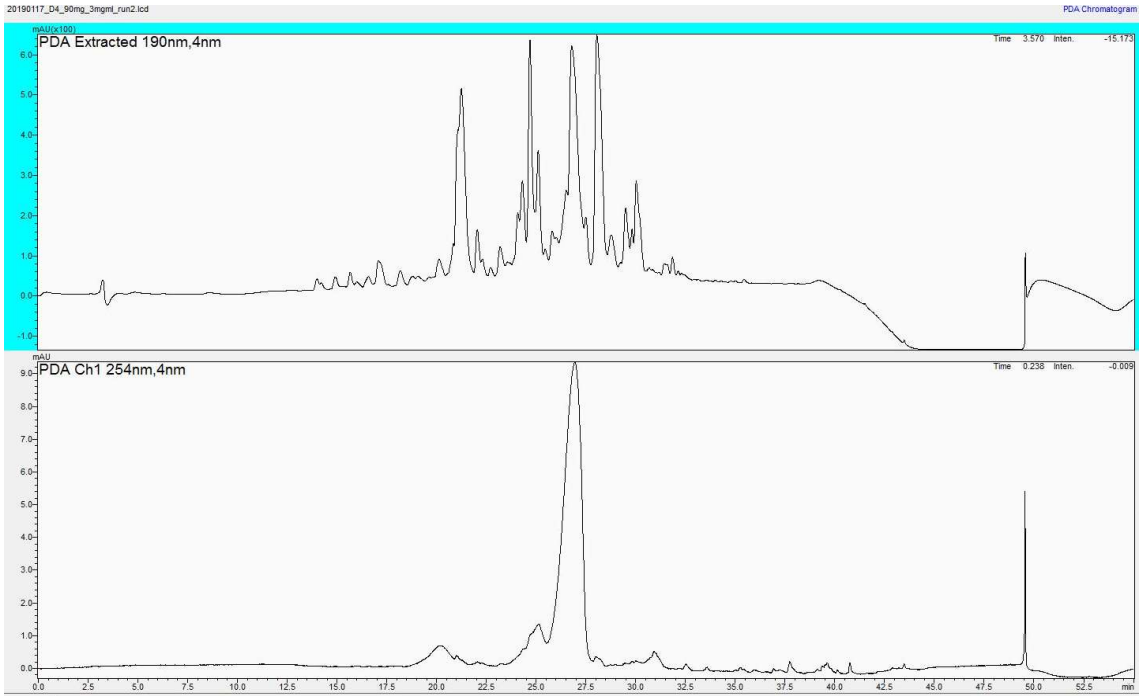

*Figure 25: HPLC chromatogram of D4 (EIEI*SQINM). The upper panel shows absorbance at 190 nm (peptide bonds). The lower panel shows absorption at 254 nm, which should be 280 nm but was set wrongly. The peak at a retention time of 26.4 min (upper panel) contained the desired peptide.*

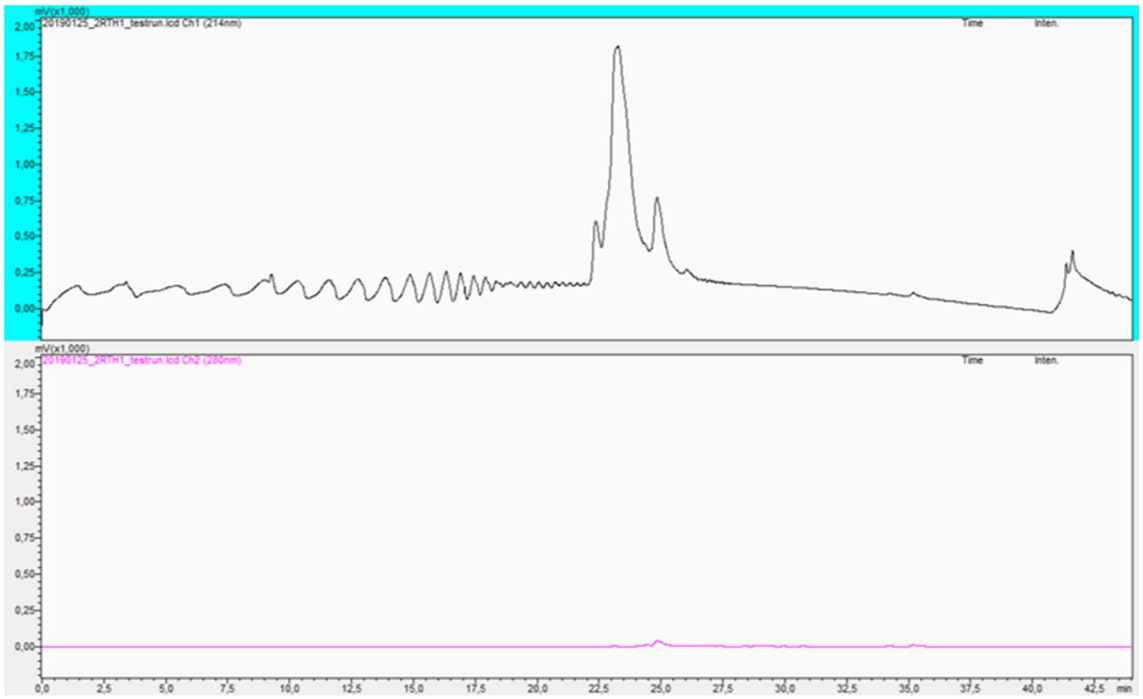

*Figure 26: HPLC chromatogram of D5 (CKIK*SQII).The black graph shows absorbance at 214 nm (peptide bonds), the pink graph shows absorbance at 280 nm (aromatic residues). The peak at a retention time of 23.3 min contained the desired peptide.*

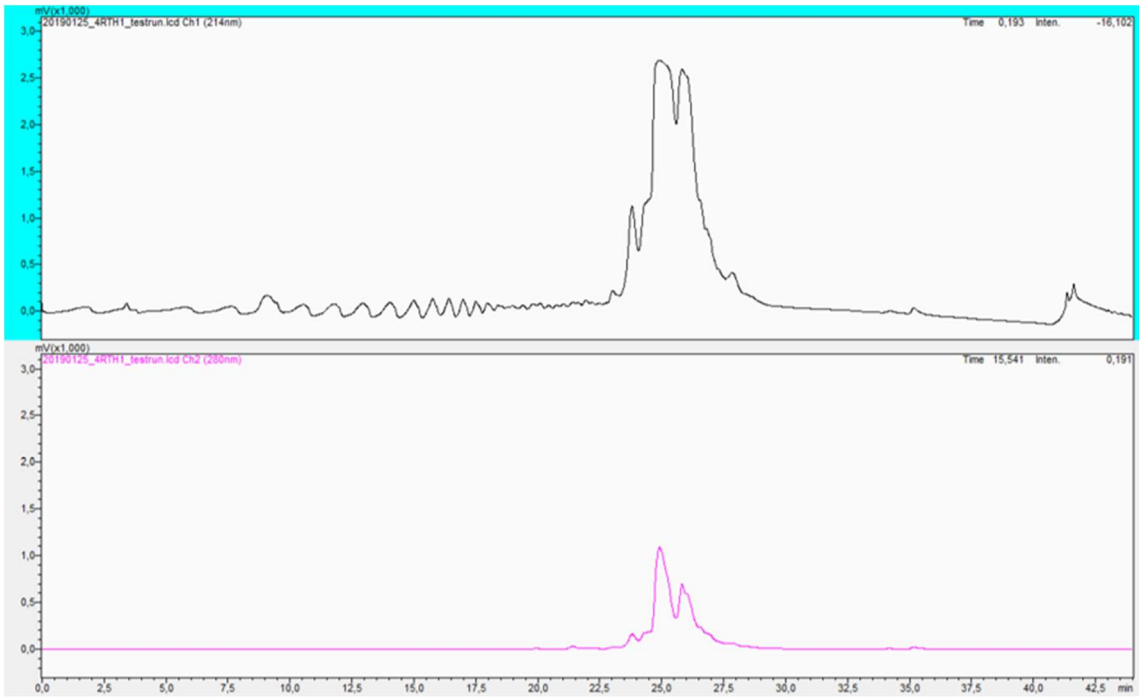

*Figure 27: HPLC chromatogram of D6 (KIKQ*SIINMWQ). The black graph shows absorbance at 214 nm (peptide bonds), the pink graph shows absorbance at 280 nm (aromatic residues). The peak at a retention time of 25.9 min contained the desired peptide.*

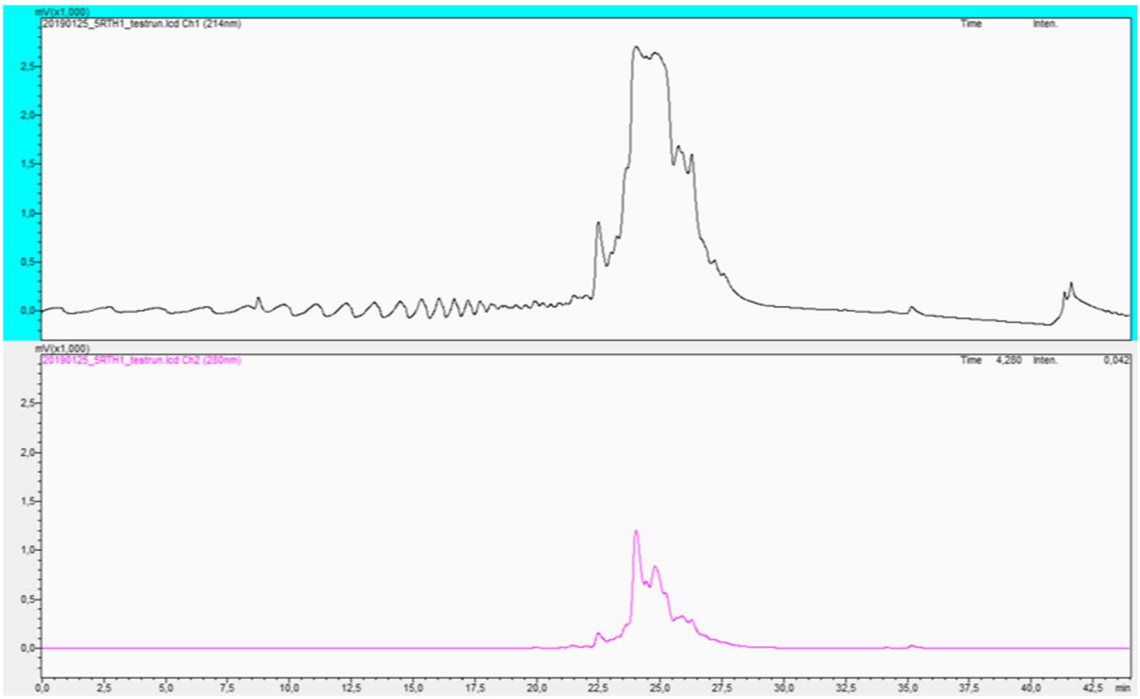

*Figure 28: HPLC chromatogram of D7 (KIKQI*SIQNMWQ). The black graph shows absorbance at 214 nm (peptide bonds), the pink graph shows absorbance at 280 nm (aromatic residues). The peak at a retention time of 24.8 min contained the desired peptide.*

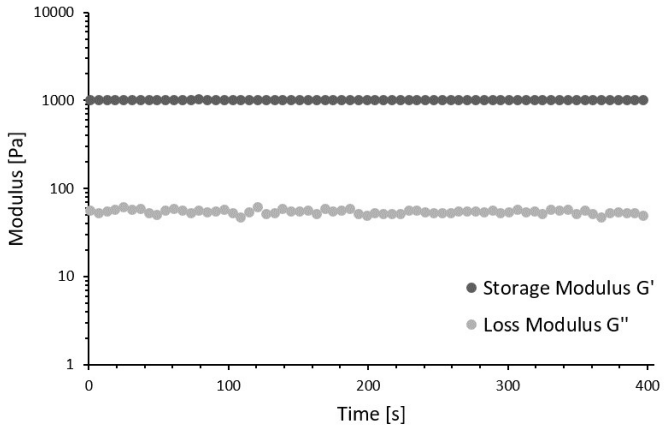

Figure 29: Oscillatory time sweep of H1 with fixed oscillatory strain (0.1 %) and fixed frequency (1 Hz). A time period of 400 s where storage modulus (G') and loss modulus (G'') were constant is displayed. Measurement was performed at 25 °C with n=1.

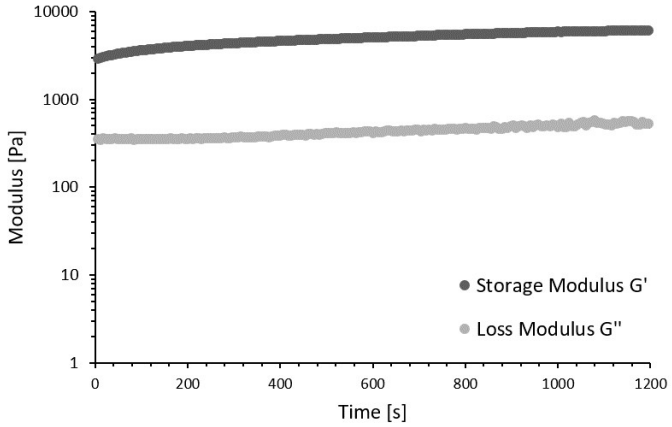

Figure 30: Exemplary gelation curve of H1+50 eq. D1 with fixed oscillatory strain (0.1 %) and fixed frequency (1 Hz). Measurement was performed at 25 °C with n=1.

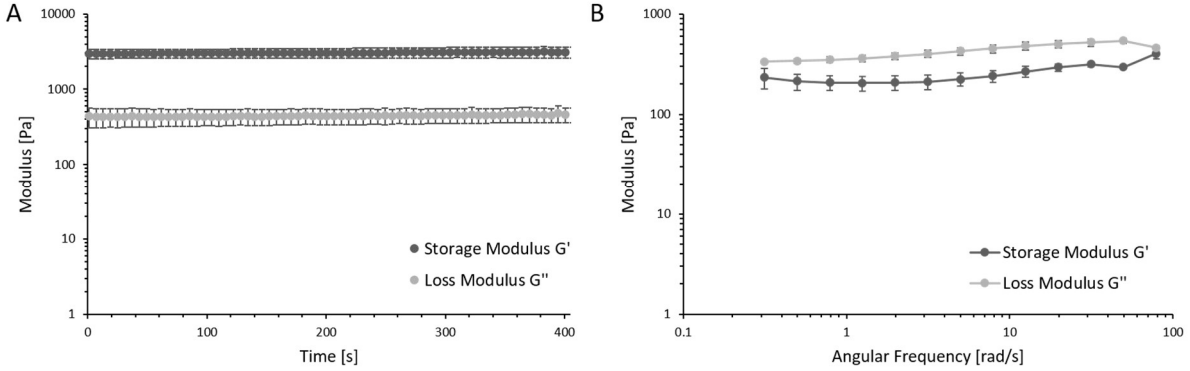

*Figure 31: Rheological characterization of H1 with additional 50 eq. of free D1 depsi peptide (KIKI*SQINM). A) Oscillatory time sweep with fixed strain (1 %) and fixed frequency (1 Hz). A time period of 400 s where storage modulus (G') and loss modulus (G'') were constant is displayed. Data is presented as mean ± s.d. with n=3. B) Frequency sweep (0.05-100 Hz) with fixed strain (1 %) (n=1). All measurements were performed at 25 °C.*

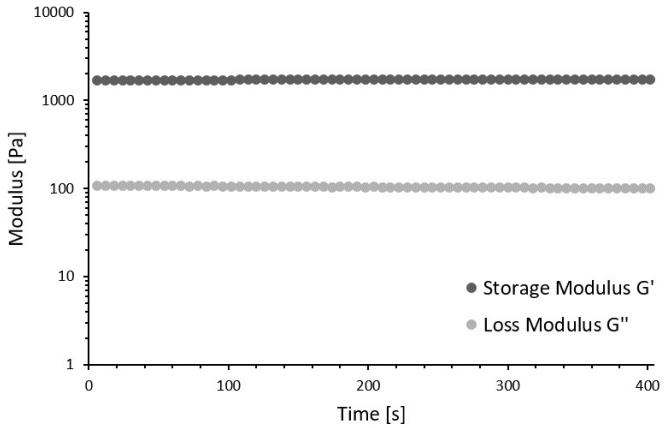

*Figure 32: Oscillatory time sweep of H1 with additional 50 eq. of free D6 depsi peptide (KIKQ*SIINMWQ) with fixed strain (1 %) and fixed frequency (1 Hz). A time period of 400 s where storage modulus (G') and loss modulus (G'') were constant is displayed. Measurement was performed at 25 °C with n=1.*

List of Abbreviations

Table 16: Abbreviations used in this thesis and their explanations listed in alphabetical order.

Abbreviation	Explanation
%	Percent
λ_{em}	Emission wavelength
λ_{ex}	Excitation wavelength
°C	Degree Celsius
µ	Micro (10^{-6})
AA	Amino acid
ACN	Acetonitrile
AD	Alzheimer's Disease
Asn, N	Asparagine
Aβ	Amyloid β
Boc	Tert-butoxycarbonyl
cHSA	Cationized human serum albumin
cHSA-PEG	Cationized and PEGylated human serum albumin
Cys, C	Cysteine
d	Day
Da	Dalton
dcHSA-PEG	Cationized, PEGylated and denatured human serum albumin
DIPEA	N,N-diisopropylethylamine
DMF	Dimethyl formamide
DMSO	Dimethyl sulfoxide
DNA	Deoxyribonucleic acid
ECM	Extracellular Matrix
EDA	Ethylene diamine
EDC	1-Ethyl-3-(3-dimethylaminopropyl)carbodiimide
eq	equivalents
Fmoc	Fluorenylmethyloxycarbonyl
FT-IR	Fourier-transform infrared spectroscopy
g	gram
G'	Storage modulus
G''	Loss modulus
Gln, Q	Glutamine

Glu, E	Glutamic acid
Gly, G	Glycine
h	Hour
HPLC	High performance liquid chromatography
HSA	Human serum albumin
Hz	Hertz
Ile, I	Isoleucine
k	Kilo (10^3)
L	Liter
LC-MS	Liquid Chromatography - Mass Spectrometry
Lys, K	Lysine
m	Milli (10^{-3})
M (weight)	Mass
Mal	Maleimide
MALDI-FT-ICR-MS	Matrix-assisted lased desorption ionisation-Fourier-transform-Ion cyclotron resonance-Mass spectrometry
MALDI-ToF-MS	Matrix-assisted laser desorption ionisation-Time of flight-Mass spectrometry
Met, M	Methionine
min	Minute
n	Nano (10^{-9})
n (statistics)	Sample size
NHS	N-hydroxysuccinimide
OtBu	Tert-butyl
Pa	Pascal
PBS	Phosphate buffered saline
PEG	Polyethylene glycol
PG	Protective group
PNF	Peptide nanofiber
PyBOP	Benzotriazol-1-yl-oxytripyrrolidinophosphonium hexafluorophosphate
RNA	Ribonucleic acid
RP-HPLC	Reversed phase high performance liquid chromatography
RPM	Rotations per minute
RT	Room temperature

s.d.	Standard deviation
sec	Second
SEM	Scanning electron microscopy
Ser, S	Serine
SPPS	Solid phase peptide synthesis
TCEP	Tris(2-carboxyethly)phosphine
TEM	Transmission electron microscopy
TFA	Trifluoroacetic acid
ThT	Thioflavin-T
TIPS	Triisopropylsilane
Trp, W	Tryptophan
Trt	Triphenylmethyl
V (Voltage)	Volt
vol.-%	Volume percent
vs.	versus
wt.-%	Weight percent
z	Charge

List of Chemicals

Table 17: Chemicals and their manufacturers used in this thesis listed in alphabetical order.

Chemical	Manufacturer
3-(maleimido)propionic acid N-hydroxysuccinimide ester	Alfa Aesar
ACN	VWR Chemicals Prolabo
Boc-Ser-OH	Sigma-Aldrich
Diethyl ether	VWR Chemicals Prolabo
DIPEA	Merck
DMF	VWR Chemicals Prolabo
DMSO	Honeywell, Riedel-de Haën®
EDA	Sigma-Aldrich
EDC	Sigma-Aldrich
Fluorescamine	PanReac AppliChem
Fmoc-Asn(Trt)-OH	Merck Novabiochem
Fmoc-Cys(Trt)-OH	Merck Novabiochem
Fmoc-Gln(Trt)-OH	Merck Novabiochem
Fmoc-Gln(Trt)-Wang resin	Merck Novabiochem
Fmoc-Glu(OtBu)-OH	Merck Novabiochem
Fmoc-Ile-OH	Merck Novabiochem
Fmoc-Ile-Wang resin	Merck Novabiochem
Fmoc-Lys(Boc)-OH	Merck Novabiochem
Fmoc-Met-OH	Merck Novabiochem
Fmoc-Met-Wang resin	Merck Novabiochem
Fmoc-Trp(Boc)-OH	Merck Novabiochem
HSA	Sigma-Aldrich
KCl	Merck
MeO-PEG(2000)-NHS ester	Rapp Polymere
PBS	Sigma-Aldrich
Piperidine	Carl Roth
PyBOP	Merck Novabiochem
Sinapinic acid	Fluka Analytical
TCEP	Acros Organics
TFA	Carl Roth
Thioflavin T	Fluka Analytical

TIPS	Sigma-Aldrich
Uranyl acetate dihydrate	Merck
Urea	AppliChem
α-cyano-4-hydroxycinnamic acid	Sigma-Aldrich

Acknowledgement

With these words, I want to thank all of you who supported me during my Master's Thesis.

First of all, I thank Prof. Dr. Tanja Weil for giving me the possibility to write my Master's Thesis in her working group. I was able to gain insight in a highly interesting field of biochemistry, in her institute in Ulm, but also at the MPI in Mainz. This was a great opportunity for me to expand my knowledge.

I thank Dr. Christopher Synatschke for the input he gave when discussing preliminary results. These discussions always showed me possibilities for follow up experiments. Furthermore, I thank him for sharing his scientific expertise during my stay at the MPI in Mainz.

A big thank you goes to Jasmina Gačanin, who was an excellent supervisor at all times. She confided this highly interesting project to me and did not hesitate to support me by sharing her expertise in all fields I worked in. She always had helpful advice for me from which I benefited a lot. Also, thank you for your friendly manner and helping me keep going with my Master's thesis.

I thank all members of AK Weil for making my stay at the institute a pleasant experience. Markus Lamla and Marco Hebel, thank you for performing MALDI measurements for me. I thank Thomas Mack for the TEM images of your peptides.

Last but certainly not least, I want to thank my husband, Manuel, and my parents, Rosie and Michael, for their emotional, mental, and financial support during my entire studies. Without you, I would not be the person I am today. Thank you for always being there for me.

Literature and Sources

Adochitei, A., and Drochioiu, G. (**2011**): Rapid Characterization of Peptide Secondary Structure by FT-IR Spectroscopy. Revue Roumaine de Chimie *56*, 783-791.

Ahmed, E.M. (**2015**): Hydrogel: Preparation, characterization and applications: A review. Journal of Advanced Research *6*, 105-121.

Akhtar, M.F., Hanif, M., and Ranjha, N.M. (**2015**): Methods of synthesis of hydrogels … A review. Saudi Pharmaceutical Journal *24*, 554-559.

Amdursky, N., Erez, Y., and Huppert, D. (**2012**): Molecular Rotors: What Lies Behind the High Sensitivity of the Thioflavin-T Fluorescent Marker. Accounts of Chemical Research *45*, 1548-1557.

Aston, R., Sewell, K., Klein, T., Lawrie, G., and Grøndahl, L. (**2016**): Evaluation of the impact of freezing preparation techniques on the characterisation of alginate hydrogels by cryo-SEM. European Polymer Journal *82*, 1-15.

Basu, A., Kunduru, K.R., Doppalapudi, S., Domb, A.J., and Khan, W. (**2016**): Poly(lactic acid) based hydrogels. Advanced Drug Delivery Reviews *107*, 192-205.

Berg, J.M., Tymoczko, J.L., Stryer, L. (**2013**): Biochemie. 7. Auflage, Springer Spektrum.

Bhattacharjee, S. (**2016**)**:** DLS and zeta potential – What are they and what are they not? Journal of Controlled Release *235*, 337-351.

Biancalana, M., Koide, S. (**2010**): Molecular mechanism of Thioflavin-T binding to amyloid fibrils. Biochimica et Biophysica Acta *1804*, 1405-1412.

Bosman, F.T., and Stamenkovic, I. (**2003**): Functional structure and composition of the extracellular matrix. The Journal of Pathology *200*, 423-423.

Byler, D.M., and Susi, H. (**1986**): Examinations of the Secondary Structure of Proteins by Deconvolved FTIR Spectra. Biopolymers *25*, 469-487.

Cabiaux, V., Brasseur, R., Wattiez, R., Falmagne, P., Ruysschaert, J.-M., and Goormaghtigh, E. (**1989**): Secondary Structure of Diphtheria Toxin and Its Fragments Interacting with Acidic Liposomes Studied by Polarized Infrared Spectroscopy. The Journal of Biological Chemistry *264*, 4928-4938.

Caló, E., and Khutoryanskiy, V.V. (**2015**): Biomedical applications of hydrogels: A review of patents and commercial products. European Polymer Journal *65*, 252-267.

Chen, J., and Zou, X. (**2019**): Self-assemble peptide biomaterials and their biomedical applications. Bioactive Materials *4*, 120-131.

Cloe, A.L., Orgel, J.P.R.O., Sachleben, J.R., Tycko, R., and Meredith, S.C. (**2011**): The Japanese Mutant Aβ (ΔE22-$Aβ_{1–39}$) Forms Fibrils Instantaneously, with Low-Thioflavin T Fluorescence: Seeding of Wild-Type $Aβ_{1-40}$ into Atypical Fibrils by ΔE22-$Aβ_{1-39}$. Biochemistry *50*, 2026-2039.

Dobson, C.M. (**2004**): Principles of protein folding, misfolding and aggregation. Seminars in Cell & Developmental Biology *15*, 3-16.

Fowler, D.M., Koulov, A.V., Alory-Jost, C., Marks, M.S., Balch, W.E, and Kelly, J.W. (**2006**): Functional amyloid formation within mammalian tissue. PLoS Biology *4*, 0100-0107.

Furuike, T., Komoto, D., Hashimoto, H., and Tamura, H. (**2017**): Preparation of chitosan hydrogel and its solubility in organic acids. International Journal of Biological Macromolecules *104*, 1620-1625.

Gačanin, J., Hedrich, J., Sieste, S., Glaßer, G., Lieberwirth, I., Schilling, C., Fischer, S., Barth, H., Knöll, B., Synatschke, C.V., and Weil, T. (**2019**): Autonomous Ultrafast Self-Healing Hydrogels by pH-Responsive Functional Nanofiber Gelators as Cell Matrices. Advanced Materials *31*.

Gačanin, J., Kovtun, A., Fischer, S., Schwager, V., Quambusch, J., Kuan, S.L., Liu, W., Boldt, F., Li, C., Yang, Z., Liu, D., Wu, Y., Weil, T., Barth, H., and Ignatius, A. (**2017**): Spatiotemporally Controlled Release of Rho-Inhibiting C3 Toxin from a Proten-DNA Hybrid Hydrogel for Targeted Inhibition of Osteoclast Formation and Activity. Advanced Healthcare Materials *6*.

Goormaghtigh, E., Cabiaux, V., and Ruysschaert, J.-M. (**1990**): Secondary structure and dosage of soluble and membrane proteins by attenuated total reflection Fourier-transform infrared spectroscopy on hydrated films. European Journal of Biochemistry *193*, 409-420.

Hoffman, A.S. (**2012**): Hydrogels for biomedical applications. Advanced Drug Delivery Reviews *64*, 18-23.

Huang, Z., Kangovi, G.N., Wen, W., Lee, S., and Niu, L. (**2017**): An RNA Aptamer Capable of Forming a Hydrogel by Self-Assembly. Biomacromolecules *18*, 2056-2063.

Hudson, S.A., Ecroyd, H., Kee, T.W., and Carver, J.A. (**2009**): The thioflavin T fluorescence assay for amyloid fibril detection can be biased by the presence of exogenous compounds. The FEBS Journal *276*, 5960-5972.

Jaradat, D.M.M. (**2017**): Thirteen decades of peptide synthesis: key developments in solid phase peptide synthesis and amide bond formation utilized in peptide ligation. Amino Acids *50*, 39-68.

Jung, I.Y., Kim, J.S., Choi, B.R., Lee, K., and Lee, H. (**2017**): Hydrogel Based Biosensors for In Vitro Diagnostics of Biochemicals, Proteins, and Genes. Advanced Healthcare Materials *6*, 1601475.

Kapoor, S., and Kundu, S.C. (**2016**): Silk protein-based hydrogels: Promising advanced materials for biomedical applications. Acta Biomaterialia *31*, 17-32.

Khan, F., and Tanaka, M. (**2018**): Designing Smart Biomaterials for Tissue Engineering. International Journal of Molecular Sciences *19*, 17.

Khurana, R., Uversky, V.N., Nielsen, L., and Fink, A.L. (**2001**): Is Congo Red an Amyloid-specific Dye? The journal of Biological Chemistry *276*, 22715-22721.

Kitagaki, J., Shi, G., Miyauchi, S., Murakami, S., and Yang, Y. (**2015**): Cyclic depsipeptides as potential cancer therapeutics. Anti-Cancer Drugs *26*, 259-271.

Knowles, T.P.J., and Mezzenga, R. (**2016**): Amyloid Fibrils as Building Blocks for Natural and Artificial Functional Materials. Advanced Materials *28*.

Kodera, Y., Matsushima, A., Hiroto, M., Nishimura, H., Ishii, A., Ueno, T., Inada, Y. (**1998**): PEGylation of proteins and bioactive substances for medical and technical applications. Progress in Polymer Science *23*, 1233-1271.

Kong, J., and Yu, S. (**2007**): Fourier Transform Infrared Spectroscopic Analysis of Protein Secondary Structures. Acta Biochimica et Biophysica Sinica *39*, 549-559.

Koutsopoulos, S. (**2016**): Self-assembling peptide nanofiber hydrogels in tissue engineering and regenerative medicine: Progress, design guidelines, and applications. Journal of Biomedical Materials Research Part A, *104A*, 1002-1016.

Kuan, S.L., Wu, Y., and Weil, T. (**2013**): Precision Biopolymers from Protein Precursors for Biomedical Applications. Macromolecular Rapid Communications *34*, 380-392.

Kumar, P., Kizhakkedathu, J.N., and Straus, S.K. (**2018**): Antimicrobial Peptides: Diversity, Mechanism of Action and Strategies to Improve the Activity and Biocompatibility In Vivo. Biomolecules *8*.

Li, C.-C., and Anseth, K.S. (**2009**): PEG Hydrogels for the Controlled Release of Biomolecules in Regenerative Medicine. Pharmaceutical Research *26*, 631-643.

Li, J., Xing, R., Bai, S., and Yan, X. (**2019**): Recent advances of self-assembling peptide-based hydrogels for biomedical applications. Soft Matter *15*, 1704-1715.

Liu, Y. and Hsu, S.-h. (**2018**): Synthesis and Biomedical Applications of Self-Healing Hydrogels. Frontiers in Chemistry *6*, 449.

Ma, X., Sun, X., Hargrove, D., Chen, J., Song, D., Dong, Q., Lu, X., Fan, T.-H., Fu, Y., and Lei, Y. (**2016**): A Biocompatible and Biodegradable Protein Hydrogel with Green and Red Autofluorescence: Preparation, Characterization and *In Vivo* Biodegradation Tracking and Modeling. Scientific Reports *6*, 19370.

Maji, S.K., Perrin, M.H., Sawaya, M.R., Jessberger, S., Vadodaria, K., Rissmann, R.A., Singru, P.S., Nilsson, K.P.R., Simon, R., Schubert, D, Eisenberg, D., Rivier, J., Sawchenko, P., Vale, W., and Riek, R. (**2009**): Functional amyloids as natural storage of peptide hormones in pituitary secretory granules. Science *325*, 328-332.

Merrifield, R.B. (**1963**): Solid Phase Peptide Synthesis. I. The Synthesis of a Tetrapeptide. Journal of American Chemical Society *85*, 2149-2154.

Noori, A., Ashrafi, S.J., Vaez-Ghaemi, R., Hatamian-Zaremi, A., and Webster, T. (**2017**): A review of fibrin and fibrin composites for bone tissue engineering. International Journal of Nanomedicine *12*, 4937-4961.

Okuda, T., Kawakami, S., Maeie, T., Niidome, T., Yamashita, F., and Hashida, M. (**2006**): Biodistribution characteristics of amino acid dendrimers and their PEGylated derivatives after intravenous administration. Journal of Controlled Release *114*, 69-77.

Parmar, A., Lakshminarayanan, R., Iyer, A., Mayandi, V., Goh, E.T.L., Lloyd, D.G., Chalasani, M.L.S., Verma, N.K., Prior, S.H., Beuerman, R.W., Madder, A., Taylor, E.J., and Singh, I. (**2018**): Design and Syntheses of Highly Potent Teixobactin Analogues against *Staphylococcus aureus*, Methicillin-Resistant *Staphylococcus aureus* (MRSA), and Vancomycin-Resistant Enterococci (VRE) *in Vitro* and *in Vivo*. Journal of Medicinal Chemistry *61*, 2009-2017.

Schilling, C., Mack, T., Lickfett, S., Sieste, S., Ruggeri, F.S., Sneideris, T., Dutta, A., Bereau, T., Naraghi, R., Sinske, D., Knowles, T.P.J., Synatschke, C.V., Weil, T., and Knöll, B. (**2019**): Sequence-Optimized Nanofibers as Growth Stimulators for Regeneration of Peripheral Neurons. Advanced Functional Materials *29*.

Selkoe, D.J., and Hardy, J. (2016): The amyloid hypothesis of Alzheimer's disease at 25 years. EMBO Molecular Medicine 8, 595-608.

Shao, Y., Jia, H., Cao, T., and Liu, D. (**2017**): Supramolecular Hydrogels Based on DNA Self-Assembly. Accounts of Chemical Research *50*, 659-668.

Sohma, Y., Sasaki, M., Hayashi, Y., Kimura, T., and Kiso, Y. (**2004**): Novel and efficient synthesis of difficult sequence-containing peptides through O-N intramolecular acyl migration reaction of O-acyl isopeptides. Chemical Communications, 124-125.

Sudhakar, S., Kalipillai, P., Santhosh, P.B., and Mani, E. (**2017**): Role of Surface Charge of Inhibitors on Amyloid Beta Fibrillation. The Journal of Physical Chemistry C *121*, 6339-6348.

Ullah, F., Othman, M.B.H., Javed, F., Ahmad, Z., and Akil, H.M. (**2015**): Classification, processing and application of hydrogels: A review. Materials Science and Engineering C *57*, 414-433.

Valastyan, J.S., and Lindquist, S. (**2014**): Mechanisms of protein-folding diseases at a glance. Disease Models & Mechanisms *7*, 9-14.

Vandermeulen, G.W.M., and Klok, H.-A. (**2004**): Peptide/Protein Hybrid Materials: Enhanced Control of Structure and Improved Performance through Conjugation of Biological and Synthetic Polymers. Macromolecular Biosciences *4*, 383-398.

Wei, Z., Yang, J.H., Zhou, J., Xu, F., Zrínyi, M., Dussault, P.H., Osada, Y., and Chen, Y.M. (**2014**): Self-healing gels based on constitutional dynamic chemistry and their potential applications. Chemical Society Reviews *43*, 8114-8131.

Wu, Y., Li, C., Boldt, F., Wang, Y., Kuan, S.L., Tran, T.T., Mikhalevich, V., Förtsch, C., Barth, H., Yang, Z., Liu, D., and Weil, T. (**2014**): Programmable protein-DNA hybrid hydrogels for the immobilization and release of functional proteins. Chemical Communications *50*, 14620-14622.

Wu, Y., Ng, D.Y.W., Kuan, S.L., and Weil, T. (**2015**): Protein-polymer therapeutics: a macromolecular perspective. Biomaterials Science 3, 214-230.

Xiao, Y.-F., Jie, M.-M., Li, B.-S., Hu, C.-J., Xie, R., Tang, B. and Yang, S.-M. (**2015**): Peptide-Based Treatment: A Promising Cancer Therapy. Journal of Immunology Research, 1-13.

Yoshiya, T., Ito, N., Kimura, T., and Kiso, Y. (**2008**): Isopeptide method: development of S-acyl isopeptide method for the synthesis of difficult sequence-containing peptides. Journal of Peptide Science *14*, 1203-1208.

Zanna, N., and Tomasini, C. (**2017**): Peptide-Based Physical Gels Endowed with Thixotropic Behaviour. Gels *3*, 39.

Zhang, Y., Tu, J., Wang, D., Zhu, H., Maity, S.K., Qu, X., Bogaert, B., and Zhang, H. (**2018**): Programmable and Multifunctional DNA-Based Materials for Biomedical Applications. Advanced Materials *30*, 1703658.

Zuidema, J.M., Rivet, C.J., Gilbert, R.J., and Morrison, F.A. (**2014**): A protocol for rheological characterization of hydrogels for tissue engineering strategies. Journal of Biomedical Materials Research Part B, *102B*, 1063-1073.